European Commission

Horizon 2020
European Union funding
for Research & Innovation

REDUCTION OF RADIOLOGICAL ACCIDENT CONSEQUENCES

Action	Research and Innovation Action NFRP-2018-1
Grant Agreement #	847656
Project name	**R**eduction of **R**adiological **C**onsequences of design basis and design extension **A**ccidents
Project Acronym	R2CA
Project start date	01.09.2019
Deliverable #	D3.2
Title	Final report on fission product releases during LOCA
Author(s)	Adam Kecek (UJV), Francois Kremer (IRSN), Asko Arkoma (VTT), Sevon Tuomo (VTT), Iurii Ovdienko (SSTC NRS), Dmytro Gumenyuk (SSTC NRS), Simone Gianfelici (ENEA), Matthias Jobst (HZDR)
Version	01
Related WP	WP3 LOCA
Related Task	T3.1. Fission product transport and release from the primary to the environment (UJV-NRI)
Lead organization	UJV-NRI
Submission date	28.02.2023
Dissemination level	PU

This project has received funding from the Euratom research and training programme 2014-2018 under the grant agreement n° 847656

Historygi

Date	Submitted by	Reviewed by	Version (Notes)
28.02.2023	A. Kecek (UJV),	S. Belon (IRSN) N. Girault (IRSN)	01

1. Contents

1. Contents 3
1 Introduction 8
2 IRSN 9
2.1 ASTEC-TR models for iodine behaviour in the containment 9
2.2 EPICUR facility test 12
2.3 ASTEC-TR models for iodine behaviour in the primary circuit 16
2.4 Summary 20
2.5 References 20
3 ENEA: 21
3.1 Models summary 21
3.2 Experiments used for validation 22
3.3 Experiments in R2CA database 22
3.4 Optimization of fuel grain size distribution 23
3.5 Conclusions 30
3.6 References 31
4 HZDR 32
4.1 Review and assessment of fission product release rate models implemented in ATHLET-CD 32
4.2 Assessment and implementation of alternative burst release fraction model 43
4.3 Summary 44
4.4 References 44
5 UJV 46
5.1 Validation of COCOSYS 46
5.2 VVER-1000/V-320 containment studies 52
5.3 Summary 58
5.4 References 58
6 SSTC NRS 59
6.1 Type of fuel assembly for which calculations have been performed 60
6.2 The used program for calculations 60
6.3 Description of the calculation model 60
6.4 The results of the calculations 67

6.5 Summary 71
6.6 References 71
7 VTT 71
7.1 Model description 72
7.2 AHMED experiment 72
7.3 Results 73
7.4 References 74
8 Summary 75

List of Figures and Tables

Figure 1. Iodine evolution in the gaseous phase (left) and total iodine concentration evolution in the main sump (right) for THAI-9 test 11
Figure 2. Total iodine concentration evolution in the elevated sump (left) and total iodine mass evolution in the condensate (right) for THAI-9 test 11
Figure 3. Inorganic and organic iodine release for EPICUR LD1 test 13
Figure 4. Inorganic and organic iodine release for EPICUR LD2 test 14
Figure 5. Inorganic and organic iodine release for EPICUR LD3 test 14
Figure 6. Inorganic and organic iodine release for EPICUR LD5 test 15
Figure 7. Inorganic and organic iodine release for EPICUR LD6 test 15
Figure 8. Iodine mass onto dry stainless steel and iodine speciation (left) and iodine concentration in the gaseous phase (right) for BIP-G1 test. 16
Figure 9: Volatile FPs release in test VERDON-1 [25] 23
Figure 10: Fuel temperature evolution for VERCORS RT1 experiment. Cladding material is (a) Zr or (b) ZrO_2 24
Figure 11: Fuel temperature evolution for VERCORS RT6 experiment. Cladding material is (a) Zr or (b) ZrO_2 25
Figure 12: Experimental and simulated Cs release during VERCORS RT6 test, along with the integral to be optimized 26
Figure 13: RT1 ASTEC/RAVEN calculations status 27
Figure 14: RT6 ASTEC/RAVEN calculations status 28
Figure 15: RT1 experiment, results with NCLG = 7, SIGM = 3.86E-6, DGRA = 13.83E-6 29
Figure 16: RT6 experiment, results with NCLG = 8, SIGM = 8.42E-6, DGRA = 2.157E-6 29
Figure 17 ATHLET-CD nodalization scheme of reactor core of generic Konvoi. 33
Figure 18 Applied power profiles for the 6 core sections. 34
Figure 19 Integral of the burst release rate (normalized to 1.0) as modelled in ATHLET-CD 37
Figure 20 Activity released from the fuel to the RCS for DBA LOCA (with application of uncertainty factors obtained from [10]) 41
Figure 21 Reduction of the fuel rod mass inventory (entire core) due to burst release during DBA LOCA (with application of uncertainty factors obtained from [10]) 42
Figure 22: Interactions of gaseous I_2 with painted surface in containment 47
Figure 23: Nodalisation of the BIP IA experiments 49
Figure 24: Prediction of iodine adsorption (original parameters) 50
Figure 25: Prediction of iodine adsorption (modified parameters) 50

Figure 26 Schematic of the RTF facility and COCOSYS nodalisation [6] 51
Figure 27 Comparison of the RTF P9T1 experimental data [8] with COCOSYS calculation (concentration of iodine in gas phase) 52
Figure 28 Comparison of iodine mass release relative to calculation with pH 5-10 (initial iodine speciation according to R.G. 1.183) 53
Figure 29 Comparison of iodine mass release relative to calculation with pH 5-10 (initial iodine speciation according to R.G. 1.195) 54
Figure 30 Results of the BEPU analysis of iodine release from VVER-1000/V-320 during LB LOCA (COCOSYS calculation) 57
Figure 31 Spearman's correlation ratio for VVER-1000/V-320 LB LOCA 57
Figure 32 Longitudinal and cross-sections of the calculation model FA-A 3.99% with the separated fuel rod of the central zone 63
Figure 33 Longitudinal and cross-sections of the calculation model FA-A 3.99% with the separated fuel rod burnable absorber 64
Figure 34 Longitudinal and cross-sections of the calculation model FA-A 4.39% with the separated fuel rod of the central zone 65
Figure 35 Longitudinal and cross-sections of the calculation model FA-A 4.39% with the separated fuel rod with burnable absorber 66
Figure 36. Aerosol concentration in the AHMED test, measurement compared with Apros and MELCOR calculations. 73

Table 1. Maximum conditions in as calculated by reactor simulations performed in Task 2.3: 10
Table 2. Conditions of tests selected from the ASTEC V2.2 database: 10
Table 3. Experimental and boundary conditions for EPICUR LD tests. 13
Table 5. CHIP GAEC: tests “IOH-1”, “IOH-2” and “IOH-3” (reducing conditions) 18
Table 5. CHIP GAEC: tests “IOH-4” and “IOH-5” (oxidizing conditions) 19
Table 6: ASTEC/ELSA Validation matrix, according to Cantrel et al. [3], and parameters of interest 21
Table 7: ASTEC/RAVEN random input parameters 27
Table 8: Optimized ASTEC parameters for RT1 and RT6 30
Table 9 Scaling factors for release of different elements 36
Table 10 Gap release values as specified by [11] 40
Table 11 ATHLET-CD results for FP releases (simulation with B.E. release rate coefficients, according to the CORSOR release fraction model) 40
Table 12 Gap release fractions for PWR as proposed by DG-1389 [12] with uncertainties taken from [13] 43
Table 13: Investigated IA tests with Amerlock coupons [6] 48
Table 14: Proposed BAS_i and XPHS parameters values for Ameron Amerlock 51
Table 15: Calculated variants 53
Table 16 List of variated parameters in VVER-1000/V-320 BEPU 56
Table 17 Spearman’s correlation ratio values at 10 000 s 58
Table 18 Isotopic composition of separately selected fuel rod with burnable absorber FA-A type 398GO depending on the depth of burnup (1 to 26 MWd/kg) 67
Table 19 Isotopic composition of separately selected fuel rod with burnable absorber FA-A type 398GO depending on the depth of burnup (28 to 54 MWd/kg) 68

Table 20 Isotopic composition of separately selected fuel rod FA-A type 398GO depending on the depth of burnup (1 to 26 MWd/kg) 68
Table 21 Isotopic composition of separately selected fuel rod FA-A type 398GO depending on the depth of burnup (28 to 54 MWd/kg) 69
Table 22 Isotopic composition of separately selected fuel rod with burnable absorber FA-A type 439GT depending on the depth of burnup (1 to 26 MWd/kg) 69
Table 23 Isotopic composition of separately selected fuel rod with burnable absorber FA-A type 439GT depending on the depth of burnup (28 to 54 MWd/kg) 70
Table 24 Isotopic composition of separately selected fuel rod FA-A type 439GT depending on the depth of burnup (1 to 26 MWd/kg) 70
Table 25 Isotopic composition of separately selected fuel rod FA-A type 439GT depending on the depth of burnup (28 to 54 MWd/kg) 71

Abbreviations

AHMED	Aerosol and Heat Transfer Measurement Device
BIP	Behaviour of Iodine Project
BU	Burn-Up
CHIP	CHimie de l'Iode dans le circuit Primaire (Chemistry of Iodine in the Primary Circuit)
DBA	Design Basis Accident
DEC-A	Design Extension Accident
EPICUR	Experimental Programme on Iodine Chemistry Under Radiation
FP	Fission Product
ISTP	International Source Term Program
LB	Large Break
LD	Long Duration
LOCA	Loss Of Coolant Accident
NPP	Nuclear Power Plant
PWR	Pressurized Water Reactor
RCS	Reactor Cooling System
SARNET	Severe Accident Research NETwork
SIC	Silver Indium Cadmium
STEM	Source Term Evaluation and Mitigation project
THAI	Thermal-hydraulics, Hydrogen, Aerosols and Iodine project
WP	Work Package

1 Introduction

The main objectives of Task 3.1 were to improve models/codes and validate or re-assess those models for the simulation of fission products behaviour in the reactor coolant system and in the containment during a LOCA transient within DBA and DEC-A conditions. It mainly concerns:

- Fission product release from the fuel rod,
- Fission product transport in the primary circuit,
- Fission product behaviour in the containment.

The contributions of the partners during these more than 2 years of work were very varied and quite disparate, depending on the degree of development of the codes used for their studies/safety analyses and their main shortcomings. The performed work covered a wide spectrum of phenomena (neutronics, FP release; FP chemistry…) ranging from isotopic inventory calculations in core assemblies to the behavior of FPs and more particularly of iodine in the reactor containment.
As regards the type of activities, they have also been very varied, covering the optimization of input parameters or model parameters, the refinement and/ development of specific models, the realization of sensitivity and uncertainty calculations. Recalculations of experimental tests selected from the database established at the beginning of the project and relevant for the LOCA accidents within DBA and DEC-A conditions as well as reactor calculations have also been performed.

Concerning the fission product releases and transport in the primary circuit, the focus, as much as possible, was made on the validity of the models dedicated to severe accidents when used to describe DBA or DEC-A conditions. Indeed, for these latter the global development of the accident and so of the releases is faster (i.e. burst releases). This difference reinforces the impact of the kinetics of the chemical and physical transformation of the radionuclides in the primary circuit and up-to the environment.

All these works had as a common objective the improvement and the validation of the calculation chains used for the source term calculation of a LOCA type accident in the DBA and DEC-A conditions to have a better evaluation of their radiological consequences.

This report describes the work and the main achievements obtained during the project by each of the six partners involved in this task.
Regarding model verification, validation, refinement and development it covers:

- Optimisation of the fuel grain size parameters used in ASTEC for the Volatile FP release in high burn-up fuel at low temperatures (typical of DBA conditions)
- Critical review of FP release models (burst/early and continuous/long term releases) and assumptions in ATHLET-CD focussing on the phenomena important for DBA LOCA transients
- Reassessment of the ASTEC models for iodine transport in RCS and iodine behaviour in containment for DBA and DEC-A conditions with a focus on the verification of chemical kinetics model built for the behaviour of (I-O-H) system behaviour in the primary coolant system
- Validation and optimisation of the model parameters in COCOSYS for FP (especially iodine) in containment covering I_2 adsorption/desorption from dry paints and iodine revolatilisation from liquid phases
- Development of a model for gravitational deposition of aerosols in APROS

The experiments in support of this work were selected in majority from the database built at the beginning of the project for the conditions (DBA and DEC-A) of interest issued from various research programmes (BIP, CHIP, EPICUR, RTF, THAI, VERCORS…).

Regarding reactor calculations it covers:

- Best-estimate calculations of the isotopic inventories for selected representative types of fuel assemblies used in VVER-1000 reactors using SCALE software package,
- FP activity releases calculations including uncertainty factors from fuel to RCS for a large break DBA LOCA transient with ATHLET-CD for a generic German PWR of type Konvoi,
- BEPU analyses with COCOSYS of iodine releases from a VVER-1000-320 reactor during a large break LOCA transient.

2 IRSN

The models existing in ASTEC-TR module (i.e. SOPHAEROS module) dealing with FP behaviour during their transport in the primary circuit and the reactor containment have been validated for what concerns iodine against a reference database mostly dedicated to severe accident (Phébus-PF [1], ISTP [2], OECD/STEM [3]) i.e. for what concerns the containment for temperatures and doses rates probably higher than those expected for DBA and DEC-A conditions. IRSN has thus re-assessed the models implemented in SOPHAEROS both for iodine transport in the primary circuit and iodine behaviour in the containment on the selected tests in the database and verified their applicability for LOCA DBA and DEC-A conditions.

2.1 ASTEC-TR models for iodine behaviour in the containment

To assess applicability of the models, the simulations of LOCA DBA and DEC-A for PWR-900 reactor performed in Task 2.3 are considered as a reference for the dose rate and temperature encountered during the accident. The conditions found in these simulations are compared to those of the different tests of the ASTEC validation database. Three tests have been found to comply with the LOCA DBA/DEC-A conditions:

- STEM/EPICUR LD [4] tests for inorganic and organic iodine releases from Epoxy paint under irradiation,
- the G1 test from the BIP program [5] for interaction of gaseous inorganic iodine with dry stainless stell,
- the Iod9 from the THAI facility [6] for iodine mass transfer and adsorption on steel wall.

The tables below provide the maximum dose rate and temperature considered as reference, as well as the dose rate and temperature of the selected validation cases of ASTEC. The LOCA range of dose rate in gas phase is covered by the EPICUR LD tests, while most of the LOCA temperature range is covered by THAI Iod-9 and EPICUR LD tests. One can note, however, that the dose rate in the liquid phase found in the LOCA calculations is not found in the ASTEC validation database.

Table 1. Maximum conditions in as calculated by reactor simulations performed in Task 2.3:

	LOCA DBA	LOCA DEC-A
Dose rate (Gas)	0.7 Gy/s	0.38 Gy/s
Dose rate (Liquid)	0.1 Gy/s	0.01 Gy/s
Temperature (Gas)	160 °C	115 °C
Temperature (Liquid)	120 °C	115 °C

Table 2. Conditions of tests selected from the ASTEC V2.2 database:

	THAI Iod-9	EPICUR LD	BIP-G1
Dose rate (Gas)	-	0.35 – 1.05 Gy/s	-
Dose rate (Liquid)	-	-	-
Temperature (Gas)	70-150 °C	80-120 °C	70 °C
Temperature (Liquid)	70-75 °C	-	-

Details on each of the selected ASTEC V2.2 database are provided below.

2.1.1 THAI facility test

The THAI facility, operated by Becker Technologies GmbH (Germany), is a cylindrical stainless-steel vessel of 9.2 m height and 3.2 m diameter, with a total volume of 60 m^3. Different inner configurations of the vessel could be used depending on the test series (HM series, HD series, HR series…).
In particular, in test "Iod-9" (of concern below), two sumps were considered. The main sump was filled with 0.625 m^3 of water that corresponds to a water height of about 0.5 m. The interfacial area between the main sump and gas was 1.6 m^2. As to the second sump (elevated sump filled with 52 l water), the water/gas interfacial area was 1.04 m^2.

The THAI Iod-9 test dealt with the study of I_2 mass transfer from the gaseous phase to the 2 sumps of the THAI facility and onto the steel surfaces of the vessel. As to the experimental protocol, the test was divided into four test phases, as follows: conditioning phase; phase with stratified main sump and I_2 injection; phase with mixed main sump; phase with steam injection and washing. In the conditioning phase the steel vessel was heated up to approximately 90°C. The relative humidity at the end of this phase was between 30% and 40%.
Main initial and boundary conditions of the THAI-9 test are summarized below:

- Temperature (gaseous phase): 70°C and then 150°C
- Temperature (main sump): 70°C
- Temperature (elevated sump): 75°C
- pH (main sump) = 2.0 and then 12.0 at washing
- pH (elevated sump) = 2.5
- pH(condensate) = 4.5
- I_2 injection rate: 2.21 mg/s for 4 minutes ($m(I_2)$ = 0.53 g)
- Vliq (main sump) = 625 L
- Vliq (elevated sump) = 52 L
- Vgas = 60 m^3
- Interfacial area (main sump): 1.6 m^2
- Interfacial area (elevated sump): 1.04 m^2

- Steel surface: 140 m^2

The ASTEC main results are summarized on the figures hereafter, focusing on how fast is the mass transfer reaction of gaseous (I_2) into the sump and its adsorption on steel walls.
More precisely, Figure 1 (left plot) shows I_2 evolution in the gaseous phase and compares it with the experimental data. "GW" refers to different heights of gaseous sampling. Figure 1 (right plot) shows the total iodine concentration evolution in the main sump. Figure 2 (left plot) shows the total iodine concentration evolution in the elevated sump. Figure 2 (right plot) shows the total iodine mass evolution in the condensate.

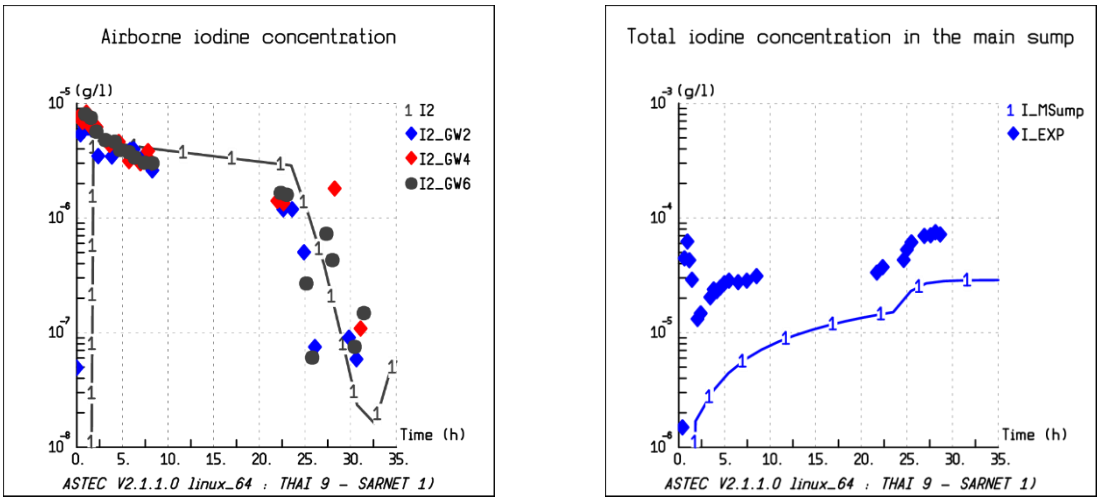

Figure 1. Iodine evolution in the gaseous phase (left) and total iodine concentration evolution in the main sump (right) for THAI-9 test

Comparison of SOPHAEROS results and experimental data

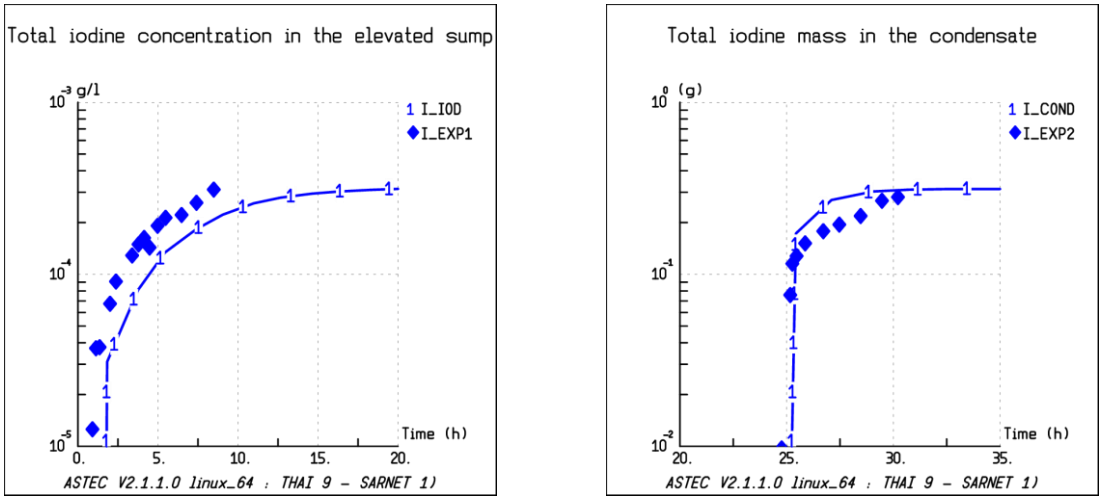

Figure 2. Total iodine concentration evolution in the elevated sump (left) and total iodine mass evolution in the condensate (right) for THAI-9 test

In summary, the iodine behaviour in THAI Iod-9 was fairly well simulated by ASTEC in both the gaseous and water phases, and also on the surfaces in the gaseous phase.

2.2 EPICUR facility test

The EPICUR experimental device (located at IRSN, France) aimed at providing experimental data to validate the chemical models for iodine in the reactor containment under accident conditions [4]. It consists of:

- A panoramic gamma-ray irradiator
- A test loop comprising:
    - an irradiation tank, irradiated by the ^{60}Co sources, which simulates the reactor vessel and its various components (sump, painted surfaces of the reactor in the air or immersed, etc.);
    - a filtration system (May-Pack) for quantitative measurement of 131-I on-line or after the test, differentiating between the different forms (iodine in aerosol form, molecular iodine I_2 or organic iodine RI).

About thirty tests were performed as part of the International Source Term Program (ISTP) from 2005 to 2010. These tests aimed at studying the behaviour of iodine in the reactor containment, particularly with the effect of irradiation on:

- Volatile iodine released from the sump;
- Organic iodides formed from iodine which are deposited on the painted containment surfaces in air or underwater;
- Iodide oxides formed from gaseous iodine and their stability.

Afterward, the EPICUR facility was used from 2011 to 2016 in the frame of the Source Term Evaluation and Mitigation (STEM) program. Numerous other tests have been therefore performed in the frame of this OECD/STEM program (and then within the follow-up STEM2 project), focusing in particular on the effect of irradiation on:

- Stability of iodine aerosols (CsI, AgI, iodine oxides, etc.);
- Interactions between iodine and aged paints in the frame of the reactor life extension;
- Re-volatilisation of iodine in the long term during an accident.

Several different test series have been conducted in the EPICUR facility, in particular the so-called LD series, whose main objectives were to quantify the inorganic and organic releases from Epoxy paint loaded with iodine and irradiated in a gaseous environment. Concretely, the LD series dealt with the irradiation of a painted coupon located in the gaseous phase. A carrier gas was injected to evaluate the kinetics of CH3I and I2 desorption from the coupon under irradiation. Six tests from the so-called LD series have been considered at IRSN to analyse the ASTEC modelling, namely the tests LD1, LD2, LD3, LD4, LD5 and LD6.

The boundary conditions are reported hereafter in Table 3 for the six EPICUR LD tests that have been simulated at IRSN with ASTEC V2.1.1. In particular, the effect of the iodine concentration was checked with LD1 to LD3, the effect of the humidity with LD4, the effect of the temperature with LD5 and the influence of the dose rate with LD6.

Table 3. Experimental and boundary conditions for EPICUR LD tests.

Test	LD1	LD2	LD3	LD4	LD5	LD6
Test duration (hours)	98	88	30	30	30	30
$[I]_i$ ($mol(I)/m^2$)	$9.0\ 10^{-3}$	$9.5\ 10^{-4}$	$9.0\ 10^{-5}$	$6.5\ 10^{-5}$	$1.7\ 10^{-4}$	$4.8\ 10^{-5}$
Dose rate (Gy/s)	0.35	0.34	0.32	0.35	0.35	1.05
Temperature (°C)	80°C	80°C	80°C	80°C	120°C	80°C
Humidity	60%	60%	60%	20%	60%	60%

As discussed and justified in 0, the raw data were then corrected for the following reasons: to consider the missing mass balance as I_2; to attribute the activity on the quartz filter (QF) on the knitmesh (KM); to correct the data on the KM and charcoal filter (CF) as the efficiency of the KM usually ranges between 85 and 98 %.
In the following, the comparisons between the iodine-paint interaction model that was developed with the LD tests series and the experimental data are focused on the release kinetics of CH_3I on the CF and I_2 on the KM.

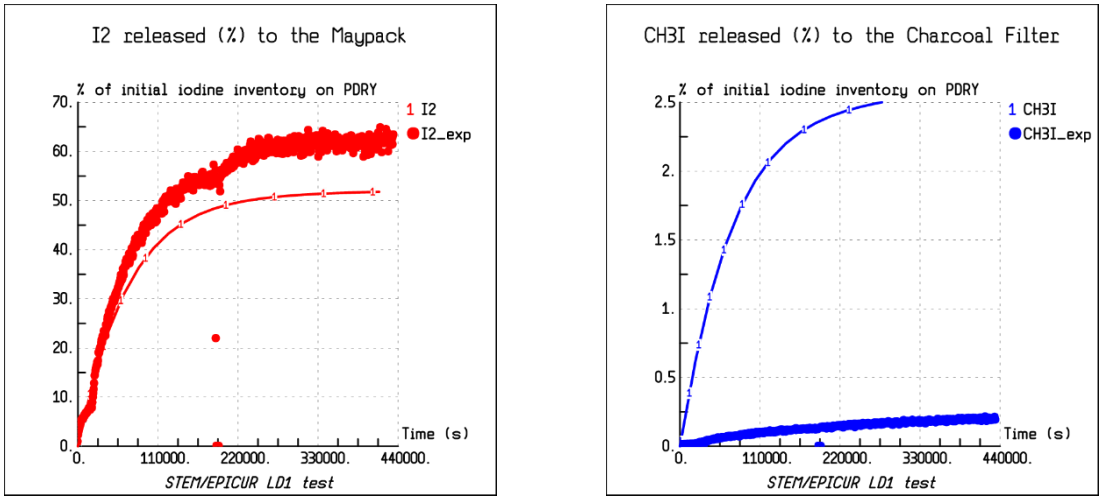

Figure 3. Inorganic and organic iodine release for EPICUR LD1 test

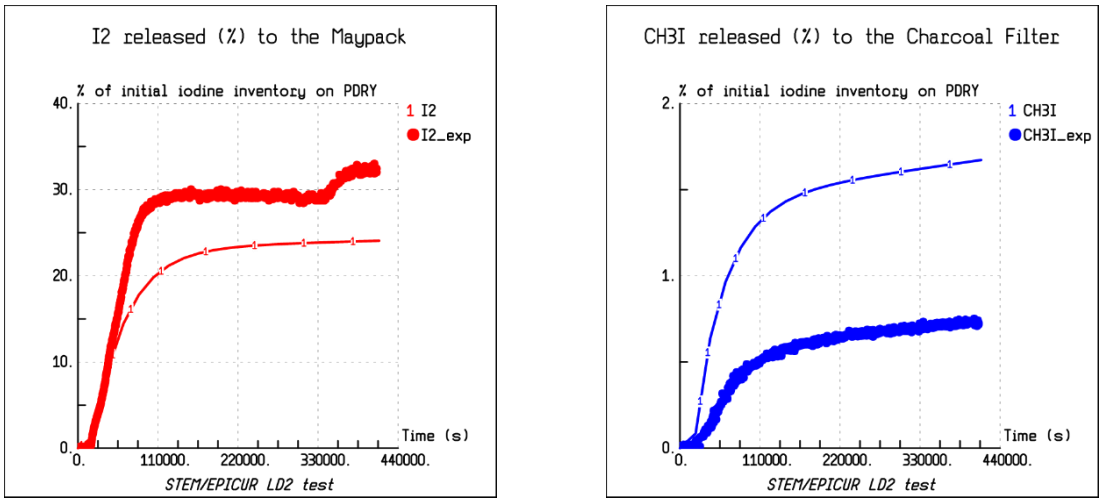

Figure 4. Inorganic and organic iodine release for EPICUR LD2 test

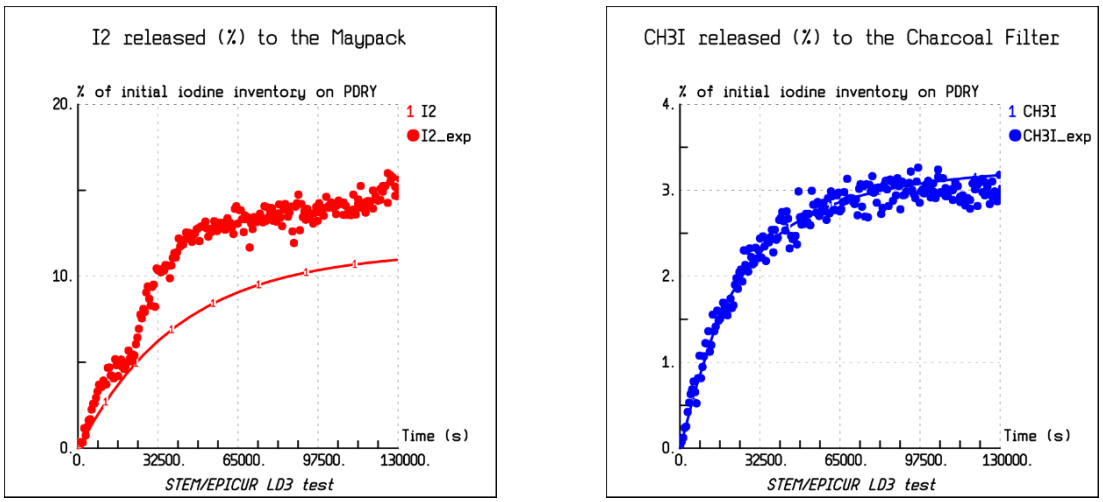

Figure 5. Inorganic and organic iodine release for EPICUR LD3 test

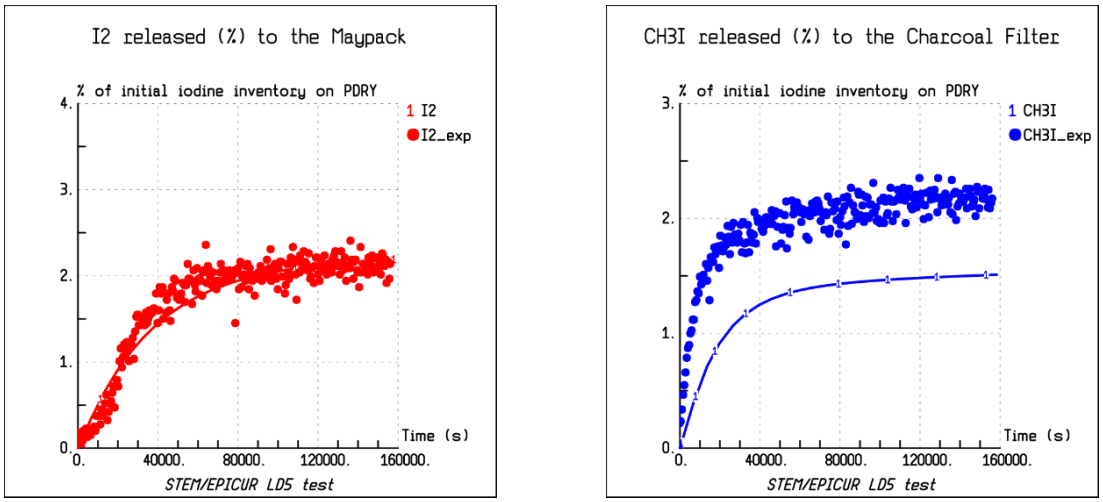

Figure 6. Inorganic and organic iodine release for EPICUR LD5 test

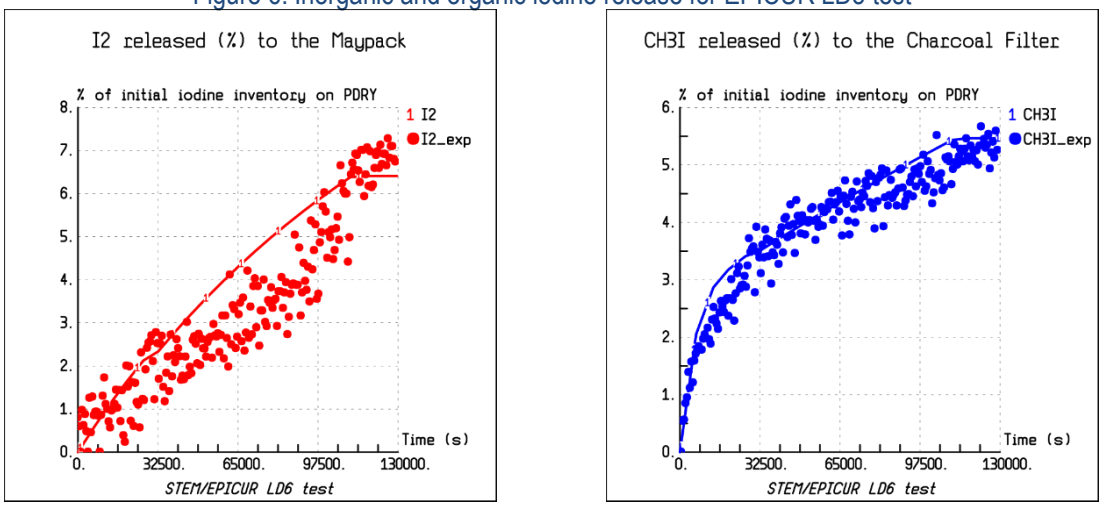

Figure 7. Inorganic and organic iodine release for EPICUR LD6 test

In summary, the experimental results obtained in the frame of the STEM and ISTP/EPICUR LD programs have led IRSN to develop a new model of iodine-Epoxy paint interaction under irradiation that considers the influence of the temperature, dose rate and iodine concentration on the paint. As illustrated above, the releases from this kind of paint are now well captured and modelled with the SOPHAEROS module.

2.2.1 BIP-G1 test

The BIP (Behaviour of Iodine Project), initiated by NEA/CSNI, was operated by AECL (Canada). It officially started in July 2007 and ended in June 2010. The G1 test dealt with the interaction of gaseous inorganic iodine I_2 with dry stainless steel. This test was therefore considered at IRSN to assess the ASTEC/SOPHAEROS modelling about iodine/steel interactions.
Main initial and boundary conditions of the G1 test are summarized below:

- Test duration: 136.9 hours
- Vliq = 0. L
- Vtot = 0.01 L
- Temperature in the sump: 70°C
- Dose rate: 0. Gy/s
- Dry steel surface: 5.07 cm^2
- $[I_2]$ = 1.0 10^{-8} mol/L
- Gas flow rate through the facility: 1 L/min

Three species were expected on the steel: I_2, FeI_2 and FeI_2O_x. The ASTEC main representative result is summarized on Figure 8.
Here, the focus is on the kinetics of adsorption and desorption of gaseous I_2 onto dry stainless steel and the iodine speciation on steel.

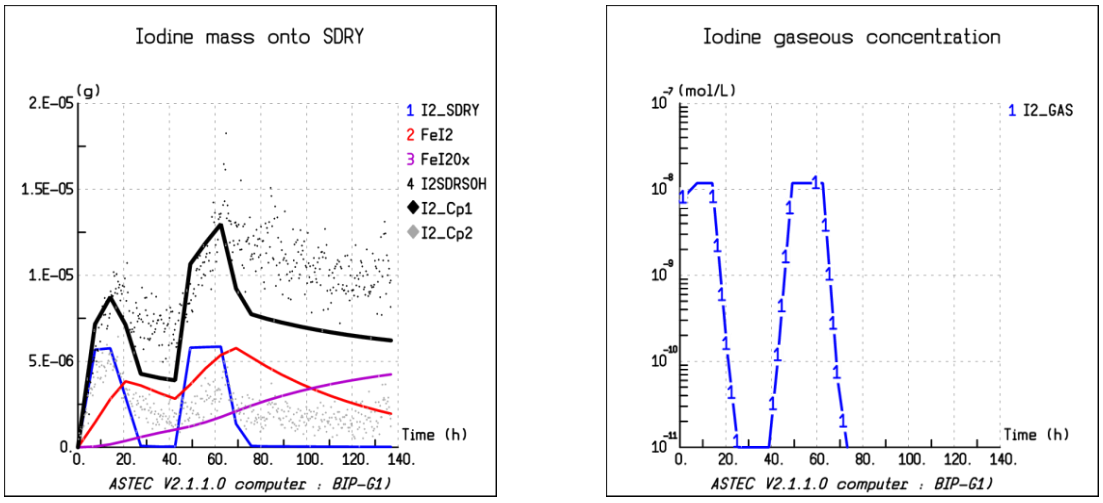

Figure 8. Iodine mass onto dry stainless steel and iodine speciation (left) and iodine concentration in the gaseous phase (right) for BIP-G1 test.
Note: On left graph, the total iodine on dry stainless steel is the thick black curve

2.3 ASTEC-TR models for iodine behaviour in the primary circuit

Among the validation grid of the models for iodine behaviour in the primary circuit, the GAEC experiments performed in the CHIP facility was focused on the {I-O-H} chemical system [7], which is relevant in the context of LOCA DBA and DEC-A accidents. The GAEC experiments consisted in the transport of iodine down a temperature gradient from 1600°C to 150°C. One can note that it is much larger than the gradient encountered in LOCA accident. However, considering that the models of ASTEC/SOPHAEROS where not fitted on the experiment, but rather developed on a physical basis and latter confronted to the experiment, it can be assumed that they are valid all along the 150-1600°C range, thus covering the temperature range encountered in the primary circuit during a LOCA.

2.3.1 Description of the CHIP facility

In the framework of the EU SARNET network [8], small-scale experiments have been specifically conducted in the last decade, in order to better understand the chemical iodine behaviour in the RCS. In that respect, one may notably mention the EXSI-PC facility [9] (operated by VTT, Finland) that was developed since 2009 to study the effect of reaction with primary circuit surface material on iodine transport, and the CHIP experimental program that was launched at IRSN in 2008 to study iodine speciation.
In particular, as part of the International Source Term Program (ISTP), the CHIP experimental program was set-up to obtain information on iodine speciation under different circuit boundary conditions in presence of other fission products (Cs, Mo) and/or control rod materials (Ag, In, Cd, B) which could be released during the reactor core meltdown. Classically, the CHIP experiments consisted in analyzing the behaviour of selected elements that were transported in a controlled thermal gradient in a tube flow reactor.
A first objective of this experimental program was to study elementary systems in order to provide step by step kinetic data for modelling the iodine chemistry in the RCS conditions, focusing on homogeneous gaseous phase reactions. In particular, the first elementary system that was studied was the {I,O,H} system through the realization of the CHIP GAEC test series.
The CHIP experimental device was operated as follows. The chemical elements including the carrier gas (H_2/H_2O/inert gas) were heated at 1600°C in a "high temperature" (HT) zone. At this temperature, all the species were supposed to be under gaseous form at thermodynamic chemical equilibrium. Downstream of the HT zone, the fluid was cooled down in the so-called "transport zone" where chemical reactions took place, producing aerosols and gases. As to the surface materials, it is worth noting that the test line consisted of an alumina tube in the HT zone while in the transport zone the tube was made of the same stainless steel as the RCS.

2.3.2 Results of ASTEC simulations vs. CHIP GAEC {I-O-H} tests

Five experiments belonging to the CHIP GAEC I-O-H test matrix ("IOH-1" to "IOH-5" tests) were therefore selected at IRSN to make a first assessment of the SOPHAEROS kinetic scheme describing the reactivity of iodine in this {I,O,H} system. In particular, this first validation allowed evaluating the modelling improvements brought by the kinetic scheme with respect to the thermodynamic equilibrium assumption that was usually made in former ASTEC versions.
For that purpose, three different calculations were consecutively achieved for each test, the first one still considering a thermodynamic equilibrium, a second one activating the new kinetic system and a third one rather similar to the second one but where only reactions including iodine were activated (i.e. assuming equilibrium for H_2 and H).
As to the test boundary conditions, one may underline the complementarity of the selected tests that allowed exploring the influence of the atmosphere: tests IOH-1, IOH-2 and IOH-3 were performed with reducing conditions while tests IOH-4 and IOH-5 were performed in oxidizing conditions.

IOH-1, IOH-2 and IOH-3 tests (reducing conditions)
IOH-1 test was conducted under hydrogen conditions with argon. It was especially dedicated to study I-H system. IOH-2 test was also performed under H_2 but the hydrogen fraction was reduced to limit HI production. IOH-3 test was under hydrogen too, but at a lower temperature and with a lower iodine injection. Details about the experimental conditions may be found in [1].

Results from the ASTEC/SOPHAEROS comparative simulations of the IOH-1, IOH-2 and IOH-3 tests are summarized hereafter in Table 32. These results are presented as released mass fractions (for HI, I_2 and I) expressed in percentage of the iodine mass injected at the circuit inlet.

Table 4. CHIP GAEC: tests "IOH-1", "IOH-2" and "IOH-3" (reducing conditions)
HI, I_2 and I fraction at the GAEC main line outlet
Comparison between experimental data, ASTEC "equilibrium" case and ASTEC "kinetic" case

			HI (% ii.)	**I_2 (% ii.)**	**I (% ii.)**
IOH-1	Experiment		85.9%	14.1%	*not av.*
	ASTEC	Thermodynamic equilibrium	100%	0.0%	0.0%
		Kinetic reactions	5.2%	87.2%	7.6%
		Kinetic reactions for iodine H_2 and H computed at equilibrium	90.5%	5.7%	3.8%
IOH-2	Experiment		79.5%	20.5%	*not av.*
	ASTEC	Thermodynamic equilibrium	99.99%	0.0	
		Kinetic reactions	3.2%	89.4%	7.4%
		Kinetic reactions for iodine H_2 and H computed at equilibrium	78.4%	16.4%	5.2%
IOH-3	Experiment		96.3%	3.7%	*not av.*
	ASTEC	Thermodynamic equilibrium	99.99%	0.0	
		Kinetic reactions	9.3%	74.5%	16.2%
		Kinetic reactions for iodine H_2 and H computed at equilibrium	87.6%	5.3%	7.1%

As to IOH-1 test, the ASTEC/SOPHAEROS calculation assuming a thermodynamic equilibrium provided only HI at the outlet, as shown on Table 4. No retention was predicted because all species were only in gaseous phase and could not condense or be sorbed on wall. HI computed at equilibrium was closer to experimental value. If kinetic system was activated, around 87% of iodine at the outlet was under I_2 which was totally in disagreement with experimental value.
Because of a disagreement between experimental values and modelled speciation at the outlet, a sensitivity study was then performed assuming that H radical amount was very likely underestimated with the SOPHAEROS complete kinetic reactions. It was assumed therefore that H_2 was in equilibrium with H radical. In that context, only reactions including iodine were activated. This updated computation performed with the carrier gas assumed to be in thermodynamic equilibrium had a significant impact on the nature of the iodine released at the outlet of the line. Indeed, in this peculiar case, SOPHAEROS computed that 90% of HI was released at the outlet of the main line.
As to IOH-2 test, due to a lower level of H_2, the measurements showed that the HI production was lower than in previous IOH-1 test. As aforementioned, three consecutive simulations were performed with ASTEC, assuming in turn either thermodynamic equilibrium, or kinetic reaction for all species or kinetic reaction only for iodine species, the latter meaning that the carrier gas is assumed in equilibrium. Similarly to the former IOH-1 test simulations, the IOH-2 test was also well modelled with ASTEC SOPHAEROS assuming carrier gas equilibrium.
As to IOH-3 test, less molecular iodine was found in sampling compared to the previous test, meaning larger iodine retention in the test line. Here again ASTEC results gave the same general trend: no molecular iodine assuming

thermodynamic equilibrium, too much molecular iodine assuming kinetic reactions for all species and closer results to the experimental values assuming kinetic reaction only for iodine species.

IOH-4 and IOH-5 tests (oxidizing conditions)

IOH-4 test was conducted under steam conditions with argon. IOH-5 test was similar to IOH-4 (also performed in presence of steam), but with a higher iodine concentration. Details about the experimental conditions may be found in [7].

Results from the ASTEC/SOPHAEROS comparative simulations of the IOH-4 and IOH-5 tests are summarized hereafter in Table 5. The way the results are presented is the same as previously for IOH-1, IOH-2 and IOH-3.

Table 5. CHIP GAEC: tests "IOH-4" and "IOH-5" (oxidizing conditions)
HI, I_2 and I fraction at the GAEC main line outlet
Comparison between experimental data, ASTEC "equilibrium" case and ASTEC "kinetic" case

			HI (% ii.)	**I_2 (% ii.)**	**I (% ii.)**	**HOI (% ii.)**
IOH-4	Experiment		3.8%	96.2%	*not av.*	*not av.*
	ASTEC	Thermodynamic equilibrium	0.0	99.99%	0.001%	0.0
		Kinetic reactions	18.9%	65.0%	4.0%	12.1%
		Kinetic reactions for iodine H_2 and H computed at equilibrium	3.3%	92.4%	4.2%	0.1%
IOH-5	Experiment		9.1%	90.9%	*not av.*	*not av.*
	ASTEC	Thermodynamic equilibrium	0.0	99.99%	0.0	0.0
		Kinetic reactions	18.1%	80.1%	0.9%	0.9%
		Kinetic reactions for iodine H_2 and H computed at equilibrium	2.7%	96.2%	0.9%	0.2%

As to IOH-4 test, similarly to the previous IOH tests, no retention in the circuit was computed by ASTEC. Assuming a thermodynamic equilibrium for all species, SOPHAEROS predicted only molecular iodine at the main line outlet, which was close to the experimental results. But no iodine at all was predicted to be released under HI form, which was not correct.

With all the kinetic systems activated, around 65% of iodine was released as molecular iodine, 19% as HI, 12% as HOI and 4% as I, which was not consistent with experimental observations. The HOI and HI fractions evaluated by SOPHAEROS were indeed too high compared to the experimental results. Furthermore, as highlighted by complementary analyses (described in [7]), molecular iodine, that was formed only with I radical, was underestimated.

A third computation was done assuming carrier gas at equilibrium, as already performed in reducing conditions. In this case, I_2 represented around 92% of total iodine at the outlet. Only 3.3% of HI was formed and 4.2% was under I radical. The analysis of the production/loss rate profile for I_2, HI and I showed that only I_2 was produced below 1000 K. Because I radical concentration was higher, there was more molecular iodine in this case.

Finally, focusing on the IOH-5 test, the SOPHAEROS computation at thermodynamic equilibrium gave only molecular iodine. With higher iodine concentration, using kinetic reactions, I_2 fraction increased but the modelling results were closer to experimental results assuming the carrier gas at equilibrium.

2.4 Summary

In summary, the CHIP GAEC experimental data was successfully used at IRSN to evaluate the physical relevance of the FP/aerosols modelling of the SOPHAEROS module from ASTEC, focusing on the RCS iodine chemistry and more particularly on the {I,O,H} system. Main objective was indeed to evaluate the capabilities of the new SOPHAEROS thermo-kinetic scheme of {I,O,H} to reproduce the experimental data from the CHIP GAEC tests. Overall, the HI and I_2 amounts measured at the outlet of the GAEC test line could be quite well predicted with a few adequate assumptions. This code-to-data comparison thus allowed validating the kinetic scheme of {I,O,H} in thermal conditions of a RCS in severe accident, and a fortiori in LOCA.

2.5 References

[1] B. Clément, R. Zeyen, "The objectives of the Phébus FP experimental programme and main findings", in Annals of Nuclear Engineering, 2013, 61, pp. 4-10

[2] B. Clément, R. Zeyen, "The phebus fission product and source term international programmes", International Conference on Nuclear Energy for New Europe, Bled, Slovenia, 5–8 September (2005)

[3] B. Clément, B. Simondi-Teisseire, "STEM: an IRSN project on source term evaluation and mitigation", in Transactions of American Nuclear Society, 2010, 103, pp. 475-476

[4] S. Guilbert et al., "Formation of organic iodide in the containment in case of a severe accident", in American Nuclear Society 2008 Annual Meeting, Anaheim, CA, 8–12 June 2008

[5] G.A. Glowa, C.J. Moore, J.M. Ball, "The main outcomes of the OECD behaviour of iodine (BIP) project", in Annals of Nuclear Engineering, 2013, 61, pp. 179-189

[6] G. Poss, K. Fischer, F. Funke, M. Sonnenkalb, "Present results and future prospects of containment research in the THAI facility", CSARP Technical Review Meeting, Bethesda, MD, USA, 16–19 September (2008)

[7] A.-C. Grégoire, Y. Délicat, C. Tornabene, F. Cousin, L. Gasnot, N. Lamoureux, L. Cantrel, "Study of the iodine kinetics in thermal conditions of a RCS in nuclear severe accident", in Annals of Nuclear Energy, 2017, 101, pp. 69–82

[8] T. Albiol, J.P. Van Dorsselaere, B. Chaumont, T. Haste, Ch. Journeau, L. Meyer, B.R. Sehgal, B. Schwinges, D.Beraha, A. Annunziato, R. Zeyen, "SARNET : Severe Research Network of Excellence", in Progress of Nuclear Energy, 2010, 52, pp. 2-10

[9] M. Gouëllo, J. Hokkinen, T. Kärkelä, A. Auvinen, "A Scoping Study of Chemical Behaviour of Caesium Iodide in Presence of Boron in Condensed Phase (650 °C and 400 °C) under Primary Circuit Conditions", in Nuclear Technology, 2018, 203, pp. 66-84.

3 ENEA:

ASTEC has been the subject of an extensive validation campaign performed by numerous European partners, also with the project EVITA, within the 5th Framework Programme of the European Union [1], [2].
The release kinetics of the fission products and structural materials are described in ASTEC, by the ELSA module. In the framework of the R2CA project it becomes important assessing the validation status of the ELSA module in the conditions of interest of the study, i.e. those expected for DEC-A and DBA.
In general, we would consider ELSA validated for such purpose in case it can effectively predict the correct results in conditions with high burn-up (BU) and rather low temperatures and has been benchmarked against experiments with such conditions.
Cantrel et al. [3] report the experiments employed for the validation: they are summarized in Table 6, along with indicative temperature and BU.

Table 6: ASTEC/ELSA Validation matrix, according to Cantrel et al. [3], and parameters of interest

Experiment	Ref.	Phenomena	Max temperature	BU (GWd/t)
VERCORS	[5]–[7]	Release from irradiated fuel pellets [4] PWR SA conditions UO_2 and MOX	1860°C – 2350°C	38.3 – 71.8
MCE/HCE	[8]–[10]	Release from CANDU fuel fragments	1780 K – 2200 K	9.8 – 10.7
EMAIC	[11]	Release from Ag-In-Cd control rods	---	---
HEVA	[12]–[15]	Release from fuel rods		36.7
ORNL HI/VI	[16]	Release from fuel rods		10 – 47
Phebus FP	[17]–[20]	Integral test UO_2	Increasing until fuel degradation	Fresh to 38

3.1 Models summary

The FP release models in ELSA distinguish the FP species into volatile, semi-volatile and low volatile, with different modelled processed each [3], [21], [22]. The ELSA theoretical manual [21] describes additional models specific for the release of control materials, structural materials (tin, steel) and from the molten pool.
The employed models and semi-empiric formulas are described in detail in the ELSA theoretical manual and in Brillant et al. [21], [22]; a detailed description of the variable relations, however, is not within the scope of this report. As a summary [3]:

- Volatile species release is guided by intra-granular diffusion, which is driven by oxygen vacancies, i.e. by fuel oxidation process (oxidation model is also described in [21], [22]) and grain-size distribution. Cladding oxidation plays a role in trapping of some isotopes (Te, Se, Sb). The release is instantaneous for the species in liquid fuel phase, occurring as soon as the fuel melting point is reached.
- Semi-volatile species also diffuse to grain boundaries with similar rate as for volatile species. Nonetheless, the main rate-limiting process occurs at the grain boundaries where the release is governed by equilibrium vapour pressures, determined by temperature and carrier gas composition. Special correlations are used for the oxides of Ba, Mo, Ru, Ce, La, Sr, Eu.
- Low-volatility species release does not depend from diffusion processes. Such species are released proportionally to volatilised fuel, i.e. depending on the vapour pressure equilibrium of UO_3.

The oxidation model (described in reports [22] and in the manual [21]), which plays an important role in the release of volatile and semi-volatile species, follows different correlations depending on the oxidising fluid being steam or air. The steam semi-empiric correlation, in particular, has been experimentally determined for temperatures in the range 1073 – 1873 K.
Nonetheless, according to Brillant et al. [4], the BU impact on the FP release was not taken into account in the model (causing discrepancies in some cases); the authors suggest that high BU UO_2 models should be developed in the future.

3.2 Experiments used for validation

Considering the relevant phenomena of concern of this report, i.e. FP releases from high burn-up fuels within LOCA DBA and DC-A conditions, VERCORS tests have been investigated in the first instance.

VERCORS [5]–[7] is an experimental program conducted at Grenoble by CEA between 1989 and 2002, following the HEVA program. The experiment focused on the FP release from an irradiated fuel rod; the conditions were representative of severe accidents in PWR.
The experiment included three test series [5]:

- *VERCORS 1-6*: UO_2 fuel, close-to-relocation temperature (1860 – 2350°C), higher than HEVA cases;
- *VERCORS HT*: focused on FP transport in the PWR primary system and interaction with neutron absorbers;
- *VERCORS RT*: focused on low-volatility and transuranic species.

In most cases the samples were re-irradiated in order to rebuild the short-lived FP inventory.
Some tests have been run for very high BU values. Such tests are [5]:

- *VERCORS 6*: UO_2, mixed steam and hydrogen flow, 60 GWd/t BU (5 cycles). During the last phases of the experiment, at 2350°C, the sample relocated.
- *VERCORS RT6*: UO_2, mixed steam and hydrogen conditions, 72 GWd/t BU (6 cycles).
- *VERCORS RT8*: UO_2, air, 70 GWd/t BU (6 cycles).

Most of the tests have been performed at high temperatures, except for:

- *VERCORS 2*: UO_2, mixed steam and hydrogen flow, 38.3 GWd/t BU, temperature plateaus at 800°C, 1000°C, 1200°C, 1500°C;
- *VERCORS 5*: UO_2, steam flow, 38.3 GWd/t BU, temperature plateaus at 800°C, 1000°C, 1300°C;
- *VERCORS RT7*: MOX, hydrogen flow, 43.0 GWd/t BU, temperature plateau at 1200°C.

None of these tests then combines fuels with high BU and low temperature plateaus. However, some of the tests performed till high temperatures includes an intermediate plateau at low temperatures.
Amongst all the VERCORS tests performed, it was decided to select for the study the VERCORS RT6 test. Then for comparison the VERCORS RT1 test with a medium burn-up fuel (47.3 GWd/t corresponding to 4 cycles) was also included.

3.3 Experiments in R2CA database

In the framework of the T2.1.3 of the R2CA project, a database of relevant experiments has been established and documented in deliverable D2.3 [25]. With the objective of improving the validation of the ELSA module for the FP

release, in particular in DEC-A and DBA conditions, one has also considered employing some of the experiments in the database.
The following experiments might prove especially interesting for extending ELSA validation:

- The *Annular Core Research Reactor – source term (ACCR-ST)* is an experiment series performed at SNL in the 1980s and 1990s with the objective of obtaining time-resolved data about FP release from irradiated fuels under SA conditions. The experiment has been performed with UO_2 fuel with a BU of 47 GWd/t.
- The *FLASH LOCA* are a series of tests performed in the 1980s in the Siloé reactor (Grenoble, France). The objectives include gathering data on FP release during LOCA type accident scenarios, including the effect of BU on FP release.
- *GASPARD* [26] has been an experimental program conducted at CEA between 2000 and 2002 aiming at the quantification of the fission gases release from high-BU PWR UO_2 fuels. The temperatures range from 300°C to 1200°C (typical LOCA temperature) and the BU was 48.5 GWd/t in one case, 71.8 GWd/t in another; results are limited to gaseous FP.
- The *VERDON* tests [27]–[29] have been conducted between 2011 and 2015 in CEA Cadarache Centre, focusing on FP release from high BU UO_2 and MOX fuels. The 5 tests employ UO_2 fuel with 68 and 72 GWd/t BU or MOX with 55.6 GWd/t BU and feature on-line FP release measurement; the temperature slowly grows up to 2800 K, so data on the release are available also for low temperatures (Figure 9).

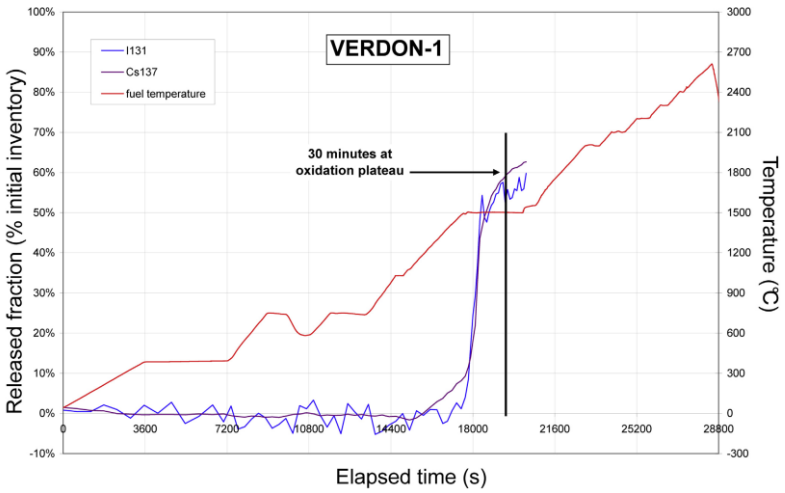

Figure 9: Volatile FPs release in test VERDON-1 [25]

Given the timeframe of the R2CA project and the associated manpower to this task, it was however not possible to study these tests in addition to the two VERCORS tests previously selected for the study. Nevertheless, it would be interesting to further apply the method developed for the analysis of the VERCORS tests to them.

3.4 Optimization of fuel grain size distribution

As already discussed, the volatile FP release in ELSA is governed by the intra-granular diffusion with no consideration to the effect of BU.
The main objective of this study is to investigate whether, in absence of a specific model, the effect of BU can be artificially caught by ELSA through the optimization of the input parameters dealing with the fuel grain size distribution.

For this purpose, two tests of VERCORS RT experiment series, focused on the release of low-volatility and transuranic species, have been selected:

- *VERCORS RT1*: UO_2 fuel, BU 47.3 GWd/t (4 cycles), H_2O+H_2 flow, maximum temperature 2300 °C;
- *VERCORS RT6*: UO_2 fuel, BU 71.8 GWd/t (6 cycles), H_2O+H_2, maximum temperature 2200 °C.

The two experiments, being characterized by similar thermal-hydraulic conditions but different BU, have been selected for the optimization study.

3.4.1 Reference calculation

The ASTEC input deck for the simulation of VERCORS test section has been provided to ENEA by IRSN and is used to run the ASTEC reference calculations with the fission products release by fuel managed by ELSA module. The temperature evolutions (Figure 10a and Figure 11a) are first checked against the experimental measurements. The simulations predict a temperature peak after the first ramp (around 12000 s for RT1 and 8000 s for RT6) due to the cladding Zr oxidation, which however could not be observed in the experimental data [7]. Hence, in order to achieve a temperature profile matching with the simulated phenomena, the Zr oxidation has been inhibited by substituting the Zr in the clad with ZrO_2. This results in simulations temperature profile in line with the expectations, as shown in Figure 10b and Figure 11b.

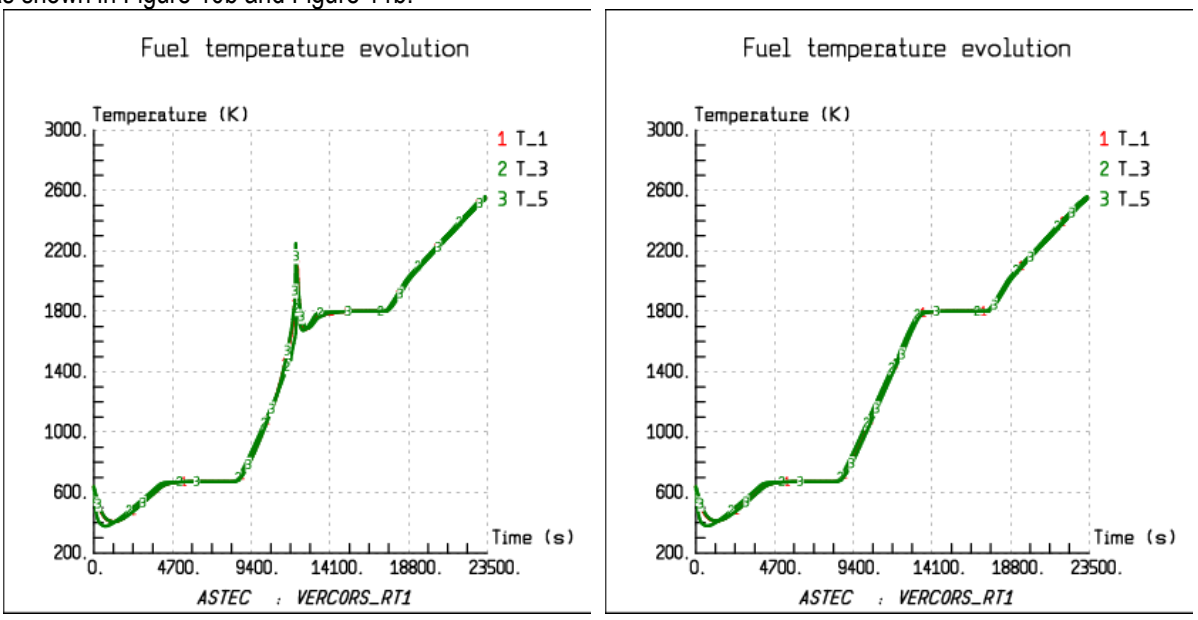

(a) (b)

Figure 10: Fuel temperature evolution for VERCORS RT1 experiment. Cladding material is (a) Zr or (b) ZrO_2.

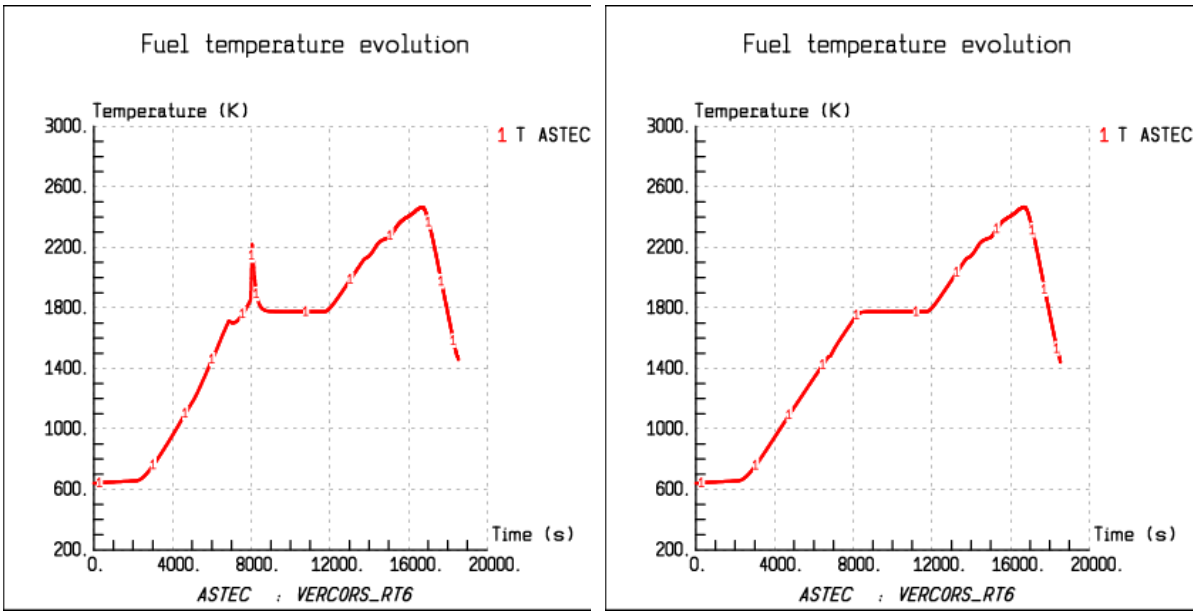

(a) (b)

Figure 11: Fuel temperature evolution for VERCORS RT6 experiment. Cladding material is (a) Zr or (b) ZrO_2.

Since the suppression of cladding oxidation, by assuming a ZrO_2 cladding, could affect the FP release computed by ELSA, a second option has been explored to agree with experimental data without skipping the oxidation of the cladding. For this purpose, the expected cladding temperatures are imposed, as boundary conditions, in both the inner and the outer surface of the Zr cladding whose oxidation can therefore take place without leading to the unwanted temperature peak. This second option allows a more realistic simulation of the experiments and, therefore, it was applied to the optimization study of the fuel grain size distribution.

3.4.2 ELSA parameter optimization

The fuel grain size is controlled in ASTEC/ELSA by different input parameters. They define the normal distribution that the grain sizes follow. In particular, the relevant keywords are:

- ***NCLG***: number of classes into which the normal distributions are subdivided;
- ***DMIN***: minimum diameter of the grain (truncation of the lower side of the Gaussian distribution);
- ***DMAX***: maximum diameter of the grain (truncation of the upper side of the Gaussian distribution);
- ***DGRA***: average diameter of the grain (mean value of the Gaussian distribution);
- ***SIGM***: variance of the Gaussian distribution describing the grain size.

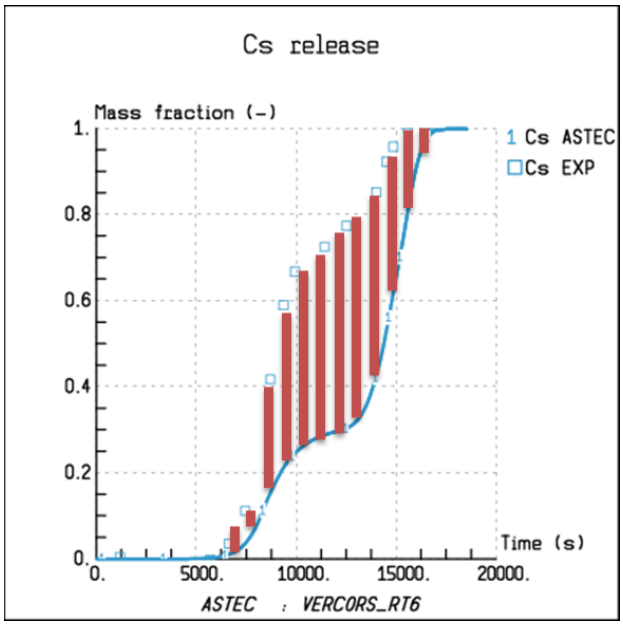

Figure 12: Experimental and simulated Cs release during VERCORS RT6 test, along with the integral to be optimized.

The objective of the optimization process is to establish the values of the key parameters above reported that lead to the best agreement between measured and computed Cs release. As an example, Figure 12 shows the Cs release experimental data (VERCORS RT6) and the preliminary reference calculation results (Zr in the clad substituted with ZrO_2). The optimization strategy aimed at closing the red gap between the experimental data and the calculation results, i.e. minimizing the integral between the experimental and simulated curves.
The optimization study was performed using RAVEN [30], [31] (Risk Analysis and Virtual ENvironment) tool coupled with ASTEC.

The settings prepared for ASTEC/RAVEN and the post-processing tools foresee the execution of 1000 calculations with variable main parameters of the ELSA model. In selecting the distributions and the ranges of the various parameters, the following assumptions were considered:

- NCLG: this parameter is randomly selected between 1 and 8, being 8 the default ELSA value;
- DMIN and DMAX: in order to study the effect of the grain diameter DGRA, DMIN and DMAX are limited to ± 1 µm with respect to DGRA;
- DGRA: this parameter is randomly selected. Considering the different burn up of the RT1 and RT6 experiments, different ranges of DGRA were tested. For the sake of brevity, only the final values are reported, going from 2 to 23 µm and from 2 to 7 µm for the experiments RT1 and RT6, respectively, considering the default value in ELSA of 12 µm;
- SIGM: this parameter is randomly selected between 1E-8 and 1E-6 µm, considering the default value in ELSA of 2E-6 µm.

The randomly selected parameters and their ranges in the final set of calculations are summarized in Table 7.

Table 7: ASTEC/RAVEN random input parameters

Experiment	NCLG	DGRA	SIGM
VERCORS RT1	From 1 to 8	From 2 to 23 µm	From 1E-8 to 1E-6
VERCORS RT6	From 1 to 8	From 2 to 7 µm	From 1E-8 to 1E-6

Post processing tools have been developed to collect the data of one set of ASTEC calculations and detect failed ones. With these tools it is possible to easily process the large amount of files generated and have a visual picture of the 3-dimensional phase space, as shown in Figure 13 for the RT1 and Figure 14 for RT6 calculations. For both experiments, red data points, corresponding to failed calculations, can be noticed. While it's easy to identify those calculations fail when is NCLG equal to 1, which is likely due to the structure of the model that considers at least 2 groups, further failures can be noticed at low values of SIGM. For RT1 calculations with NCLG different from 1, all the calculations with SIGM lower than 7E-8 fail, and lower than 8E-8 in the case of RT6. While a low value of SIGM may limit the possibility of the ELSA model to converge, the exact threshold value does not seem to depend on the DGRA value. Most of the simulation have been performed successfully and postprocessed.

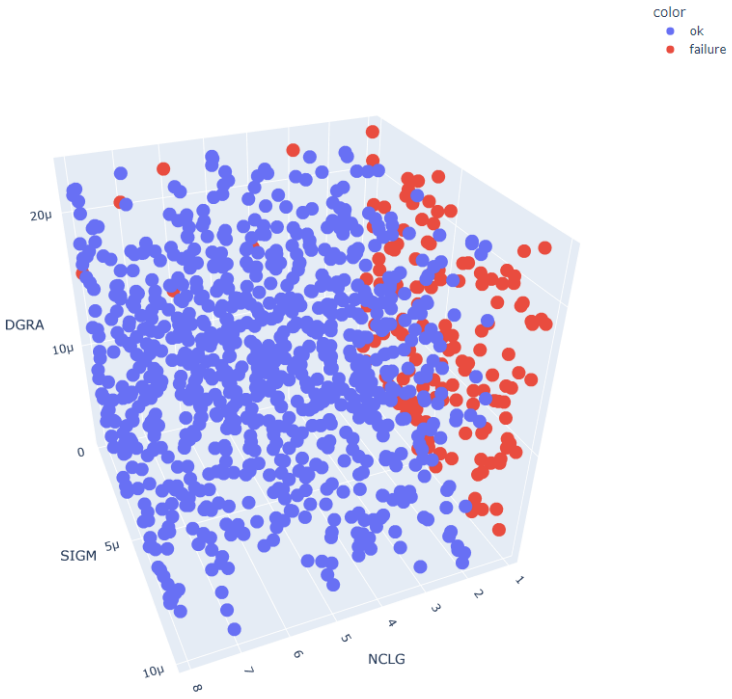

Figure 13: RT1 ASTEC/RAVEN calculations status

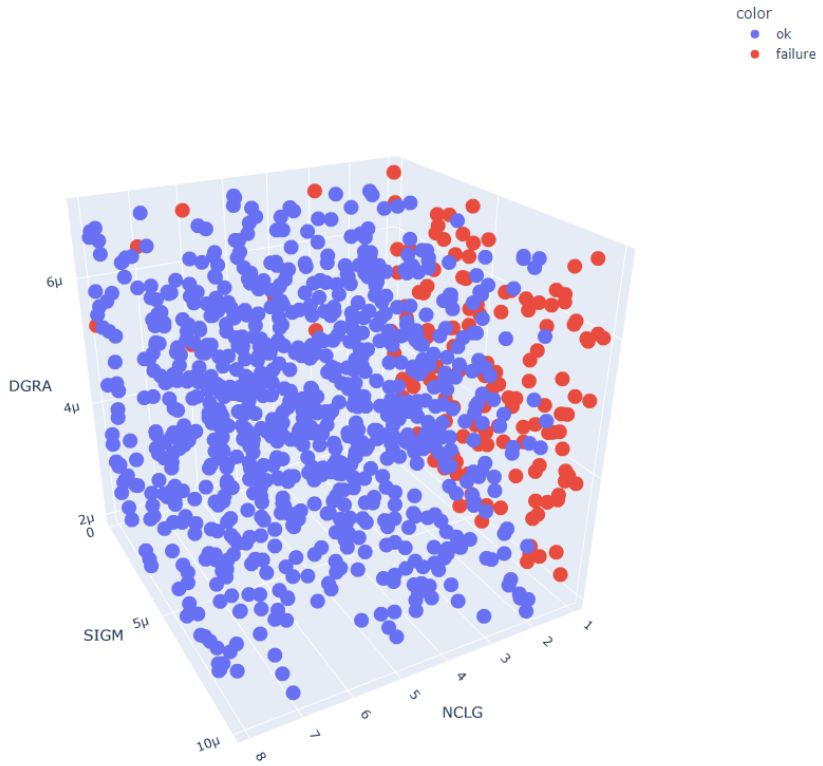

Figure 14: RT6 ASTEC/RAVEN calculations status

*Note: on the two previous graphs the SIGM values reported were arbitrarily enlarged for better readability)

In order to identify the set of ELSA parameter that provides the best results when compared to the outcome of the experiments, a criterium has been selected and implemented in the post processing tools: the best set is considered to be the one that minimizes the quadratic difference between the ASTEC/RAVEN results and experimental data, as formulated in equation (1).

$$\min\left[\sum_{x\in data_{EXP}}(x_{ASTEC}-x_{EXP})^2\right] \quad (1)$$

The results of this analysis are shown in Figure 15 and Figure 16 for experiment RT1 and RT6, respectively. Optimized values are reported in Table 8. In the case of the RT1 calculation, ASTEC tends to overestimate the Cs release during the transient and underestimate the final release value: simulations that better follow the release trend during the transient have lower than expected final values of the Cs release; vice versa, simulations where the final values are met show a greater discrepancy in the release during the transient. Since the selection criterium is meant to find the best fit for all data points, the optimized trend tries to interpolate all the available values.

For RT6 the experimental and simulated trends are quite similar, although according to ASTEC the release of Cs ends earlier as compared to the experimental data.
According to these results, the main parameter influencing the outcome of the calculation is DGRA, however the behaviour of the ELSA model in case of step changes in the FP gas release rate should be further investigated.

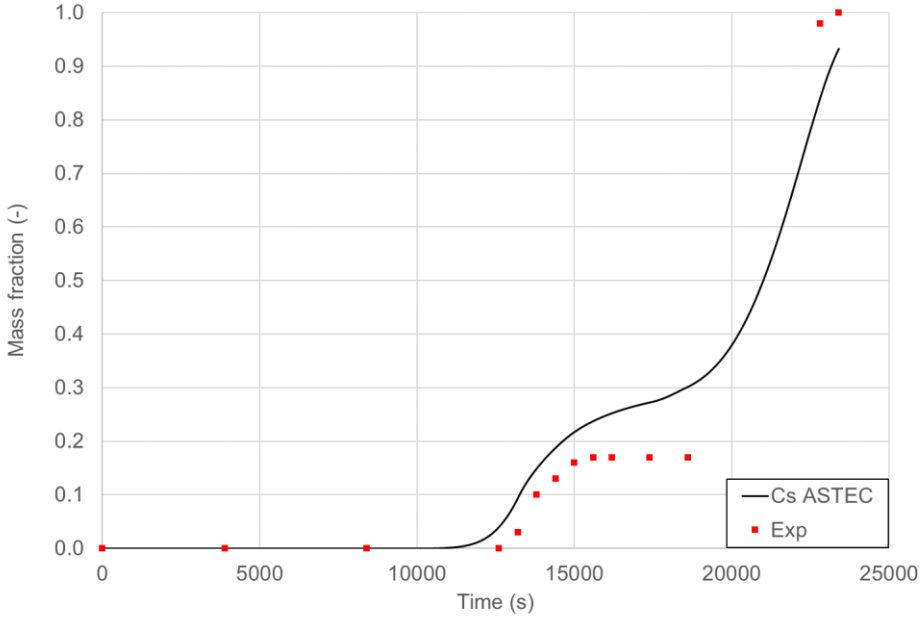

Figure 15: RT1 experiment, results with NCLG = 7, SIGM = 3.86E-6, DGRA = 13.83E-6

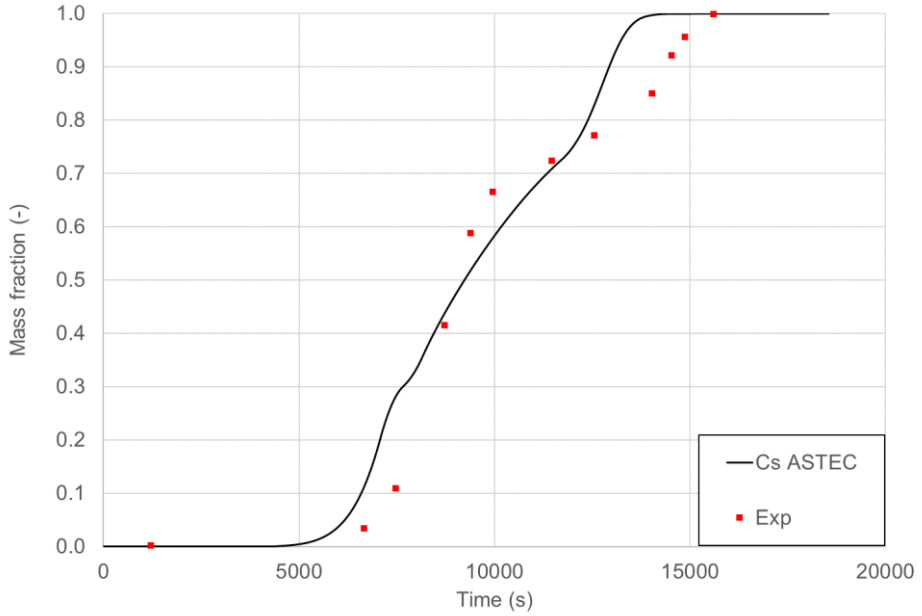

Figure 16: RT6 experiment, results with NCLG = 8, SIGM = 8.42E-6, DGRA = 2.157E-6

Table 8: Optimized ASTEC parameters for RT1 and RT6

Experiment	NCLG	DGRA	SIGM
VERCORS RT1	7	13.83E-6	3.86E-6
VERCORS RT6	8	2.157E-6	8.42E-6

3.5 Conclusions

In the framework of the R2CA project it is important to assess the validation status of the ELSA module of ASTEC in DEC-A and DBA conditions, i.e. whether ASTEC is validated for accidental scenarios with low fuel temperatures and high burn-up.

The employed formulas and models are reported in details in Brillant et al. [22] and in the theory manual of ELSA [21]: they include models for the oxidation, for the release of volatile, semi-volatile and low-volatility species. In addition, simpler models do exist for control materials, structural materials and for the release from the molten pool.

Based on the validation matrix reported by Cantrel et al. [3] (which includes VERCORS, MCE/HCE, EMAIC, HEVA, ORNL HI and VI, and Phebus FP experimental programs), the data having the conditions of interest for this project are very limited. Among these, only the VERCORS experiment includes very high-BU fuel tests though they were run till high temperatures. However, some data from these tests are available at lower temperatures (plateaus at 800°C and 1000°C). Their burn-up, except for some tests were not very high. Phebus FP has low temperature data too but, also in this case, the BU is quite low.

It is noteworthy that, according to Brillant et al. [4], the release models in ASTEC/ELSA do not consider the BU effect on the FP releases, causing some discrepancies in high BU validation cases; for this reason the authors suggest that high BU UO_2 models should be developed in the future.

A complete validation of ELSA for DEC-A and DBA, hence, would require a modelling effort taking into account the BU influence and further benchmark experiments. In the framework of the R2CA project an experimental database [25] has been constructed, and some test cases could prove important in such task. The recent VERDON tests, in particular, are focused on FP release from very high-BU fuels and include data at low temperature. However, this study focussed on VERCORS RT tests. A study with ASTEC/ELSA has been performed to simulate the Cs release in VERCORS RT1 and RT6 experiments, characterized by similar thermal-hydraulic conditions and different BU. The main objective was to analyse whether, in absence of a specific model, the effect of BU can be artificially caught by ELSA through the optimization of the input parameters dealing with the fuel grain size distribution.

The Preliminary simulations of RT1 and RT6 reference cases showed temperature peaks, due to the Zr cladding oxidation, which have not been observed during the experimental measurements; therefore, the reference cases have been refined in order to achieve a reasonable agreement with the experimental data.

The optimization study has been performed with the RAVEN tool coupled with ASTEC. The outcome of the calculations is in reasonable agreement with the experimental results, especially for the VERCORS RT6 test using high burn-up fuel. This study however would require to be further checked on the other identified tests of interest (such as the VERDON tests).

3.6 References

[1] H. J. Allelein *et al.*, "European validation of the integral code ASTEC (EVITA)," in *Nuclear Engineering and Design*, Apr. 2003, vol. 221, no. 1-3 SPEC., pp. 95–118, doi: 10.1016/S0029-5493(02)00346-1.
[2] H. J. Allelein, K. Neu, and J. P. V. Dorsselaere, "European Validation of the Integral Code ASTEC (EVITA): First experience in validation and plant sequence calculations," in *Nuclear Engineering and Design*, Feb. 2005, vol. 235, no. 2–4, pp. 285–308, doi: 10.1016/j.nucengdes.2004.08.051.
[3] L. Cantrel, F. Cousin, L. Bosland, K. Chevalier-Jabet, and C. Marchetto, "ASTEC V2 severe accident integral code: Fission product modelling and validation," *Nucl. Eng. Des.*, vol. 272, pp. 195–206, Jun. 2014, doi: 10.1016/j.nucengdes.2014.01.011.
[4] G. Brillant, C. Marchetto, and W. Plumecocq, "Fission product release from nuclear fuel II. Validation of ASTEC/ELSA on analytical and large-scale experiments," *Ann. Nucl. Energy*, vol. 61, pp. 96–101, Nov. 2013, doi: 10.1016/j.anucene.2013.03.045.
[5] Y. Pontillon, G. Ducros, and P. P. Malgouyres, "Behaviour of fission products under severe PWR accident conditions VERCORS experimental programme—Part 1: General description of the programme," *Nucl. Eng. Des.*, vol. 240, no. 7, pp. 1843–1852, Jul. 2010, doi: 10.1016/j.nucengdes.2009.06.028.
[6] G. Ducros, P. P. Malgouyres, M. Kissane, D. Boulaud, and M. Durin, "Fission product release under severe accidental conditions: General presentation of the program and synthesis of VERCORS 1-6 results," *Nucl. Eng. Des.*, vol. 208, no. 2, pp. 191–203, Sep. 2001, doi: 10.1016/S0029-5493(01)00376-4.
[7] G. Ducros, Y. Pontillon, and P. P. Malgouyres, "Synthesis of the VERCORS experimental programme: Separate-effect experiments on Fission Product release, in support of the PHEBUS-FP programme," *Ann. Nucl. Energy*, vol. 61, pp. 75–87, Nov. 2013, doi: 10.1016/j.anucene.2013.02.033.
[8] D. S. Cox *et al.*, "Model for the release of low-volatility fission products in oxidizing conditions," in *Annual International Conference - Canadian Nuclear Association*, 1991, pp. 280–289.
[9] R. D. Barrand, R. S. Dickson, Z. Liu, and D. D. Semeniuk, "Release of fission products from CANDU fuel in air, steam and argon atmospheres at 1500-1900 deg C: the HCE3 experiment," in *6. International conference on CANDU fuel*, 1999, pp. 271–280.
[10] L. W. Dickson and R. S. Dickson, "Fission-product releases from CANDU fuel at 1650°C: the HCE4 experiment," in *7. International CANDU fuel conference proceedings*, 2001, pp. 3B.21-3B.30.
[11] B. Rabu *et al.*, "Silver- indium- cadmium- tin aerosol releases and control rod behaviour in PWR accidental conditions," *J. Aerosol Sci.*, vol. 30, no. Suppl. 1, 1999, doi: 10.1016/S0021-8502(99)80066-4.
[12] G. Le Marois, "Report CEA DMG n° 64/87," 1987.
[13] G. Le Marois, "Report CEA DMG n° 58/88," 1988.
[14] G. Le Marois, "Report CEA DMG n°34/89," 1989.
[15] J.-P. Leveque, B. Andre, G. Ducros, G. Le Marois, and G. Lhiaubet, "The HEVA Experimental Program," *Nucl. Technol.*, vol. 108, no. 1, pp. 33–44, Oct. 1994, doi: 10.13182/nt94-a35041.
[16] P. E. Domagala, J. Rest, and S. A. Zawadzki, "Assessment of improved fission-product transport models in VICTORIA against ornl HI and VI tests," in *AIChE Symposium Series*, 1991, vol. 87, no. 283, pp. 182–189.
[17] H. Scheurer and B. Clement, "PHEBUS Data Book - FPT1," Cadarache, France, IS/92/49, 1997.
[18] D. Jacquemain, S. Bourdon, A. de Braemaeker, and M. Barrachin, "PHEBUS FTP1 Final Report," Cadarache, France, SEA/00/IP//oo/479, 2000.
[19] M. Schwarz, G. Hache, and P. von der Hardt, "PHEBUS FP: A severe accident research programme for current and advanced light water reactors," *Nucl. Eng. Des.*, vol. 187, no. 1, pp. 47–69, Jan. 1999, doi: 10.1016/S0029-5493(98)00257-X.

[20] B. Clément and R. Zeyen, "The objectives of the Phébus FP experimental programme and main findings," *Ann. Nucl. Energy*, vol. 61, pp. 4–10, Nov. 2013, doi: 10.1016/j.anucene.2013.03.037.
[21] K. Chevalier-Jabet, "ASTEC V2.2 ELSA module: fission products and structural elements release from intact and degraded cores - Theoretical manual," France, IRSN/PSN-RES/SAG/2015-00110, 2015.
[22] G. Brillant, C. Marchetto, and W. Plumecocq, "Fission product release from nuclear fuel I. Physical modelling in the ASTEC code," *Ann. Nucl. Energy*, vol. 61, pp. 88–95, Nov. 2013, doi: 10.1016/j.anucene.2013.03.022.
[23] D. Jacquemain, *Nuclear power reactor core melt accidents*, EDP scienc. France, 2015.
[24] B. Clément *et al.*, "Thematic network for a Phebus FPT1 international standard problem (THENPHEBISP)," *Nucl. Eng. Des.*, vol. 235, no. 2–4, pp. 347–357, 2005, doi: 10.1016/j.nucengdes.2004.08.057.
[25] Z. Hózer *et al.*, "D2.3. Review of experimental database," 2020.
[26] Y. Pontillon *et al.*, "Experimental and theoretical investigation of fission gas release from UO2 up to 70 GWd/t under simulated LOCA type conditions: The GASPARD program," 2004, Accessed: Jul. 04, 2021. [Online]. Available: https://www.researchgate.net/publication/286956984_Experimental_and_theoretical_investigation_of_fission_gas_release_from_UO2_up_to_70_GWdt_under_simulated_LOCA_type_conditions_The_GASPARD_program.
[27] A. Gallais-During *et al.*, "Overview of the VERDON-ISTP Program and main insights from the VERDON-2 air ingress test," *Ann. Nucl. Energy*, vol. 101, pp. 109–117, Mar. 2017, doi: 10.1016/j.anucene.2016.09.045.
[28] Y. Pontillon *et al.*, "Fission products and nuclear fuel behaviour under severe accident conditions part 1: Main lessons learnt from the first VERDON test," *J. Nucl. Mater.*, vol. 495, pp. 363–384, Nov. 2017, doi: 10.1016/j.jnucmat.2017.08.021.
[29] C. Le Gall *et al.*, "Fission product speciation in the VERDON-3 and VERDON-4 MOX fuels samples," *J. Nucl. Mater.*, vol. 530, p. 151948, Mar. 2020, doi: 10.1016/j.jnucmat.2019.151948.
[30] C. Alfonsi *et al.*, "RAVEN Theory Manual", INL/EXT-16-38178, Idaho National Laboratory (INL), (2020).
[31] C. Alfonsi *et al.*, "RAVEN User Guide", INL/EXT-18-44465, Idaho National Laboratory (INL), (2020).

4 HZDR

HZDR work was dedicated to a detailed analysis of the fission product release from fuel for DBA-LOCA conditions. The analysis was performed with the code ATHLET-CD [1, 2] (which is part of the AC^2 code package).

4.1 Review and assessment of fission product release rate models implemented in ATHLET-CD

The ATHLET-CD code models the release of fission products (FPs) from a reactor core to the reactor coolant system (RCS) with the module FIPREM (fission product and aerosol release). A general description of the model is given in [1], [2]. The current assessment is focused on the phenomena relevant for fission product release during a DBA LOCA of a pressurized water reactor.

All assessments shown in this report were performed for a generic German PWR of type Konvoi (Siemens-KWU design with 1300 MW_{el}), with an ATHLET-CD input dataset developed and applied in task 2.3 of the current project (first round of reactor calculations). That model represents the reactor core by six concentric core sections. Each

section is represented by a thermal-hydraulic channel (PV-COR1 for the inner-most section to PV-COR6 for the outer-most section in Figure 17). The 57900 fuel rods of the core are represented by one representative fuel rod per core section (plus additional control rods, except for section 6). It is assumed, that core section 1 represents the rods with maximum power (10% of all rods). The power profiles applied to the 6 core sections are shown by Figure 18 (with identical profile for sections 2-5). The peak power for section 1 is 465 W/cm, which corresponds to a local peak power factor P' ≈ 2.5.

For the investigated DBA LOCA scenario, only the representative fuel rod in core section 1 burst, which means that the release of fission products is limited to this core section. It has to be mentioned, that the model is not appropriate to estimate the correct number of burst fuel rods in contrast to the detailed core model developed in Task 3.2. Due to the very long calculation times necessary for the new detailed model (1-3 months per run), it was not possible to apply the new model for the analyses in Task 3.1. However, for a general demonstration and assessment of the release models, the simple model is useful and may even facilitate the analyses (faster run times, lower amount of generated data, simplified post processing).

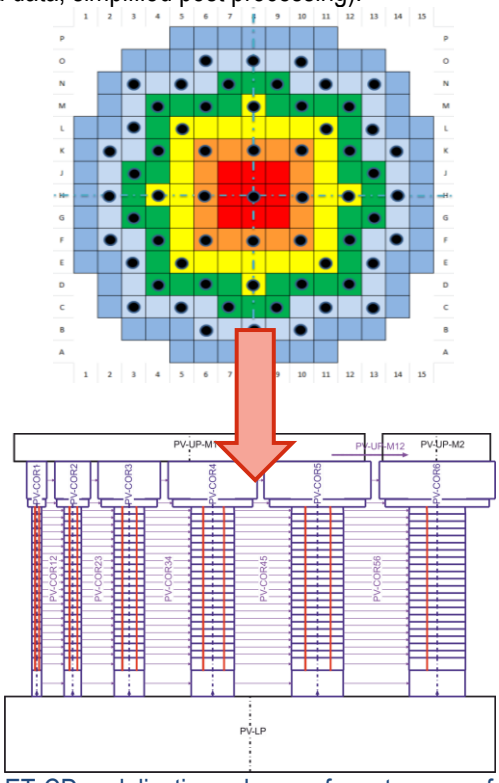

Figure 17 ATHLET-CD nodalization scheme of reactor core of generic Konvoi.

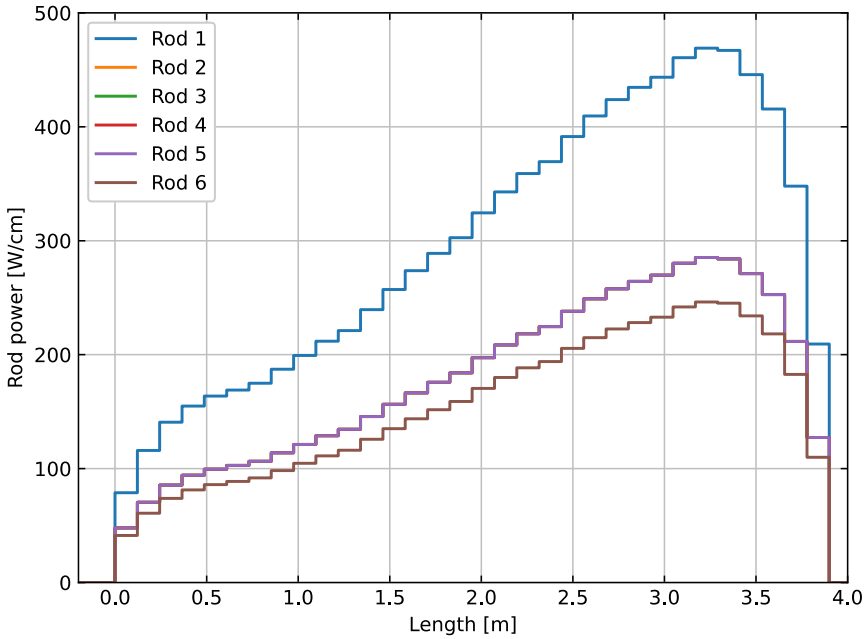

Figure 18 Applied power profiles for the 6 core sections.

In general, for DBA and beyond design basis accidents (severe accidents) there are several release phases which have to be taken into account [3]: the gap release (or burst release) phase, the early in-vessel release phase, ex-vessel release phase and late-in-vessel release phase. For the accidents investigated in the framework of the R2CA project (DBA and DEC-A LOCA accidents), only the gap release (spontaneous release after cladding burst) and (in case of partial heat-up of the core for DEC-A conditions) the release during the early in-vessel phase (which is continuous release of fission products due to elevated fuel rod temperature) are important.

During the steady state operation of the reactor, fission gases (Xe, Kr) and volatile fission products (I, Cs) are accumulated in the fuel rod gap and fuel rod plenum volume. In case of burst of fuel rods during the LOCA accident[1] these fission products are released from the fuel rod to the primary circuit and from there are transported to the containment. The accumulation process during normal operation of the reactor is not modelled by ATHLET-CD. Instead, the process of release is described by a burst release model, with fractions of FPs accumulated in the gap which are taken from experimental data. There are different models implemented in ATHLET-CD, which will be discussed later. However, the amount of FPs release during this phase is in the order of a few per cent up to 10%. E.g. NUREG-1465 states a release of 5% for the noble gases, halogens and alkali metals [3]. According to the German guidelines for pressurized water reactors, the following values have to be assumed as spontaneous releases during the DBA LB-LOCA for evaluation of the radiological consequences (in relation to the inventory of a single fuel rod) [4]:

- 10 % of noble gases

[1] For the German Siemens-KWU design of PWR with ECCS injection combined from cold leg and hot leg, the typical fraction of failed rods during LOCA is in the order of 10% or less. However, as shown in Task 3.2 of the current project, the fraction of failed rods might exceed the 10% criterion if conservative initial and boundary conditions are applied.

- 3 % of halogens
- 2 % of volatile fission products
- 0.1 % of other solid fission products

For the later release phases, the ATHLET-CD code predicts the continuous fission product release from the fuel rods based on the integral release rate approach [2] in the form:

$$\mathrm{X} = A \cdot R \cdot e^{(-Q/T)} \quad (2)$$

with the release rate X (1/s), a scaling factor A (-), the release rate coefficient R (1/s). Q (unit K) is the activation energy related to the general gas constant and T (K) is the temperature. Typically, the release rate coefficient for fission gas Xe is given as a basis, e.g. 200/s according to data from ORNL [5] and the scaling factors are defined in relation to the Xenon release.
In total 27 element groups are taken into account by ATHLET-CD (however, for some of the elements, the below listed models do not provide any release rate coefficients):

- Fission products (15 groups): Xe, Kr, I, Cs, Rb, Br, Te, Se, Ag, Ba, Sr, Ru group (including Pm, Sm, Eu, Gd, Nb, Nd, Pr, Ce, La, Y), Mo group (including Pd, Tc, Rh), Sb, Zr
- Fuel and actinides (3 groups): U, Pu, Np group (including Am, Cm, Bk, Cf, Es)
- 9 groups to model the release from structural materials (non-radioactive)

Three different sets of rate equations are available in ATHLET-CD, which differ for selected elements as follows:

1. Rates according to ORNL data and CORSOR rates for release of silver, indium and cadmium
2. Rates according to ORNL data [5] and as a function of partial pressures for silver, indium, and cadmium
3. Rates according to ORNL data [5] and as a function of partial pressures for several materials

In the past, more options were available, as described in [6]. However, the application of those alternative models is no longer recommended by the ATHLET-CD developer [7]. That is why they are no longer accessible by the standard user input (despite the equations are still implemented in the code).

For the first set of release rate equations, the scaling factors for different elements are given by

Table 9, with volatile FPs marked with yellow, semi-volatiles with green and non-volatiles with blue. As could be seen from the table, all factors are less or equal to 1.0. Several model parameters (specified by ATHLET-CD input) are available to modify the release rate coefficient for different elements. For Xe, Kr, Cs and I, the release rate coefficient is modelled burn-up dependent. For low burn-up, the rate coefficients are only 50% of those valid for high burn-up (see

Table 9). However, the current version of ATHLET-CD does not take the local burn-up distribution into account for calculation of these factors. Instead, it is specified by the input data file (parameter ILOBUP) for the entire fuel of the core. Consequently, the high burn-up release model coefficients should be selected to obtain conservative result.

For Ba, Sr, Eu, Mo, Ce, U, Ru, Mn and Fe, the release rate coefficients are modelled dependent on the fuel oxidation. Again, that value is not calculated by the code, but has to be specified by the user and only a single value can be given for the entire fuel of the core. According to the ORNL data, the values for reduced fuel and fully

oxidized fuel can differ several orders of magnitude and oxidized conditions show for some elements higher, for other elements lower values. Therefore, the user should assess both conditions separately.

For Te, Sb and Sn, the release rates are modelled dependent on the cladding oxidation. The local value of cladding oxidation (cladding oxidation layer thickness) is calculated by the code. If that value exceeds 90% of the total cladding thickness, the release rate coefficients for fully oxidized cladding are applied (scaling factor between 0.4 and 0.8), otherwise the lower values for not fully oxidized cladding are applied (scaling factor of 0.02).

Table 9 Scaling factors for release of different elements

Rod condition	Elemental Scaling factors A_x								
	Xe	Kr	Cs	I					
High burn-up	1.0	1.0	1.0	0.8					
Low burn-up	0.5	0.5	0.5	0.4					
	Te	Sb	Sn						
Cladding fully oxidized	0.8	0.5	0.4						
Cladding not fully oxidized	0.2	0.2	0.2						
	Ba	Sr	Eu	Mo	Ce	U	Ru	Mn	Fe
Fuel oxidation UO_{2+x} $x \leq 0$	0.2	0.1	0.1	0.01	$2 \cdot 10^{-3}$	$6 \cdot 10^{-5}$	$4 \cdot 10^{-5}$	0.0	0.0
Fuel oxidation UO_{2+x} $x > 0$	0.02	0.01	$6 \cdot 10^{-5}$	0.25	$2 \cdot 10^{-4}$	$6 \cdot 10^{-4}$	0.02	0.1	0.02
	Zr	Pu							
No change	$2 \cdot 10^{-4}$	$2 \cdot 10^{-5}$							

For the DBA LB-LOCA case, cladding temperature does not exceed 1200°C (as defined e.g. by the German guidelines for pressurized water reactors, [4]), and the peak fuel temperature is reduced within a few seconds from its initial steady state value to 1200°C or lower[2]. The duration until complete quenching of the core is usually in the order of 100 s. Consequently, the release rates from the fuel under these conditions are very low, as indicated by the following example:

For Xenon, A = 1.00, R = 200/s, upper boundaries for the release rates can be estimated as follows:

$$X_{\mathrm{Xe,DBA,max,before\ 5\ s}} = 1.0 \cdot \frac{200}{\mathrm{s}} \cdot e^{(-27680\mathrm{K}/1800\mathrm{K})} \approx 4.2 \cdot 10^{-5} \frac{1}{\mathrm{s}} \quad (3)$$

$$X_{\mathrm{Xe,DBA,max,after\ 5\ s}} = 1.0 \cdot \frac{200}{\mathrm{s}} \cdot e^{(-27680\mathrm{K}/1473\mathrm{K})} \approx 1.38 \cdot 10^{-6} \frac{1}{\mathrm{s}} \quad (4)$$

The results obtained by equations (3) and (4) only hold for a small part of the core (with peak temperatures) and are lower elsewhere. Assuming (conservatively) that the whole core has reached the maximum allowed

[2] Steady state peak fuel temperature at nominal power and realistic power profile with maximum linear heat rate of 360 W/cm is typically below 1600 K, in case of the conservative assumption of a top-peaked power profile with maximum linear heat rate of 465 W/cm less than 1800 K.

temperature of 1200 °C during the entire time span of 100 s till complete quenching, the Xe fraction released from the fuel would be less than 0.014% (equal or even lower values apply according to the ORNL data for the other FP species). Compared to the burst release fractions quantified above, the continuous release described by the rate equation approach eq. (2) is negligible. Therefore, the assessment of fission product release models in Task 3.1 is focused on the burst release model.

The release of the fission products (accumulated in the gap) is initiated in ATHLET-CD by two different criteria, either by reaching a user-defined cladding temperature or by reaching the burst of cladding which is simulated by the mechanical fuel rod model. The application of the mechanical fuel rod model is recommended as it provides a more accurate modelling of the burst initiation. The mechanical model provides several burst criteria and has been assessed within in Task 3.2 to estimate the number of burst fuel rods within a detailed model of the PWR core.
]
If the cladding failure criterion is reached, the fission products accumulated in the fuel rod gap are first released. This gap release is distributed over a time interval of 300 s according to a beta-function (with distribution parameters PB=6.0, QB=6.0) and superimposed on the continuous release (which is actually negligible for the DBA LOCA case). Figure 19 shows the integral of the gap release rate (with integral value normalized to 1.0 at the end of the 300 s period).

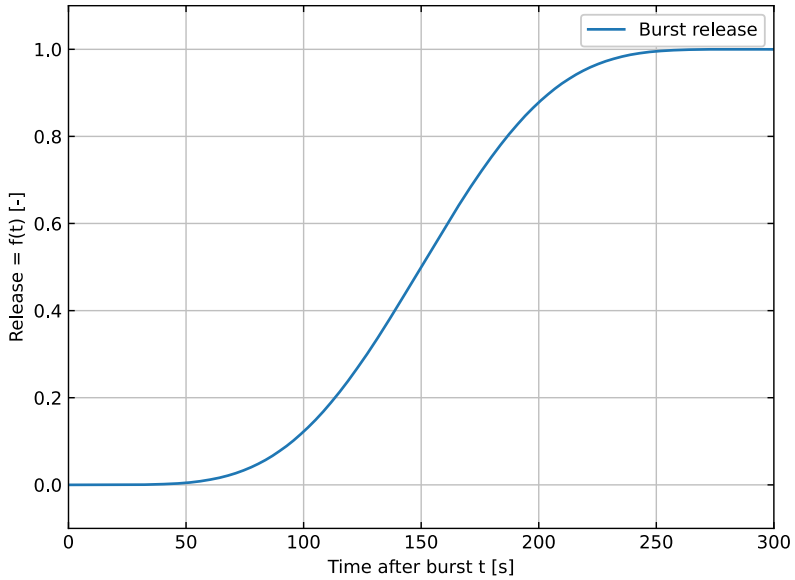

Figure 19 Integral of the burst release rate (normalized to 1.0) as modelled in ATHLET-CD

Three different burst release models are implemented in the ATHLET-CD code, which define the elements taken into account for burst release and their burst release fractions [8]:

1. Model based on CORSOR [9],
2. Model based on the WASH-1400 report (WASH-fraction model) [10], [11],
3. Model based on French measurements [8].

The CORSOR burst release model assumes the following release rates:

- 3% for Kr and Xe,
- 1.7% for I,
- 5% for Cs,
- 10^{-4} for Te and Sb,
- 10^{-6} for Ba and Sr.

The release rates are applied to the whole reactor core (i.e. in the model it is effective to those representative rods, that reach the burst criterion).

The WASH-fraction model calculates the releases as follows: The release factor depends on the power factor P', which is evaluated locally for each control volume of the reactor core. If $P' < 1.35$, no release is calculated. For $P' \geq 1.35$, a reduction factor F is calculated based on P':

$$\mathrm{F} = 0.13(P' - 1.35) \tag{5}$$

With F the release fractions RF are calculated [8]:

- Xenon: $\mathrm{RF_{Xe}} = 0.05 \cdot F$
- Krypton: $\mathrm{RF_{Kr}} = 0.1 \cdot F$
- Iodine: $\mathrm{RF_{I}} = 0.7 \cdot F$
- Cesium: $\mathrm{RF_{Cs}} = 0.15 \cdot F$

For all further FP species, no release from the gap is assumed. In the current analysis, the peak power factor for core section 1 is 2.5 (see above). Therefore, the maximum release fractions (from the control volume with $P' = 2.5$) are according to the WASH-fraction release model:

- Xenon: $\mathrm{RF_{Xe,max}} \approx 0.75\%$
- Krypton: $\mathrm{RF_{Kr,max}} \approx 1.5\%$
- Iodine: $\mathrm{RF_{I,max}} \approx 10.5\%$
- Cesium: $\mathrm{RF_{Cs,max}} \approx 2.24\%$

However, during the assessment of the ATHLET-CD results for the WASH-fraction release model it was observed, that the code does not calculate any release of FPs. After assessment of the ATHLET-CD source code a wrong calculation of the power factors was identified as possible reason and the issue was reported to the ATHLET-CD code developers and is currently still under investigation.

For the third model based on French measurements, no original reference could be identified, except the GRS report from 1997 with description of model scope of ATHLET-CD [8]. The model distinguishes between a high-power case (with maximum linear heat generation rate $\dot{q}'_{\mathrm{max}} \geq 250\ \mathrm{W/cm}$, evaluated at the moment of burst, separately for each representative fuel rod) and a low power case (< 250 W/cm, i.e. reactor is shut down due to SCRAM). For the low power case, a further distinction is made according to the system pressure:

- High pressure case (p ≥ 2.0 MPa): release fractions of Xe and Kr are 1%, and release fractions of I and Cs are 0.3%
- Low pressure case (p < 2.0 MPa): release fractions of Xe and Kr are 3%, release fraction of I is 1.7% and release fraction of Cs is 5%.

For the high-power case, the following values are applied (no distinction according to the system pressure):

- Xe and Kr: : $\mathrm{RF}_{\mathrm{Xe/Kr}} = 2.07 \cdot 10^{-5} \cdot \left(\frac{\dot{q}'_{\max}}{\mathrm{W/cm}} - 100 \right) - 0.3$
- 1.7% for I and 5% for Cs.

No burst release fraction is defined for any other FP species. For the DBA LOCA of the generic Konvoi investigated in the project, only the low power case with low system pressure is relevant. For those conditions the release fractions defined according to the French measurements are identical to the CORSOR model (for Xe, Kr, I, Cs).[3] The FP releases are calculated for each of the representative rods that reached the burst criterion. As for the simplified Konvoi model, burst occurs only in core section 1 (which contains 10% of all rods), the fraction of released FPs to the total inventory of the core is basically 0.1 times the above defined release fractions, which is verified in the following.

The CORSOR model as implemented in ATHLET-CD was taken from the CORSOR code [9]. Therefore, the origin of the release rates modeled in the CORSOR code was of interest. From the CORSOR manual it was found that the WASH-1400 report was also the basis of the implemented burst release rates. In contrast to the above mentioned WASH-fraction model (which is based on a contribution described in appendix VIII of [10]), the CORSOR values are based on a table given in appendix VII of [10], summarizing several contributions to that study (and reproduced by Table 10). Table 10 defines values for the gap release fraction (accumulation of FPs from the fuel in the gap) and further a gap escape fraction (that fraction of the accumulated FPs that escape from the gap after the burst of cladding). The product of both values defines the total gap release value. The values applied in CORSOR are identical to those given in last table column. However, burst release rates for Br, Rb, and Se were not implemented into CORSOR (nor were they implemented in ATHLET-CD).

Important to mention are the uncertainty factors given in Table 10, which are quite significant. For the noble gases the uncertainty factor is 4 (either lower or higher values possible). For other FP species the uncertainty factors for gap release and that for gas escape have to be multiplied to obtain the total uncertainty (which can be up to a factor of 12 for Iodine and up to 400 for the semi-volatile FPs Sr, Ba, Te and Sb).

[3] In addition, general application of the model is not recommended at this time, as code problems similar to the WASH-fraction model have been identified (incorrect calculation of $\dot{q}'_{\max}$).

Table 10 Gap release values as specified by [11]

TABLE VII 1-2 GAP RELEASE COMPONENT VALUES

Fission Product Species	Gap Release Fraction	Gap Escape Fraction	Total Gap Release Value
Xe, Kr	0.03 (a)	1	0.03
I-Br	0.05 (a)	1/3 (c)	0.017
Cs, Rb	0.15 (b)	1/3 (c)	0.05
Sr, Ba	0.01 (a)	10^{-4} (d)	0.000001
Te, Se, Sb	0.10 (a)	10^{-3} (d)	0.0001
Others	-	-	Negligible (e)

(a) Values can be higher or lower by a factor of 4

(b) Value can be higher by a factor of 2 or lower by a factor of 4

(c) Values can be higher or lower by a factor of 3

(d) Values can be higher or lower by a factor of 100

(e) While no numerical value was developed for these various species, the number should not exceed that used for strontium-barium.

To study the influence of these uncertainties in the DBA LOCA case, the ATHLET-CD code was extended such that the user can define uncertainty factors in the ATHLET-CD input dataset. The LOCA has been calculated three times, with results shown by Figure 20 and Figure 21: first calculation was performed with best estimate (B.E.) release rates (blue curves), with maximum and with minimal release rate values (red and green curves, respectively). The simulations were performed with a developer version of the code (3.3). For verification purpose, results obtained with the official release 3.2 patch 1 were added (grey curves, identical to the new calculation with B.E. release rates). The figures show the S-shaped curves for the FP burst releases, starting at 35 s (cladding burst) and reaching a plateau 300 s later (as defined by the underlying beta function).

Table 11 ATHLET-CD results for FP releases (simulation with B.E. release rate coefficients, according to the CORSOR release fraction model)

FP species	Total initial inventory [kg]	Released mass [kg]	Fraction of released FPs to total initial inventory
Xe	682.3	2.017	0.3 %
Kr	43.98	0.1299	0.3 %
I	29.24	0.0492	0.17 %
Cs	343.6	1.676	0.5 %

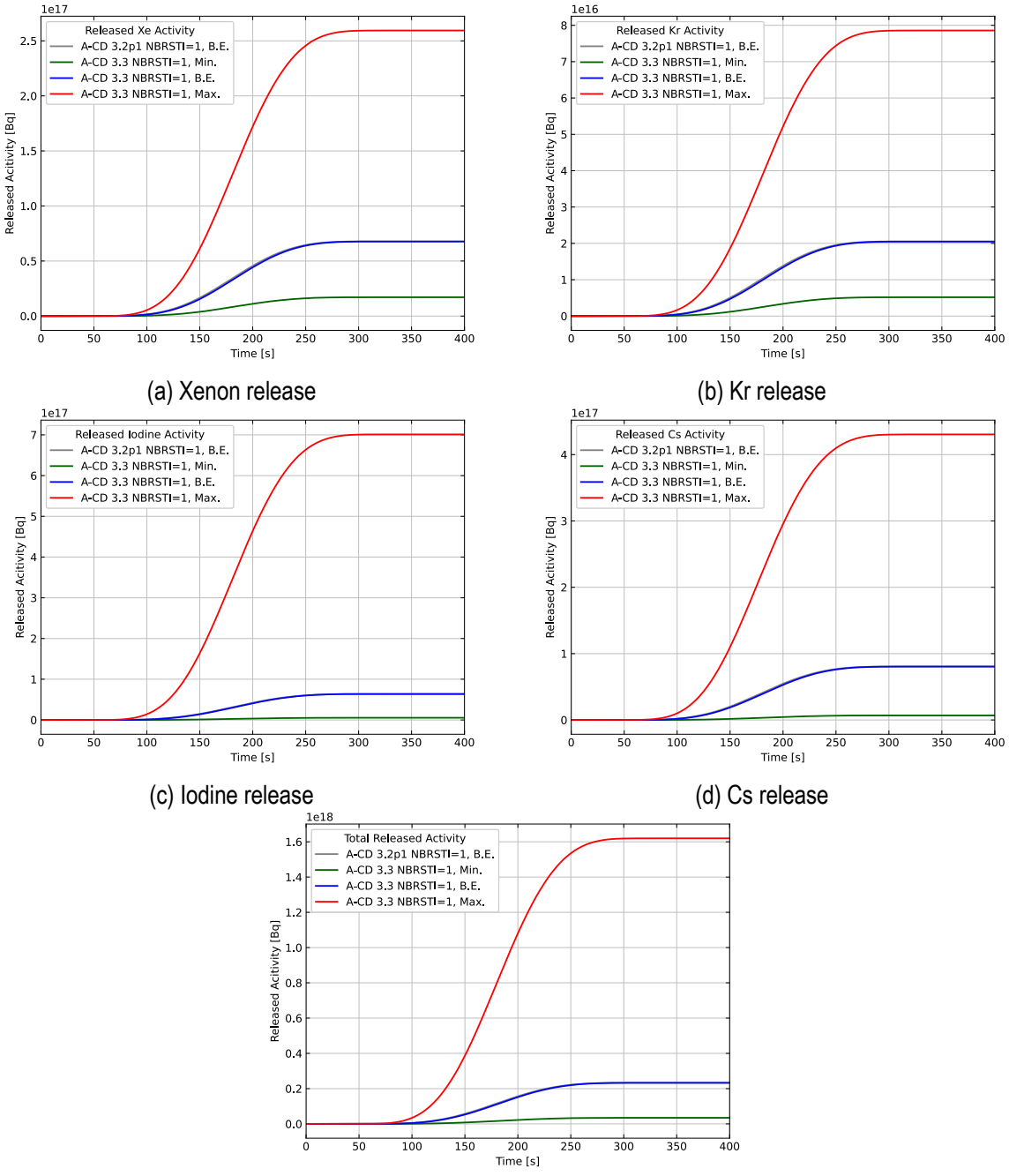

(a) Xenon release

(b) Kr release

(c) Iodine release

(d) Cs release

(e) Total release

Figure 20 Activity released from the fuel to the RCS for DBA LOCA (with application of uncertainty factors obtained from [10])

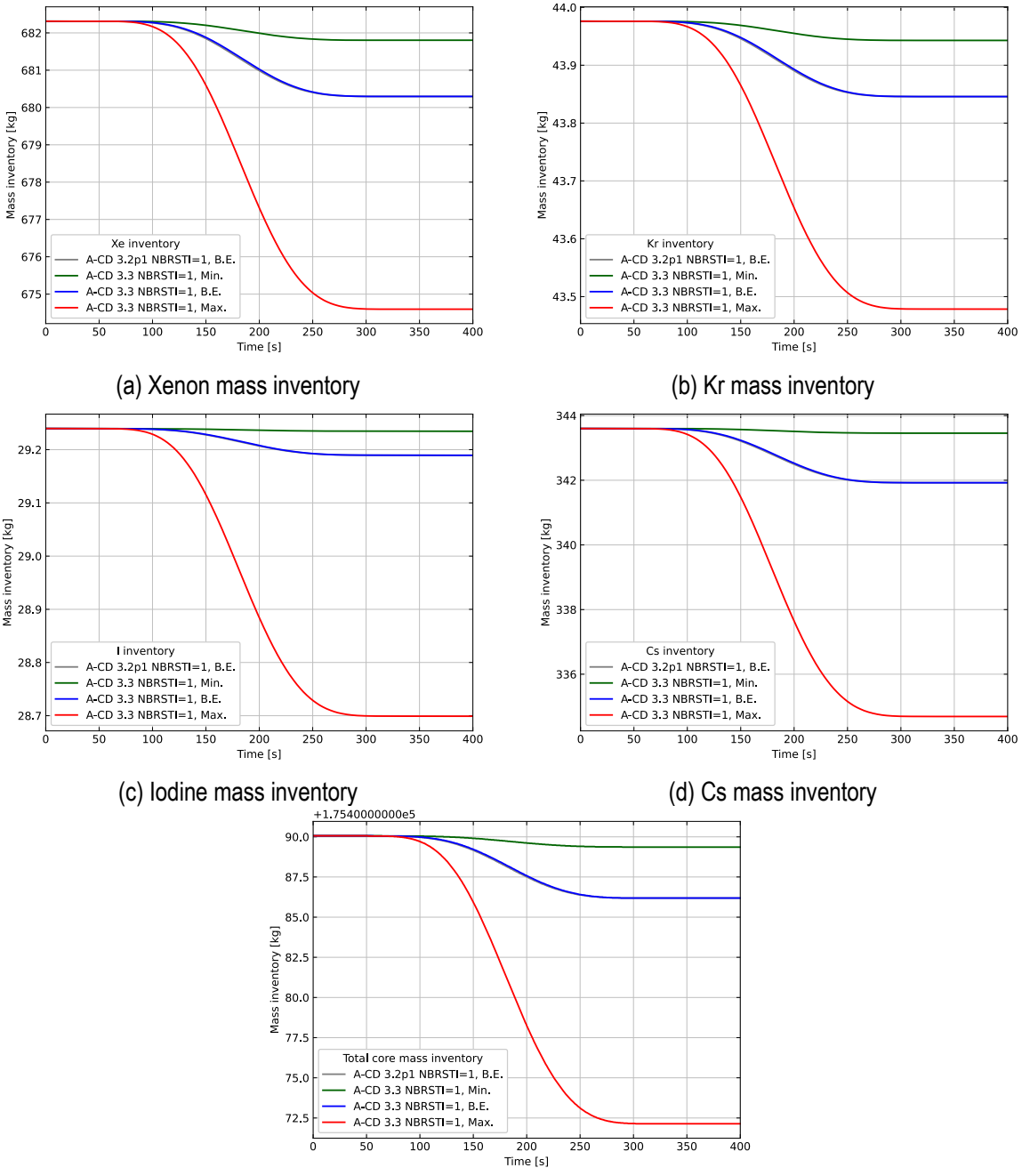

(a) Xenon mass inventory

(b) Kr mass inventory

(c) Iodine mass inventory

(d) Cs mass inventory

(e) Total mass inventory

Figure 21 Reduction of the fuel rod mass inventory (entire core) due to burst release during DBA LOCA (with application of uncertainty factors obtained from [10])

4.2 Assessment and implementation of alternative burst release fraction model

In 2022, US NRC issued draft regulatory guide DG-1389 with a proposal for updated gap release fractions [12], which is based on the report published in 2011 [13]. The proposed release fractions are given by Table 12 and are hybridized accident source terms that utilize the maximum release fractions from low- and high burnups results [12] and are applicable to full-lengths uranium dioxide fuel rod designs operating up to 68 GWd/MTU rod average burnup.

Table 12 Gap release fractions for PWR as proposed by DG-1389 [12] with uncertainties taken from [13]

FP Group	FP species in the group	Gap release fraction	Gap release uncertainty
Noble Gases	Xe, Kr	0.022	±0.002
Halogens	I, Br	0.007	±0.002
Alkali Metals	Rb, Cs	0.005	±0.002
Tellurium Metals	Te, Se, Sb	0.007	±0.003
Alkaline Earths	Sr, Ba	0.0014	±0.0006

The estimated release fractions were obtained from MELCOR 1.8.5 computer code analyses performed for 12 different PWR accident sequences [13]. The investigated accident sequences had in common a “substantial meltdown” of the reactor core, i.e. beyond the scope of the DBA and DEC-A conditions which are investigated in the R2CA project. The given gap release fractions are fractions of the total core inventory that are released to the containment (in-containment source term) during a so-called gap release phase and take the retention of radionuclides in the reactor coolant system into account [13].

The gap release phase was judged to have ended when 5% of the initial, total core inventory of xenon had been released from the fuel to the RCS[4] [13]. At that moment, 2.2% of the noble gases were released to the containment, which means that approximately 50% the FPs were (at least temporarily) retained in the RCS. High retention factors were also included for the halogens and alkali metals. For example, the CORSOR model defines a gap release fraction of 5% for Cs, while the gap release fraction given by DG-1389 is by a factor of 10 lower. On the other hand, the gap release rates for tellurium metals, strontium and barium are significantly higher than defined by the CORSOR model. The reason is that in the underlying MELCOR analyses are performed for an entire reactor core. During the gap release phase, the first cladding rupture occurs in the hottest part of the core, with gap release from those fuel rods. Afterwards, those rods are further heated-up and show significant releases of further FPs, until the 5% xenon release criterion (calculated for the entire core) is reached. For example, the CORSOR gap release fraction for Sr and Ba is 10^{-6}, while DG-1389 states $1.4 \cdot 10^{-3}$.

For test purposes, the gap release fractions as given by Table 12 were implemented into ATHLET-CD and first calculations were performed. However, on the base of the aforementioned reasons, the coefficients seem to be inappropriate to model the gap release from the fuel to the RCS.

[4] Note that for the definition of the end of gap release phase, the release from fuel to RCS is considered and not the release to containment.

4.3 Summary

HZDR reviewed the fission product release models which are implemented in the ATHLET-CD code with a focus to the phenomena important for DBA LOCA. The review was supplemented by ATHLET-CD analyses for a generic German PWR of type Konvoi (Siemens KWU design). For this purpose, the code was extended, that the user can apply uncertainty factors for the release rate coefficients of selected fission product species separately.

It was found that the continuous release rates (based on experimental data published by ORNL) do not play a significant role for DBA LOCA, as the fuel temperatures are too low for the major part of the accident until the entire core is quenched at approximately 100 s after the beginning of the transient. The main releases originate from the fission products accumulated in the fuel rod gap, which are spontaneously released after burst of cladding. However, ATHLET-CD does not model the process of accumulation, but instead a burst release model is applied which is based on experimental data. Three different burst release models are available in ATHLET-CD. For two of the implemented models, issues were found which led to incorrect results (wrong calculation of power shape factors). The third model is based on the CORSOR code and was investigated in more detail and uncertainty factors originating from analyses reported in the Reactor Safety Study (WASH-1400) were applied. It was found that these uncertainty factors are huge and do not correspond to current state of knowledge. Therefore, more recently published release rate coefficients were searched. One recent publication with updated gap release coefficients is the Draft Regulatory Guide DG-1389 was analyzed. However, these coefficients describe the in-containment source term during the so-called gap-release phase (which is defined by an arbitrarily selected criterion, i.e. the time until 5% of the total amount of xenon had been released from the fuel to the reactor coolant system). Therefore, they are inappropriate to model the gap release from the fuel to the reactor coolant system (needed in ATHLET-CD).

Consequently, the gap release model based on CORSOR-fraction is the only gap release model that seems to be correctly implemented in ATHLET-CD and it is currently the only one that is recommended for application. However, more detailed mechanistic analyses with fuel performance codes (such as TRANSURANUS) are needed to estimate the accumulation of fission products in the fuel rod gap and the release from the gap after cladding burst more precisely.

4.4 References

[1] Lovasz, L., Austregesilo, H., Bals, C., Hollands, T., Köllein, C., Luther, W., Pandazis, P., Schubert, J.D., Tiborcz, L., Weber, S., and Wielenberg, A., ATHLET-CD 3.3 User's Manual, GRS-P-4/Vol. 1 Rev. 8. 2021, Ges. für Anlagen- und Reaktorsicherheit (GRS).

[2] Lovász, L., Bals, C., D'Alessandro, C., Hollands, T., Köllein, C., Austregesilo, H., Pandazis, P., Tiborcz, L., and Weber, S., ATHLET-CD Mod 3.3 Models and Methods, GRS-P-4/Vol.2 Rev. 0. 2021, Gesellschaft für Anlagen- und Reaktorsicherheit (GRS) gGmbH.

[3] US NRC, Accident source terms for light-water nuclear power plants, NUREG-1465. 1995.

[4] RSK, RSK guidelines for pressurized water reactors, 3rd edition of October 14th, 1981 with modifications. 1998.

[5] Lorenz, R.A. and Osborne, M.F., A summary of ORNL fission product release tests with recommended release rates and diffusion coefficients. 1995, Nuclear Regulatory Commission.

[6] Bals, C., Köllein, C., Cester, F., Hollands, T., Luther, W., Schubert, J.D., and Weber, S., Entwicklung von Kühlkreislaufmodellen zur Spätphase von Kernschmelzeunfällen (ATHLET-CD und ASTEC) Abschlussbericht, GRS-A-3646. 2012, Gesellschaft für Anlagen- und Reaktorsicherheit (GRS) gGmbH: Köln.
[7] Trambauer, K., Austregesilo, H., Bals, C., Cester, F., Deitenbeck, H., Klein-Heßling, W., Lerchl, G., Müller, C., Papukchiev, A., and Schubert, J.-D., Weiterentwicklung ATHLET / ATHLET-CD Vorhaben RS 1162 Abschlussbericht, GRS-A-3461. 2009, Gesellschaft für Anlagen- und Reaktorsicherheit (GRS) gGmbH.
[8] Trambauer, K., Modellumfang ATHLET-CD, GRS-A-2508. 1997, Gesellschaft für Anlagen- und Reaktorsicherheit (GRS) gGmbH.
[9] Kuhlmann, M.R., Lehmicke, D.J., and Meyer, R.O., CORSOR User's Manual, NUREG/CR-4173. 1985, Battelle's Columbus Laboratories.
[10] US NRC, Reactor Safety Study, WASH-1400. 1975.
[11] Carbiener, W.A., Cybulskis, P., Denning, R.S., Genco, J.M., Miller, N.E., Ritzman, R.L., Simon, R., and Wooton, R.O., Physical Processes in Reactor Meltdown Accidents, Appendix VIII to Reactor Safety Study (WASH-1400). 1975.
[12] US NRC, Draft Regulatory Guide DG-1389. Alternative Radiological Source Terms for Evaluating Design Basis Accidents at Nuclear Power Reactors. 2022.
[13] Powers, D.A., Leonard, M.T., Gauntt, R., Lee, R.Y., and Salay, M., Accident Source Terms for Light-Water Nuclear Power Plants Using High-Burnup or MOX Fuel, SAND2011-0128. 2011.

5 UJV

The subject of the UJV activities is the COCOSYS (Containment Code SYStem) code, which is developed and maintained at GRS gGmbH [5]. Within the framework of the R2CA project [7] the version 2.4v5 [09] and 3.0 have been used. COCOSYS is extensively used at UJV for numerous applications in nuclear power plants safety analyses. Historically, the code was used for thermal hydraulic calculations only. During last few years, the thermal hydraulic models have been extended to provide fission product transport calculations. This led to the need of validation of the fission product transport calculation.
The activities conducted at UJV within the task 3.1 comprises of two main fields

1. Validation of COCOSYS
2. Sensitivity study and application of BEPU at VVER-1000/V-320

5.1 Validation of COCOSYS

The validation of COCOSYS code was aimed at the iodine behaviour mainly because iodine is a dominant contributor to the radiological consequences [2], [3]. The work is distinguished between two main areas. Firstly, on deposition of iodine on dry painted surface. Iodine is one of the most important fission products regarding the radiological consequences [4]. NPP containments have typically large surfaces covered with epoxy paint, which works as an efficient sink for the gaseous iodine preventing from larger release into the environment. Correct representation of this phenomena in a computational code and model is a key part to a more realistic estimation of the source term and a possible reduction of the radiological consequences. The dry deposition is defined as a system of chemical interactions of airborne elemental iodine with painted surface in conditions with very low or negligible condensation on surface, i.e. without the existence of a water film. The threshold between dry and wet (high condensation rates, water film) is set by the user and the code chooses which set of correlations to use accordingly.

Secondly, the work aims at validation of iodine revolatilization from containment sumps. This effect becomes more important in later phases of loss-of-coolant accidents, where significant amount of water within the containment may form sumps in numerous containment volumes [4]. Iodine trapped in the sumps may be revolatilized depending on the sump pH, yielding to possibly higher concentrations in the atmosphere and consequent release to the environment.

The calculation of iodine behaviour is done by the so-called AIM module, which considers 53 chemical reactions and 18 physical processes in each compartment (computational volume). Iodine transport between compartments by gas and water flows is provided by the thermal hydraulic (THY module) part of the calculation and aerosol behaviour of the particulate iodine species is treated by the aerosol fission product calculation (AFP module) [1].

5.1.1 Recalculation of BIP experiments

In general, the COCOSYS AIM-3 (Advanced Iodine Model) calculates concentrations of considered species resulting from many coupled processes as a function of time. General form of chemical process in COCOSYS is

described in equation (5), where k_1 is the reaction rate constant for the forward reaction where the reactants are compounds A, B and C, D are the products and k_2 is for the reverse reaction (C, D are the reactants and A, B are the products) [1].

$$A + B \underset{k_2}{\overset{k_1}{\rightleftharpoons}} C + D \tag{6}$$

A kinetic equation is formulated in AIM-3 for each iodine species. The resulting set of differential equations is solved for each iodine compartment. To calculate reaction rate constants k_i at elevated temperatures (T [K]) the Arrhenius equation (6) is mostly applied. In equation (6) BAS_i is reaction rate constant at the temperature of 25 °C, R is the gas constant 8.3144 J mol^{-1} K^{-1} and $EAKT_i$ is an activation energy [J mol^{-1}].

$$k_i = \mathrm{BAS_i} \cdot e^{\mathrm{EAKT_i}\left(\frac{T-298,15}{RT\cdot 298,15}\right)} \tag{7}$$

The constants BAS_i and $EAKT_i$ can be, in some cases, modified by the user [1].

Molecular iodine I_2 is a reactive and water-soluble gas which can deposit and resuspend from surfaces. Following equations are important for iodine adsorption on dry painted surface:

- Physisorbed I_2 is weakly bounded to paint (with reaction rate constant k_{76}) and can be desorbed (resuspended) back to gas phase (k_{62}). Further equation (7) describes this reversive reaction. In COCOSYS $I_2(g)$ is for gaseous I_2 and $I_2(dep,p,g)$ is for I_2 deposited on paint from gas phase [1].

$$\mathrm{I_2}(g) \underset{k_{62}}{\overset{k_{76}\cdot \mathrm{FSATP}\cdot \mathrm{XPHS}}{\rightleftharpoons}} \mathrm{I_2}(dep,p,g) \tag{8}$$

- Chemisorbed I_2 is strongly bounded to paint also with k_{76}. The reaction described by the equation (8) in COCOSYS is technically reversive but the value of k_{77} is set to 0 in this version of the code system. $I_2(g)$ is also for gaseous I_2 and $I_{chs}(dep,p,g)$ is for I_2 chemisorbed on paint from gas phase [1].

$$\mathrm{I_2}(g) \underset{k_{77}}{\overset{k_{76}\cdot \mathrm{FSATP}\cdot (1-\mathrm{XPHS})}{\rightleftharpoons}} \mathrm{I_{chs}}(dep,p,g) \tag{9}$$

Schemes of both equations (7) and (8) are shown in Figure 22.

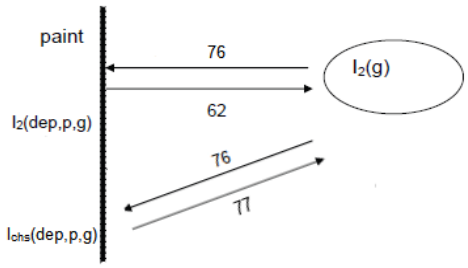

Figure 22: Interactions of gaseous I_2 with painted surface in containment

Furthermore, COCOSYS allows the user to modify the XPHS splitting factor, which determines the fraction of physisorbed and chemisorbed iodine of the total adsorbed iodine for specific kind of paint. FSATP is a dimensionless function of the absolute steam density to describe the influence of humidity and temperature, it cannot be changed by user [1].
The adsorption model is in original conditions set up for the GEHOPON paint [1].

Within the task 2.1.3 a database of validation experiments was created, where one of the described experimental series was the BIP project, which aim fits the intended application. The OECD (Organisation of Economic Co-operation and Development) initiated the Behaviour of Iodine Project with AECL (Atomic Energy of Canada Limited) as operating agent to achieve better understanding of iodine behaviour in NPP containments. Project performed work in 3 areas: adsorption of molecular iodine on surfaces (IA), organic iodides formation from containment paints loaded with iodine (OIF) and provision of Radioiodine Test Facility (RTF). Previous studies at AECL have determined that adsorption of gaseous molecular iodine in dry conditions is strongly dependent on the temperature and relative humidity of the air-steam mixture containing iodine. One of the paints used for BIP IA experiments is the Ameron Amerlock which is used on inner surface in NPP Temelin containment [6]. The list of the experiments, including thermal hydraulic conditions of the tests is presented in Table 13.

Table 13: Investigated IA tests with Amerlock coupons [6]

Test #	Coupon material	Temperature [°C]	Humidity [%]	Other information
G5	Aged Amerlock	70	15-40-60	Humidity was raised in stages
G8	Aged Amerlock	30	70	Temperature effect
G9	Aged Amerlock	50	70	Temperature effect
G12	Fresh Amerlock	70	70	1 adsorption/desorption cycle
G14	Aged Amerlock	70	15-40-60	Humidity was raised in stages
G19	Aged Amerlock	30	80	The same partial pressure of steam
G20	Aged Amerlock	50	27,5	
G21	Aged Amerlock	70	10,89	

The computational model for COCOSYS consists of three types of nodes (Figure 23). The BUFF1 to BUFF6 represent large volumes, which contain the gaseous mixture of desired pressure, temperature, humidity, and iodine concentration. The VESSEL represents the experimental cell with coupon and the ENVIRON collects the mass released from the VESSEL. The mass flow between the BUFFx and VESSEL is maintained by a corresponding ventilation component. Activating and deactivating of these ventilation systems allow precise control of gaseous mixture entraining in the experimental cell. The ventilation system FREM removes the mass from the VESSEL into the zone ENVIRON. This approach helps to keep stable thermal hydraulic conditions in the system.

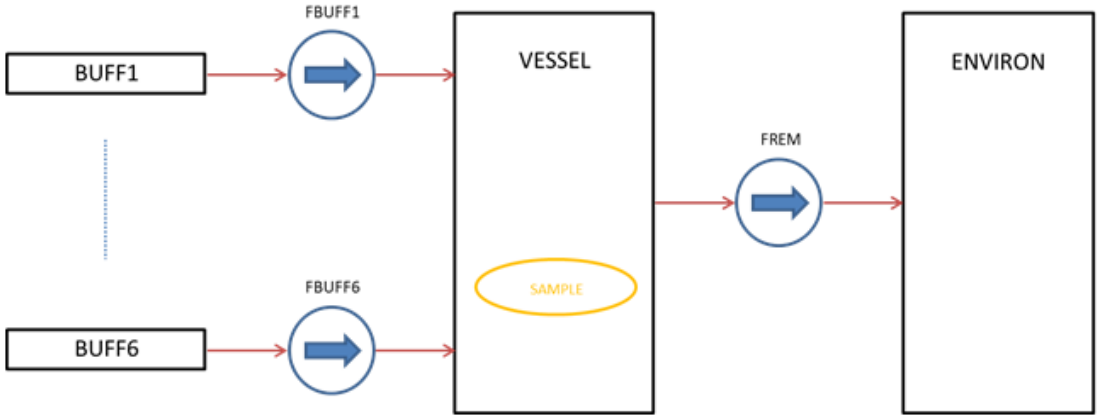

Figure 23: Nodalisation of the BIP IA experiments

A typical experiment with painted coupon starts with injection of gas mixture containing iodine. This yields to adsorption (chemisorption and physisorption) of iodine onto the coupon, cf. Figure 24. At certain time point, the iodine injection stops. The physisorbed iodine is then released from the surface. This release ends at a certain point, where the adsorbed iodine is mainly composed of the strong bound chemisorbed iodine. The experimental results are labelled Coupon 1, 2, 3. The sum of the calculated physisorbed and chemisorbed iodine is labelled m_{total} (the orange curve). Physisorption and chemisorption are represented individually, where the physisorbed iodine mass is labelled $m_{I2\ paint}$ (the yellow curve), and the chemisorbed iodine mass is labelled $m_{Ich\ paint}$ (the blue curve).

The recalculation of the Ameron Amerlock experiments revealed significant underestimation of the adsorbed iodine mass, as presented on the G-20 test, cf. Figure 24. This led to following assumption:

- Adsorption should be increased (BAS_{76})

Furthermore, the desorption of physisorbed iodine (deposited mass drop after the end of iodine injection around 80 000 s] was not interpreted correctly. This led to following assumptions:

- XPHS should be reduced to increase the adsorption of physisorbed iodine (BAS_{76})
- Desorption of physisorbed iodine should be increased (BAS_{62})

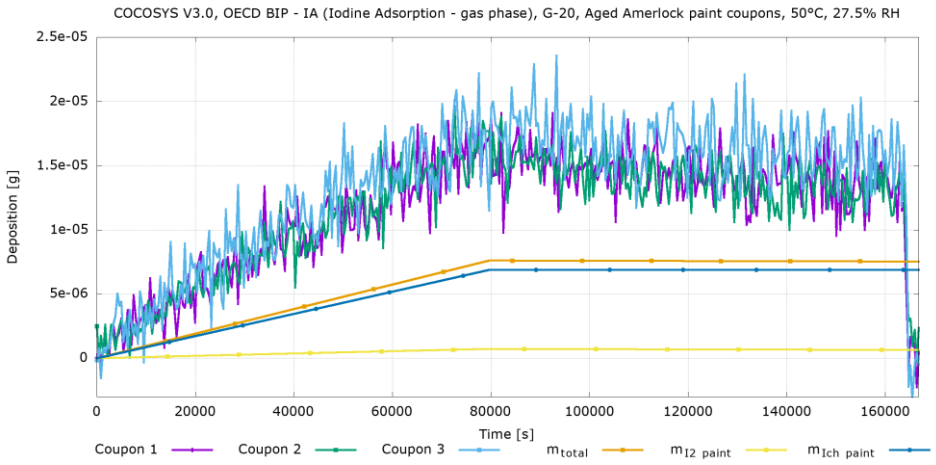

Figure 24: Prediction of iodine adsorption (original parameters)

Following the assumptions mentioned earlier, over 500 calculations were performed. The fine-tuning of the model parameters was done with a demand on realistic representation of the investigated phenomena for all the tests in Table 13. The calculation with modified model parameters (XPHS and BAS) led to more realistic estimate of the adsorption and desorption on dry Ameron Amerlock painted surfaces, cf. Figure 25.

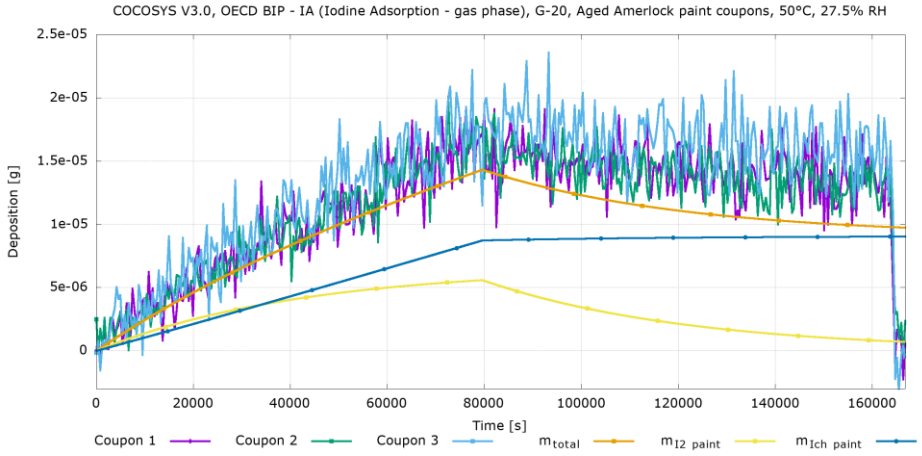

Figure 25: Prediction of iodine adsorption (modified parameters)

The work conducted in this study proved the ability of COCOSYS V3.0 to simulate the iodine adsorption and desorption on dry painted surface. It should be noted that this type of fine tuning should be done for each investigated surface type and coating. Values presented in Table 14 are valid for the Ameron Amerlock only and may be further modified based on other experiments.

Table 14: Proposed BAS_i and XPHS parameters values for Ameron Amerlock

Parameter	$BAS_i(76)$	$BAS_i(62)$	XPHS
Modified value	7.5E-3	2.0E-6	0.6

Future work should be aimed at other single effect and integral tests and on implementation of the validation results into the models used for the NPP safety analyses and further reduction of radiological consequences.

5.1.2 Recalculation of RTF experiments

The RTF test facility consists of a cylindrical main vessel with a total 350 litres volume, which is partially filled with water, cf. Figure 26. In some tests, radiation source was present. The P9T1 experiment used a stainless-steel vessel. The temperature was maintained at 60°C and the dose rate was 0.78 kGy/h. The test started with pH equal to 10, then the pH was reduced in steps to 5 and finally increased to 9. Each decrease of pH was followed by increase of iodine concentration in the atmosphere. Finally, the pH increase led to reduction of airborne iodine concentrations [8].

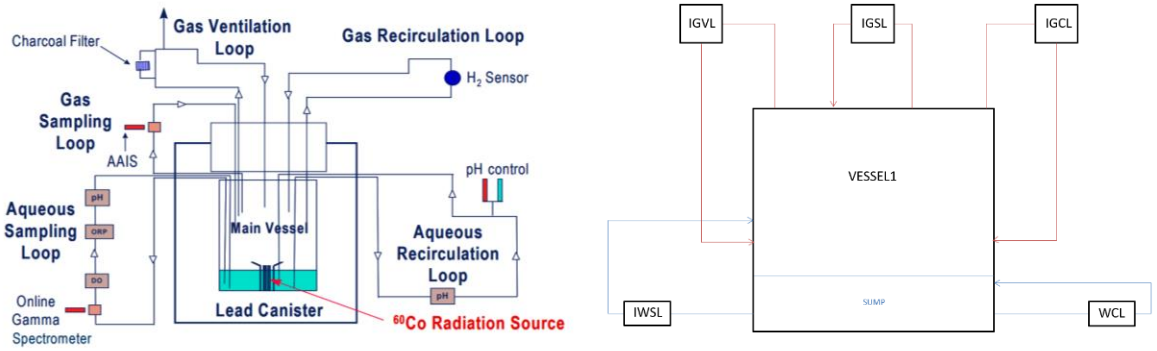

Figure 26 Schematic of the RTF facility and COCOSYS nodalisation [6]

For the validation, a tailored COCOSYS nodalisation was introduced, representing all major volumes as well as the instrumentation (circulation pumps and piping) and surface. The comparison of calculated and measured values can be observed in Figure 27. The trends are in good consonance with the experiment. Slightly lower iodine concentration in the gas phase may be influenced by overestimated iodine adsorption on vessel steel surface. Generally, the pH may have impact to iodine release from containment during loss-of-coolant accidents and should be tested on power plant model.

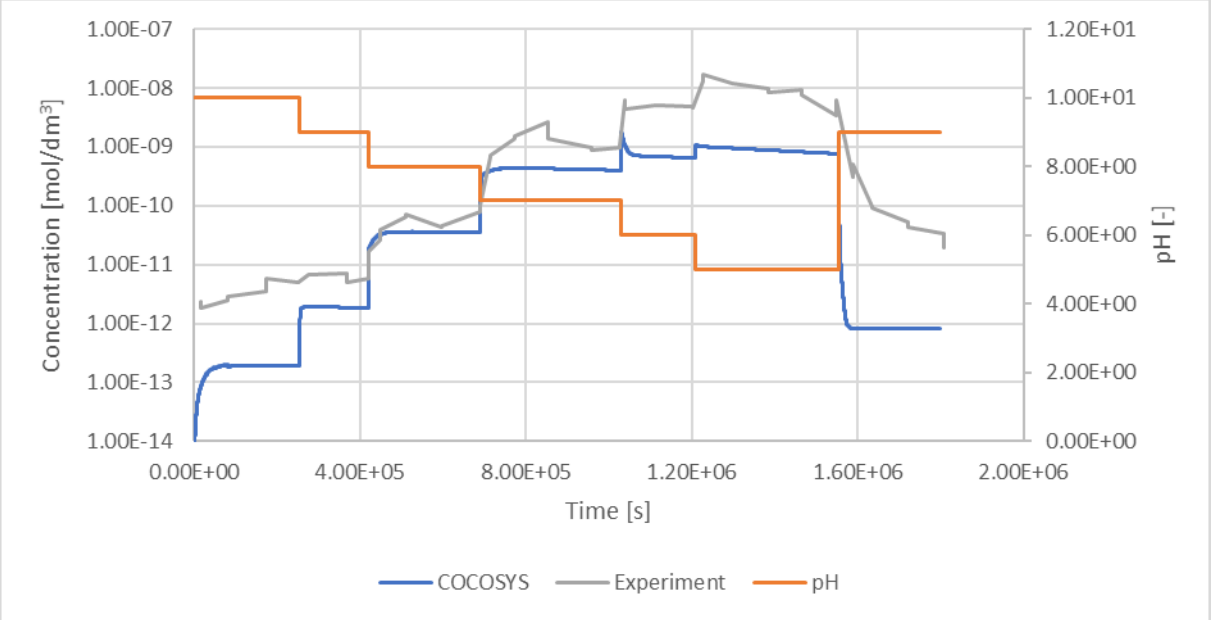

Figure 27 Comparison of the RTF P9T1 experimental data [8] with COCOSYS calculation (concentration of iodine in gas phase)

5.2 VVER-1000/V-320 containment studies

The experience gathered within the validation activities were reflected in the application at LB LOCA. It was decided to study more deeply the initial and boundary conditions. Firstly, the sensitivity to sump pH was tested, secondly a BEPU approach using the GRS methodology and Spearman's correlation ratio was used to evaluate the sensitivity of the system.

5.2.1 Containment pH sensitivity study

The validation on RTF experiment created answers, whether the sump pH could be an important initial and boundary condition for iodine release. Furthermore, it was decided to check, whether an assumption that a lower pH should lead to higher iodine concentrations in the atmosphere yielding to higher release into the environment. During normal VVER-1000/V-320 operation, only two significant water volumes are in the containment – the spent fuel pool and the containment sump. The pH of these volumes is maintained nearly constant, but when a LB LOCA occurs, ejecting primary coolant may change the sump pH and concentration in containment atmosphere.
Typically, the pH of the VVER-1000/V-320 is maintained in the range from 7 to 7.2 [11], [12]. For the calculations, a range from 5 to 10 was chosen to cover the range from the P9T1 experiment as well as to cover conditions with increased and decreased chemical compound concentrations. For each of the calculations, the pH was set constant, i.e. no pH calculation based on chemical compound concentration was done by COCOSYS. Furthermore, it was decided to test the sensitivity for two different initial iodine chemical compositions based on the R.G. 1.183 [14] and R.G. 1.195 [15][15] respectively.

Table 15: Calculated variants

Iodine speciation	pH values	Further information
R.G. 1.183 95 % CsI, 4.85 % I_2, 0.15 % CH_3I	5 to 10	Release of iodine to the containment atmosphere only Injection timing 30 – 1800 s after initiating event
R.G. 1.195 91 % I_2, 5 % CsI, 4 % CH_3I	5 to 10	Release of iodine to the containment atmosphere only Injection timing 30 – 1800 s after initiating event

The comparison is done for the two chemical speciation separately. The variants with chemical speciation based on the R.G. 1.183, i.e. dominant aerosol iodine, revealed highest release for lowest pH, cf. Figure 28. This is in consonance with the expectation based on the RTF results, cf. Figure 27. Significant decrease of the released mass can be observed from pH 6 and higher. From pH 8 the released iodine mass shows lower sensitivity to the changing pH.
Interesting results may be observed for pH 5 to 6, where slight increase of the released iodine mass can be observed in comparison to the reference calculation. This effect is not in consonance with the experiment. The origin of this effect may come from complex containment behaviour, i.e. presence of spray systems, painted surface etc. These factors are not present in the simplified RTF test facility. Further discrepancies in the expected trend can be observed for pH 8 and further.
The range of the results vary between the maximal and minimal value by almost 20 %. It should be noted that the highest sensitivity is close to the typical primary circuit pH range.

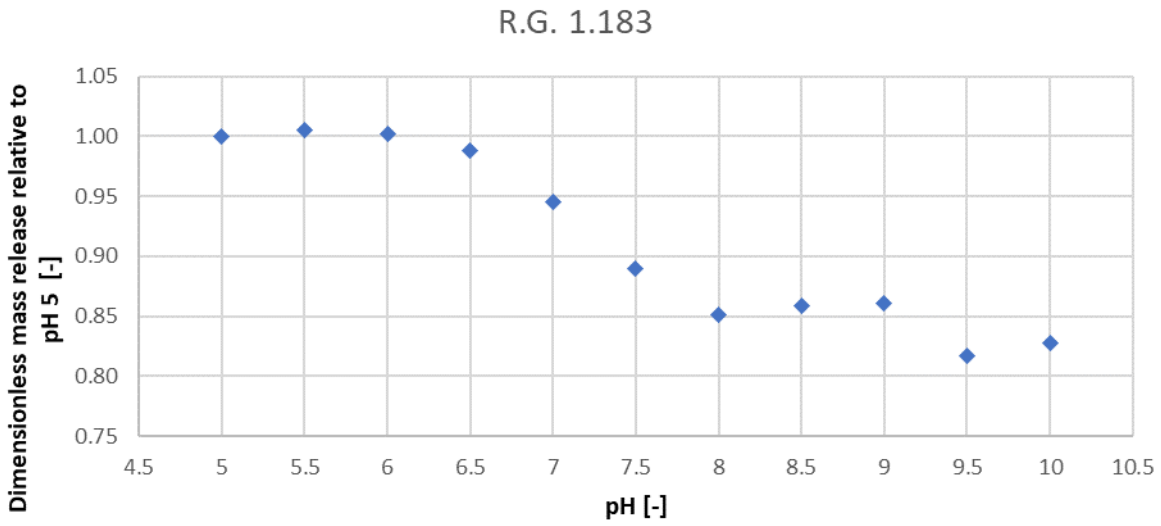

Figure 28 Comparison of iodine mass release relative to calculation with pH 5-10 (initial iodine speciation according to R.G. 1.183)

The variants with chemical speciation based on the R.G. 1.195, i.e. dominant elemental iodine, confirmed the consonance with the basic assumption, cf. Figure 29. Compared to the previous sets, the decrease of the released iodine mass starts with pH 5.5. The sensitivity of the system is most significant for the pH between 6 and 7. From

pH 8, the released iodine mass is nearly pH independent. Unlike the previous variants, the sensitivity follows the basic assumption without any disruption in expected trend. The variation between minimal and maximal iodine mass release is higher, reaching almost 40 % from the reference pH 5 calculation.

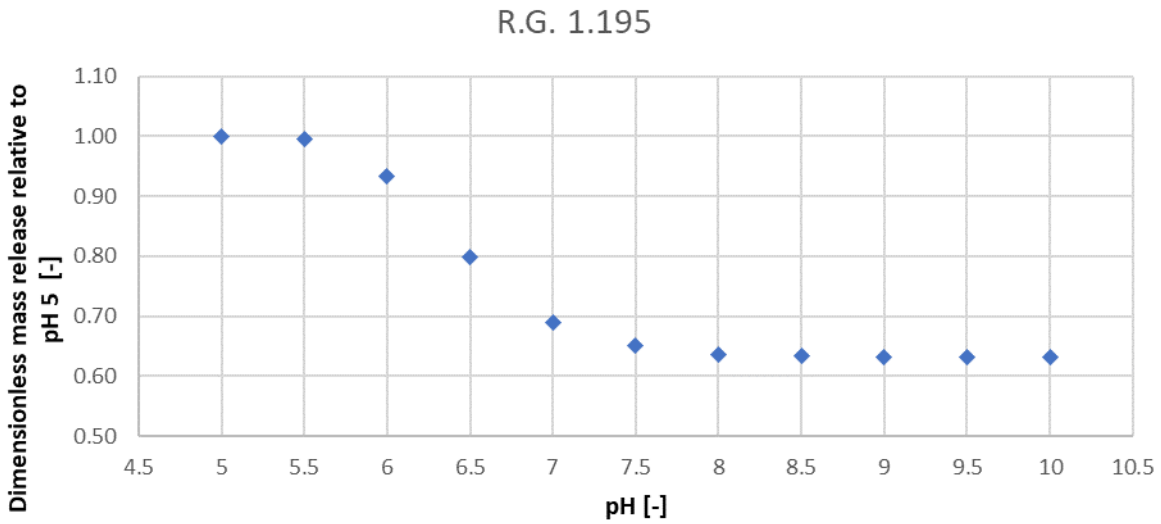

Figure 29 Comparison of iodine mass release relative to calculation with pH 5-10 (initial iodine speciation according to R.G. 1.195)

The recalculation of the variants proved that the iodine mass release from the containment is influenced by the sump pH value. The general behaviour is in consonance with the validation at RTF facility. The evaluation revealed different sensitivity for different initial chemical speciation. The variants with dominant molecular iodine exhibit stronger sensitivity (i.e. R.G. 1.195) to the change of the sump pH.
Furthermore, the conducted study proved that for conservative analyses pH 5 should be used with initial iodine speciation following the R.G. 1.195. For the speciation following the R.G. 1.183, pH 5.5 should be used.
For realistic calculations, further evaluation of pH evolution in the containment sumps should be done, because the sensitivity for both iodine speciation is highest for pH values typical for normal primary circuit operation. This can be done both by standalone containment calculation with appropriate modelling of the mass transfer back to the primary circuit, or with a coupled approach, which is a favourable option.

5.2.2 BEPU analysis

The improved plant model was further used in BEPU analysis. The BEPU methodology used for this task was the GRS methodology based on Wilks law. The law defines the number *n* of necessary calculations to get the desired accuracy, α and γ represent the tolerance limits

$$\alpha = 1 - \sum_{i=n-m+1}^{n} \binom{n}{i} \gamma^i (1 - \gamma^{n-i})$$

The first order, where $m = 1$ is suitable for one sided tolerance limit, i.e. values which are bound from the one side only.
For double sided interval, i.e. for parameter which range is bound between two values, a second order with $m=2$ yields to

$$\alpha = 1 - n\gamma^{n-1} - (n-1)\gamma^n$$

For a general application in the safety analysis field, the tolerance limit of 95 % is accepted. Assuming these values for both sided intervals, at least 93 calculations should be made.
The sensitivity analysis is based on Spearman's correlation ratio, which evaluates the order of watched values. Let $(x_i, y_i), \ldots, (x_n, y_n)$ be a random choice from continuous two-dimensional distribution. For each x_i and y_i a x_{ri} and y_{ri} is estimated based on the upwardly organized values $x_1, \ldots, x_n$ and $y_1, \ldots, y_n$. Then, the difference of order of watched values is calculated as $d_i = x_{ri} - y_{ri}$. In general, the Spearman's correlation ratio assesses monotonic relationships. If there are no repeated data values, a perfect correlation ratio of 1 or -1 occurs when each of the variables is a perfect monotone function of the other.

$$r = 1 - \frac{6}{n(n^2-1)}\sum_{i=1}^{n} d_i^2$$

For correct assessment, definition of critical r value is necessary. If the r value is below critical value, it is assumed that the there is no relational between the quantities. If the r is above critical value, the quantities may be correlated. In this case, the critical value of r is 0,204.

The choice of variated initial and boundary conditions included thermal hydraulic values such as temperature, humidity, and pressure as well as dose rate within the containment volumes etc. The original number of 75 variated parameters was then reduced due to relation between them, i.e. the atmosphere temperature in the reactor hall is correlated to the temperature of other volumes. The final list of variated parameters is given in Table 16.

Table 16 List of variated parameters in VVER-1000/V-320 BEPU

Parameter No.	Description
1	Environment pressure
2	Environment temperature
3	Environment relative humidity
4	Atmosphere temperature in GA701 (reactor hall)
5	Relative air humidity in GA701 (reactor hall)
6	Containment sump water volume
7	Containment spraying angle
8	Spray droplet diameter
9	Dose rate in GA701 atmosphere
10	Dose rate in containment sump
11	Containment sump pH

The aim of the BEPU analysis was to reveal possibly significant initial and boundary conditions, which may have impact on iodine release. Such conditions might be interesting for further investigation to reduce the existing margins and reduce the radiological consequences accordingly.

Majority of the iodine release during LB LOCA escapes the containment within first hour, cf. Figure 30. That is why the evaluation was done for the 10 000 s only. Most of the investigated initial and boundary conditions proved to be without significant impact on the results, i.e. the absolute value of Spearman's correlation ratio was below the critical value. The possibly significant initial and boundary conditions are initial environment pressure, spray droplet diameter and spray angle and finally the pH, which was thoroughly investigated earlier. The final values are presented in Table 17. Figure 31 presents the Spearman's correlation ratio in time.

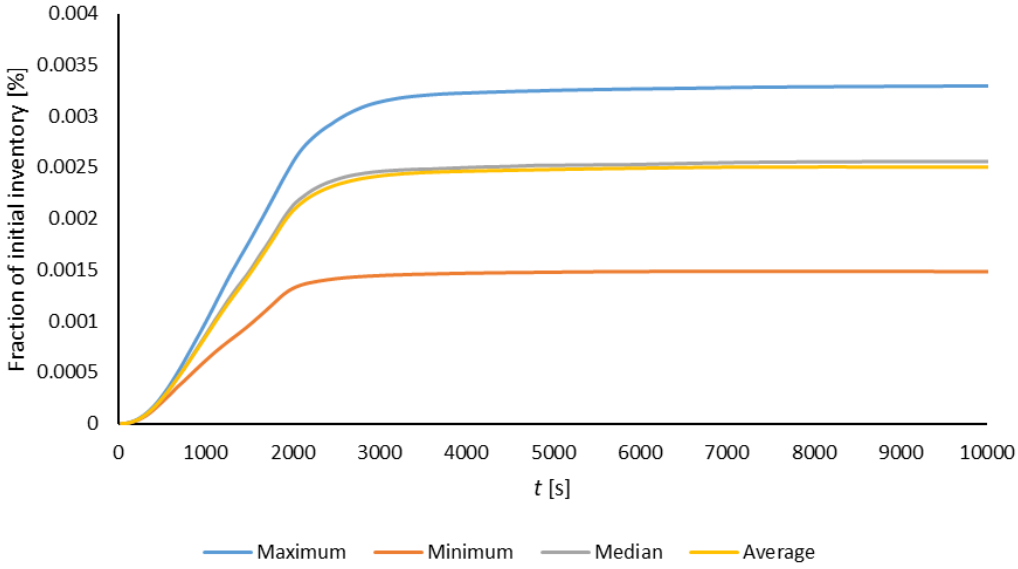

Figure 30 Results of the BEPU analysis of iodine release from VVER-1000/V-320 during LB LOCA (COCOSYS calculation)

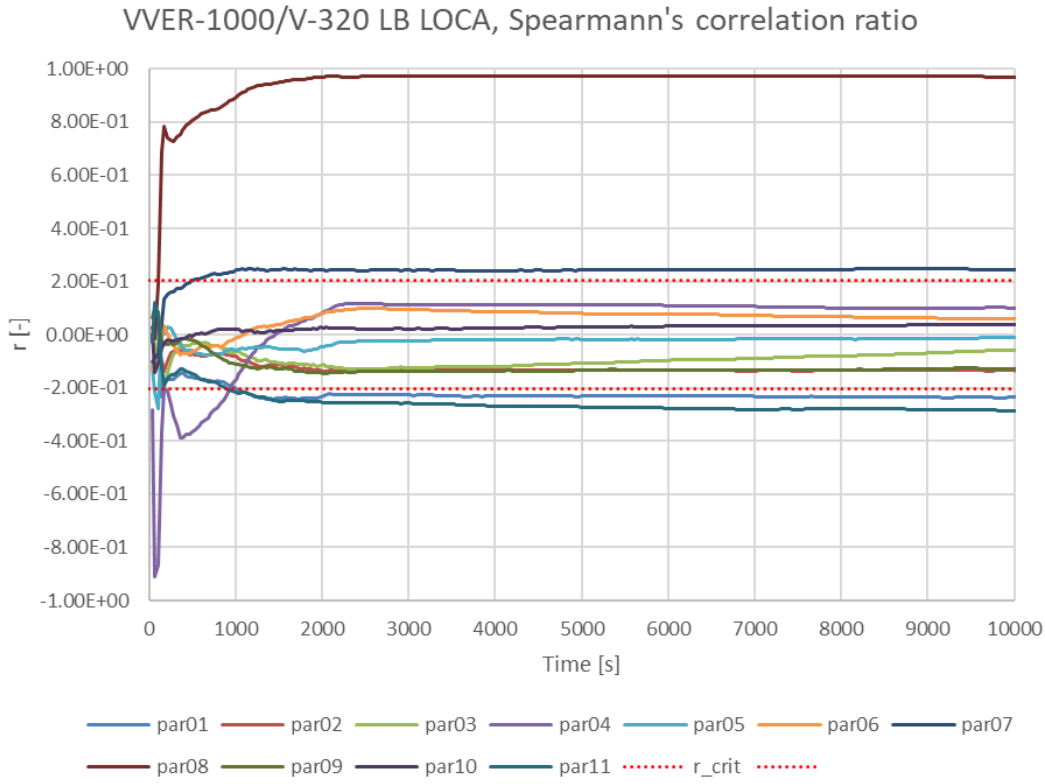

Figure 31 Spearman's correlation ratio for VVER-1000/V-320 LB LOCA

Table 17 Spearman's correlation ratio values at 10 000 s

Parameter No.	Description	r [-]	$\|r\| > \|r_{crit}\|$
1	Environment pressure	-0.235	Yes
2	Environment temperature	-0.135	No
3	Environment relative humidity	-0.057	No
4	Atmosphere temperature in GA701 (reactor hall)	0.101	No
5	Relative air humidity in GA701 (reactor hall)	-0.012	No
6	Containment sump water volume	0.062	No
7	Containment spraying angle	0.243	Yes
8	Spray droplet diameter	0.970	Yes
9	Dose rate in GA701 atmosphere	-0.127	No
10	Dose rate in containment sump	0.038	No
11	Containment sump pH	-0.286	Yes

5.3 Summary

The work conducted within this task aimed at two main areas. Firstly, the COCOSYS code was validated on two experiments aiming at iodine behaviour. The existing COCOSYS dry paint deposition model was fine tuned to Ameron Amerlock, which is used on inner surface of Temelin NPP containment. The code was further validated on RTF experiment for iodine volatilization from aqueous phase. The results achieved within this section were used in the second phase, where a consonance between the experiment and the containment analysis was observed. Finally, the second part included a BEPU analysis, which selected several initial and boundary conditions, which may have significant impact to iodine release during such conditions. These initial and boundary conditions may indicate areas, which should be investigated in the future, to reduce the margins and radiological consequences.

5.4 References

[1] Arndt, S., Band, S., Beck, S., Eschricht, D., Iliev, D., Klein-Heßling, W., Nowack, H., Reinke, N., Sonnenkalb, M., Spengler, C., Weber, G., Brückner, N.: COCOSYS 3.0.1 User Manual. Ed.: Gesellschaft für Anlagen- und Reaktorsicherheit (GRS) gGmbH (GRS), GRS-P-3 / Vol. 1, Rev. 54, June 2019

[2] IAEA, Deterministic safety analysis for nuclear power plants, IAEA SAFETY STANDARDS SERIES No. SSG-2 (Rev. 1), International Atomic Energy Agency Vienna, Austria, 2019

[3] W. Bleam, Soil and Environmental Chemistry, Academic Press, Madison, USA, 2017, pp. 1-38.

[4] OECD NEA, State of the Art Report on Iodine Chemistry, NEA/CSNI/R(2007)1, Nuclear Energy Agency, Committee on the Safety of Nuclear Installations, Paris, France, 2007.

[5] H.-J. Allelein, S. Arndt, W. Klein-Heßling, S. Schwarz, C. Spengler, G. Weber, COCOSYS: "Status of development and validation of the German containment code system", Nuclear Engineering and Design, Volume 238 (Issue 4), 2008

[6] AECL, Behaviour of Iodine Project, Final Summary Report (Rev. 0), 153-126530-440-015, Atomic Energy Canada Limited, Ontario, Canada, 2011

[7] Website r2ca-h2020.eu/
[8] OECD NEA, International Standard Problem (ISP) No. 41 – Containment Iodine Computer Code Exercise Based on a Radioiodine Test Facility (RTF) Experiment, NEA/CSNI/R(2000)6/VOL1, PARIS (2000)
[9] W. Klein-Heßling, S. Arndt, H. Nowack, C. Spengler, S. Schwarz, D. Eschricht, S. Beck, COCOSYS V2.4v5 User's Manual, Gesellschaft für Anlagen- und Reaktorsicherheit (GRS) gGmbH, Cologne, Germany (2018)
[10] Bezpečnostní návod BN-JB-2.10 (Rev. 0.0) Deterministické bezpečnostní analýzy událostí abnormálního provozu a základních projektových nehod, State Office for Nuclear Safety, Prague, Czechia (2020)
[11] Denk, L.: Metodika výpočtů radiačních následků pro bezpečnostní zprávu, ÚJV Z5085 T, ÚJV Řež, a. s., 2018
[12] Miklos, M. et al.: Review of the Primary Coolant Chemistry at NPP Temelín and its Impact on the Fuel Cladding, Proceedings of the WWER2011 Conference, (2011)
[13] EPRI, Review of VVER Primary Water Chemistry and the Potential for its Use in PWRs: Potassium Hydroxide and/or Ammonia Based Water Chemistries, Technical report 1003382, USA (2002)
[14] US NRC, Alternative Radiological Source Terms for Evaluating Design Basis Accidents at Nuclear Power Reactors, R.G. 1.183, United States Nuclear Regulatory Commission, USA (2000)
[15] US NRC, Methods and Assumptions for Evaluating Radiological Consequences of Design Basis Accidents at Light-Water Nuclear Power Reactors, R.G. 1.195, United States Nuclear Regulatory Commission, USA (2003)

6 SSTC NRS

The assessment of radiological consequences should include an evaluation of the isotopic composition of radionuclides released from the loaded into reactor core fuel into the atmosphere. The characterization of used in the core fuel is important component of safety substantiation.

The given part of subtask contributes to project outcome with information on the WWER-1000 fuel isotopic inventory and source term during in-core irradiation. The information will be based on the nuclear fuel characterization and using validated and best-estimate computer codes, NPP realistic data for burnup, and the modern nuclear data libraries.

The study is performed for the selected representative types of fuel assemblies used in WWER-1000 reactors of Ukrainian NPPs by numerical simulation using best-estimate models for the SCALE software package.
The expected outcome of the performed activities:

- state-of-art methods, calculation techniques and models for fuel characterization during in-core irradiation;
- improving relevant knowledge on WWER-1000 fuel characteristics and its evolution characterization during in-core irradiation;
- best-estimated evaluation of source term for LOCA radiological consequences analysis.
-

6.1 Type of fuel assembly for which calculations have been performed

The description of the fuel assembly (FA) is provided in the report on Subtask3.2.

6.2 The used program for calculations

The SCALE software package [1] was used for calculations. The SCALE software package is a modular system of standardized computer analysis for licensing purposes. This program was developed and is constantly being improved by the Oak Ridge National Laboratory of the USA's specialists by order of the US Nuclear Regulatory Commission (US NRC).

The SCALE program package is constantly used both in the US and around the world for modelling radiation parameters of nuclear fuel and various fuel handling systems starting with the first version of SCALE, which was released in 1980.
The SCALE program has the following structure:

- Data libraries – libraries of neutron physical characteristics;
- Functional modules – programs used in the SCALE package;
- Control modules – problem-oriented sets of programs (software modules) used in the SCALE package to solve specific physical problems (nuclear safety – criticality, radiation safety - activity, determination of isotopic composition, residual energy release, etc.);
- Auxiliary programs – preparing input files, processing output files, viewing models and obtaining results.

Calculations were performed using the TRITON software module. The ORIGEN program is the main component of the TRITON software module that allows a three-dimensional calculation of the burnup distribution and radiation characteristics of the spent fuel. This calculation was performed using the KENO program based on the correction depending on the burnup of libraries of neutron-physical constants (NFC) and three-dimensional modelling of the flow and spectrum of neutrons. The KENO program was developed based on the Monte Carlo method.

The standard 44-group NFC library of the SCALE package was used for the calculations. This library is based on the ENDF/B-V estimated data file.

The most complete description of the structure of the SCALE program package (libraries of NFC, programs, and software modules), program capabilities and features of use and data on validation and verification are given in the document «SCALE User's Manual. NUREG/CR 0200».
Initially, the SCALE program package was developed to model the fuel systems of PWR and BWR. Currently, this software package has been validated and widely implemented for the simulation of fuel handling systems of VVER.

6.3 Description of the calculation model

All geometric and material FA parameters used in the calculation model correspond to the data provided in the document [2].
All calculations were performed using the TRITON module of the SCALE software package, which allows the modelling of fuel systems in three dimensions.
Fuel burnup is modelled in SCALE step by step with calculation at each step of the isotopic composition of the fuel and structural materials, as well as libraries of NFC of the model. All calculations were performed with a burnup

step of 1 MW·days/kgU (at the beginning and the end of the burnup) and 2 MW·days/kgU (for the rest of the time). As the model testing showed, further meshing the calculation step of burnup does not lead to changes in the calculation results.

All calculations were carried out for the specific power of FA of 40 MW/tU. This is a conservative assumption since the operation of FA at a lower power level leads to a decrease in activity values with the same burnup (the real power of FA at the end of the refuelling interval is much smaller than the average values). Taking into account other factors within their possible fluctuations during fuel operation, consistent results were obtained. Considering this, the following characteristics of the fuel burnup mode were selected for the calculations:

- the concentration of boric acid– 3 g/kg;
- fuel temperature– 1005 K;
- coolant temperature – 558 K;
- inter-cassette gap– 2 mm.

FA was modelled carefully with the exact determination of the materials, configuration, and geometry of all elements within the fuel zone by the height of the system in accordance with the data given in [2]. The exception is spacing grids, the exact modelling of which by means of the SCALE package would lead to an unjustified complication of the calculation model and additional costs of calculation time. The material of the spacer grids was modelled in the form of two cylindrical bushings located in the upper and lower parts of the fuel rods.

WWER - 1000 FA includes 312 fuel rods (fuel pins and pins with Gadolinium burnable absorber), as well as 18 guide channels of control and protection system, which are connected to each other by spacer grids, a lower grid and a central pipe. On top of the fuel rods bundle is the FA upper end part, and on the bottom - the bottom end part.

The composition of FA-A type 398GO, which was modelled in the calculations, includes 306 fuel rods with Uranium dioxide having an enrichment of 4.0%, as well as 6 rods with a homogeneous mixture of Uranium dioxide with an enrichment of 3.3%, and 5% by weight of Gadolinium oxide. The average estimated mass fraction of Uranium-235 in such FA-A is 3.99%.

The composition of FA-A type 439GT, which was modelled in the calculations, includes 306 fuel rods with Uranium dioxide having an enrichment of 4.4%, as well as 6 rods with a homogeneous mixture of Uranium dioxide with an enrichment of 3.6% and 5% by weight of Gadolinium oxide. The average estimated mass fraction of Uranium-235 in such FA-A is 4.39%.

The fuel in fuel rods was modelled as a cylindrical core with an inner hole and a gap between the core and the shell. It was believed that the composition of Uranium in fresh fuel includes only two isotopes – U-235 and U-238. Impurities of other Uranium isotopes were not taken into account.

Fuel density (Uranium dioxide) in fuel rods was modelled by determining the average effective fuel density based on the geometric characteristics of the cylindrical fuel pellet (height, inner and outer diameters of the cylindrical core by the data given in [2]) and the average mass of fuel with the addition of a technological tolerance for the mass of fuel in FA – 4.5 kgUO2.

The calculated value of the fuel density in the fuel rods was determined at the level of 10.32 g/cm3. For more correct modelling of the neutron spectrum in the central and peripheral regions of the FA during the burning process in the central and peripheral regions of the FA, the fuel was designated by different types, see Figures 28-31. In this case, neutron spectra at each burnup step are calculated separately for each fuel type.

For calculations of changes in breeding properties of FA depending on burnup and enrichment, the calculation cell was modelled as a periodic cell, in the center of which is a hexagonal prism with a fuel cassette, surrounded by a layer of water.

The geometry of the prism corresponds to the pitch of the fuel cassettes in the WWER - 1000. The height of the prism was determined by adding a layer of water at the top and bottom of the cassette. At the boundary of the model, the conditions of periodicity were set in the axial direction and the presence of a water reflector in the axial direction.

Figure 32 to Figure 35 present the results of the visualization of FA-A calculation models, obtained using the graphical capabilities of the SCALE package.

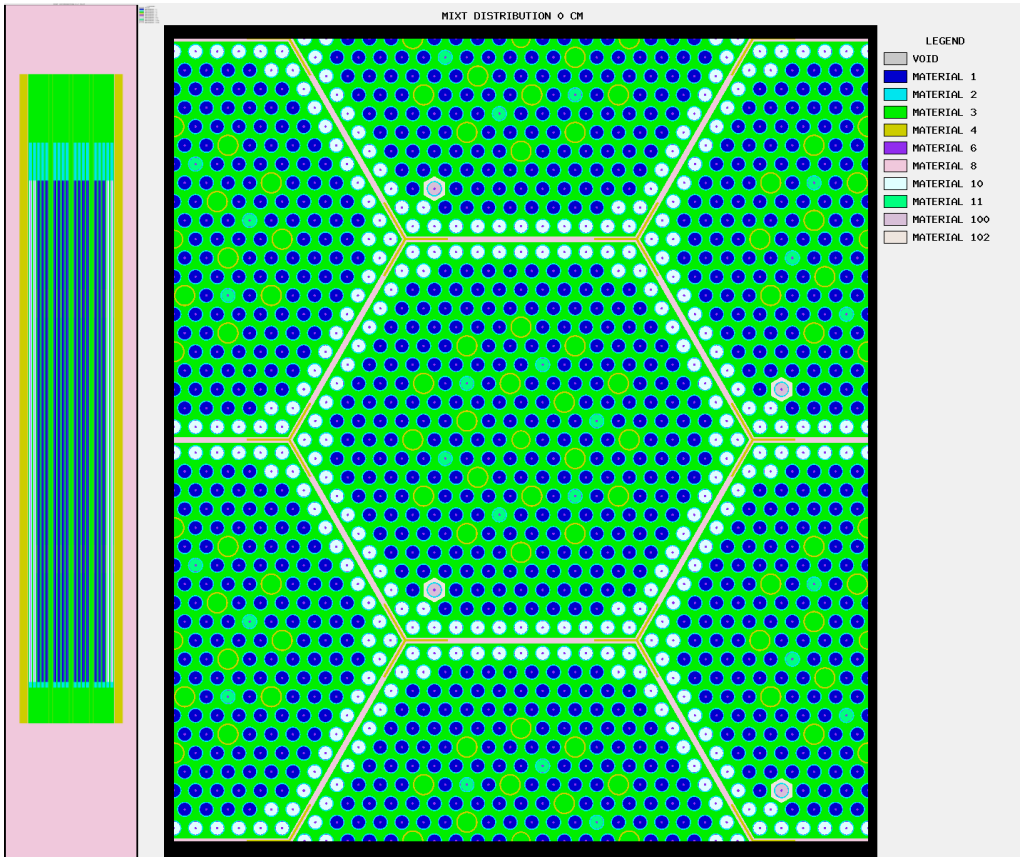

MATERIAL 1 – a fuel pellet of fuel rod of the central zone (enrichment 4.0%);
MATERIAL 100 a fuel pellet of a separately allocated fuel rod of the central zone (enrichment 4.0%)
MATERIAL 10 – a fuel pellet of fuel rod of the peripheral (enrichment 4.0%);
MATERIAL 11 – a fuel pellet of fuel rod with burnable absorber (enrichment 3.3%);
MATERIAL 2 – the cladding of the fuel rod;
MATERIAL 3 – water in the inner space FA;
MATERIAL 102 – water around the separately allocated fuel rod of the central zone;
MATERIAL 4 – central pipe, guide channels, and angles;
MATERIAL 6 – the internal space of the fuel rod which is filled with helium;
MATERIAL 8 – water in the space between the cassettes.

Figure 32 Longitudinal and cross-sections of the calculation model FA-A 3.99% with the separated fuel rod of the central zone

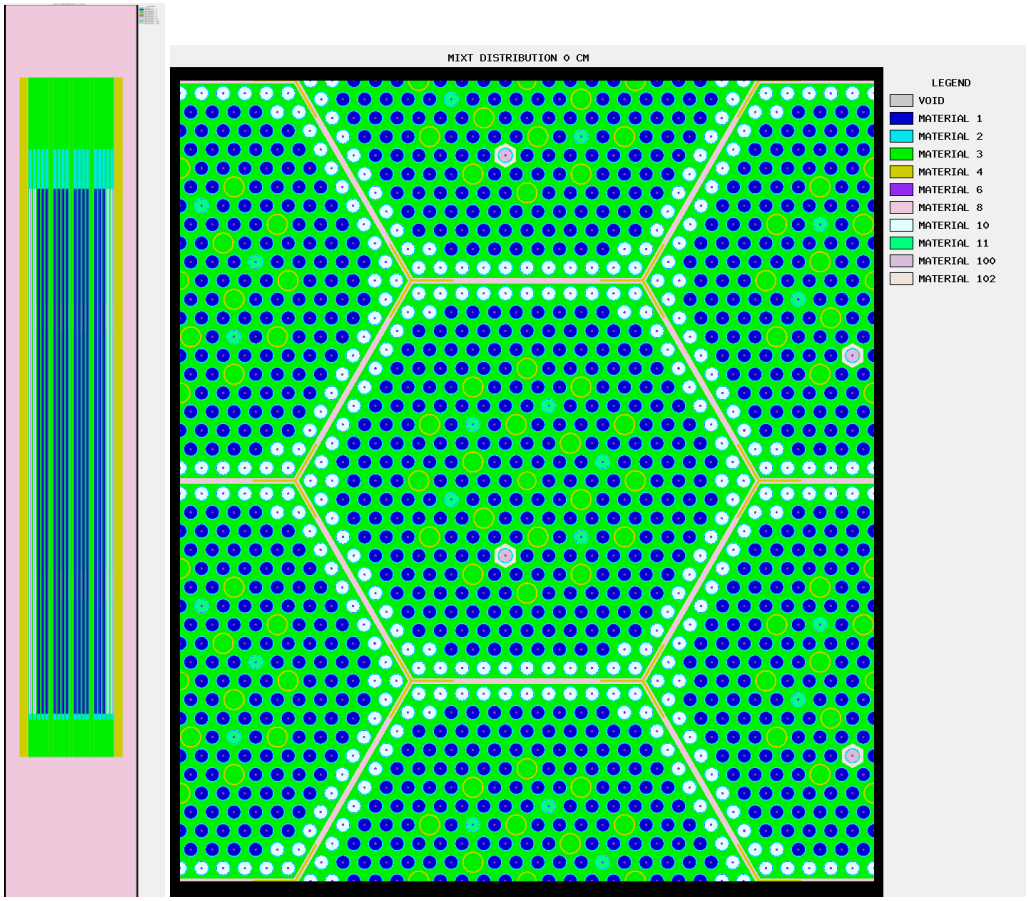

MATERIAL 1 – a fuel pellet of fuel rod of the central zone (enrichment 4.0%);
MATERIAL 10 – a fuel pellet of fuel rod of the peripheral (enrichment 4.0%);
MATERIAL 11 – a fuel pellet of fuel rod (enrichment 3.3%);
MATERIAL 100 – a fuel pellet of a separately allocated fuel rod with burnable absorber (enrichment 3.3%);
MATERIAL 2 – the cladding of the fuel rod;
MATERIAL 3 – water in the inner space FA;
MATERIAL 102 – water around the separately allocated fuel rod of the central zone;
MATERIAL 4 – central pipe, guide channels, and angles;
MATERIAL 6 – the internal space of the fuel rod cassettes.

Figure 33 Longitudinal and cross-sections of the calculation model FA-A 3.99% with the separated fuel rod burnable absorber

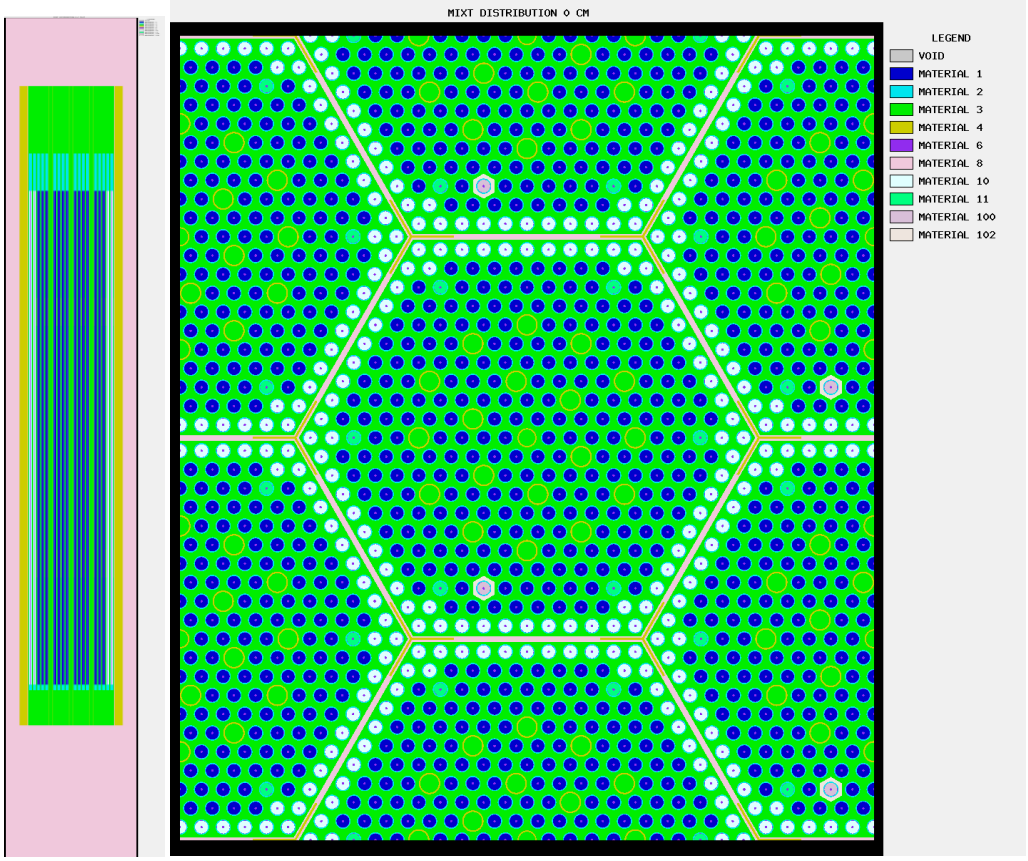

MATERIAL 1 – a fuel pellet of fuel rod of the central zone (enrichment 4.4%);
MATERIAL 100 – a fuel pellet of a separately allocated fuel rod with burnable absorber of the central zone (enrichment 4.4%);
MATERIAL 10 – a fuel pellet of fuel rod of the peripheral (enrichment 4.4%);
MATERIAL 11 – a fuel pellet of fuel rod (enrichment 3.6%);
MATERIAL 2 – the cladding of the fuel rod;
MATERIAL 3 – water in the inner space FA;
MATERIAL 102 – water around the separately allocated fuel rod of the central zone;
MATERIAL 4 – central pipe, guide channels, and angles;
MATERIAL 6 – the internal space of the fuel rod which is filled with helium;
MATERIAL 8 – water in the space between the cassettes.

Figure 34 Longitudinal and cross-sections of the calculation model FA-A 4.39% with the separated fuel rod of the central zone

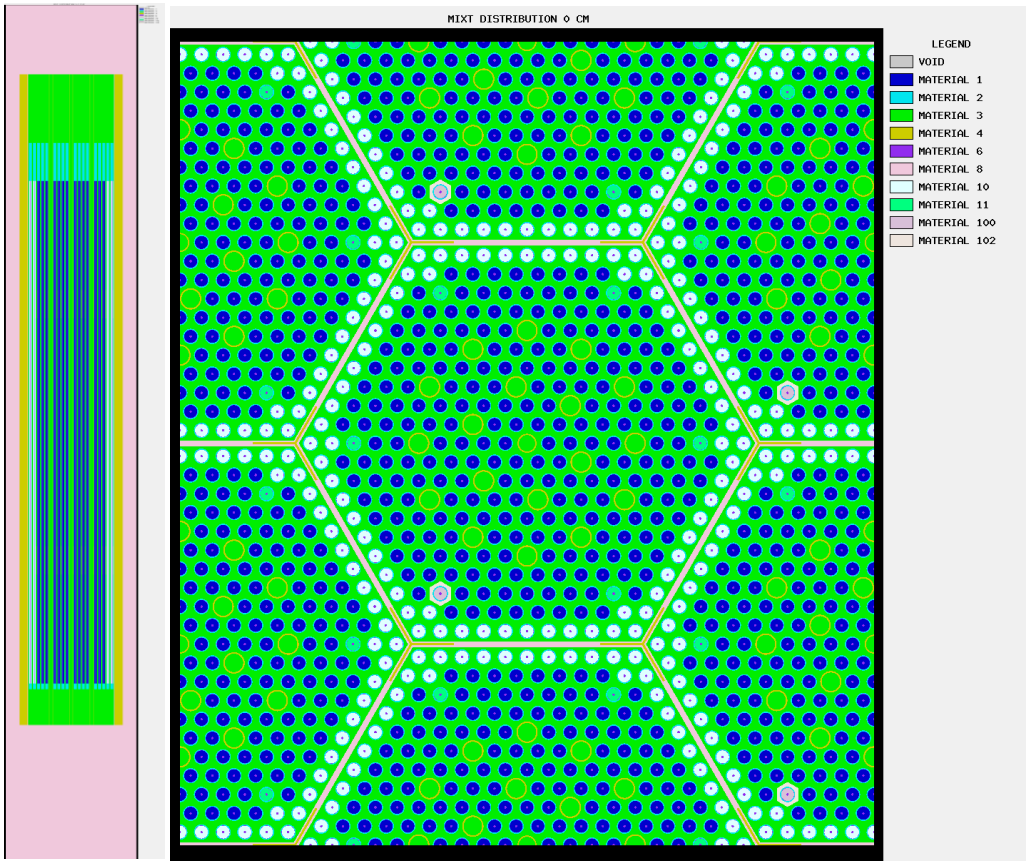

MATERIAL 1 – a fuel pellet of fuel rod of the central zone (enrichment 4.0%);
MATERIAL 10 – a fuel pellet of fuel rod of the peripheral zone (enrichment 4.0%);
MATERIAL 11 – a fuel pellet of fuel rod with burnable absorber (enrichment 3.3%);
MATERIAL 100 – a fuel pellet of a separately allocated fuel rod with burnable absorber (enrichment 3.3%);
MATERIAL 2 – the shell of the fuel rod;
MATERIAL 3 – water in the inner space FA;
MATERIAL 102 – water around the separately allocated fuel rod of the central zone
MATERIAL 4 – central pipe, guide channels, and angles;
MATERIAL 6 – the internal space of the fuel rod which is filled with helium;
MATERIAL 8 – water in the space between the cassettes.

Figure 35 Longitudinal and cross-sections of the calculation model FA-A 4.39% with the separated fuel rod with burnable absorber

6.4 The results of the calculations

As part of the task, the concentration (Becquerel per ton of heavy metals in fresh fuel) was calculated depending on the burnup (MW*day/kg) of the following isotopes:

Cs - 134, 135, 137, 138, 139;
I - 129, 131, 132, 133, 134, 135;
Xe - 133, 135, 137, 138;
Kr - 85, 87, 88.

The results of the calculations are given in Table 18 through Table 25.

Table 18 Isotopic composition of separately selected fuel rod with burnable absorber FA-A type 398GO depending on the depth of burnup (1 to 26 MWd/kg)

Burnup	1.00	2.00	4.00	6.00	8.00	10.00	12.00	14.00	16.00	18.00	20.00	22.00	24.00	26.00
cs134	6.511E+09	3.336E+10	1.431E+11	2.981E+11	4.955E+11	7.485E+11	1.059E+12	1.424E+12	1.820E+12	2.275E+12	2.772E+12	3.318E+12	3.904E+12	4.521E+12
cs135	1.119E+06	2.196E+06	3.966E+06	5.412E+06	6.746E+06	8.046E+06	9.332E+06	1.061E+07	1.188E+07	1.314E+07	1.438E+07	1.561E+07	1.684E+07	1.806E+07
cs137	1.271E+11	2.642E+11	5.633E+11	8.811E+11	1.206E+12	1.531E+12	1.855E+12	2.178E+12	2.500E+12	2.821E+12	3.140E+12	3.458E+12	3.775E+12	4.090E+12
cs138	8.963E+13	9.506E+13	1.026E+14	1.055E+14	1.064E+14	1.060E+14	1.055E+14	1.049E+14	1.044E+14	1.039E+14	1.035E+14	1.030E+14	1.025E+14	1.021E+14
cs139	8.493E+13	8.976E+13	9.654E+13	9.906E+13	9.980E+13	9.936E+13	9.880E+13	9.819E+13	9.763E+13	9.710E+13	9.667E+13	9.610E+13	9.567E+13	9.519E+13
xe133	8.511E+13	9.532E+13	1.005E+14	1.041E+14	1.056E+14	1.057E+14	1.056E+14	1.054E+14	1.053E+14	1.051E+14	1.050E+14	1.049E+14	1.047E+14	1.045E+14
xe135	5.916E+13	5.459E+13	4.481E+13	3.569E+13	3.252E+13	3.156E+13	3.122E+13	3.095E+13	3.064E+13	3.037E+13	2.980E+13	2.946E+13	2.920E+13	2.858E+13
xe137	8.411E+13	8.950E+13	9.702E+13	9.971E+13	1.006E+14	1.006E+14	1.004E+14	1.001E+14	9.989E+13	9.967E+13	9.954E+13	9.932E+13	9.910E+13	9.893E+13
xe138	8.419E+13	8.876E+13	9.519E+13	9.758E+13	9.823E+13	9.776E+13	9.710E+13	9.650E+13	9.589E+13	9.532E+13	9.489E+13	9.432E+13	9.380E+13	9.337E+13
i129	2.141E+04	4.803E+04	1.121E+05	1.842E+05	2.604E+05	3.391E+05	4.196E+05	5.016E+05	5.855E+05	6.703E+05	7.559E+05	8.428E+05	9.306E+05	1.019E+06
i131	3.493E+13	4.241E+13	4.877E+13	5.107E+13	5.212E+13	5.255E+13	5.281E+13	5.307E+13	5.325E+13	5.346E+13	5.359E+13	5.377E+13	5.390E+13	5.403E+13
i132	6.111E+13	6.646E+13	7.328E+13	7.581E+13	7.685E+13	7.724E+13	7.750E+13	7.772E+13	7.789E+13	7.811E+13	7.820E+13	7.837E+13	7.850E+13	7.859E+13
i133	9.167E+13	9.802E+13	1.075E+14	1.106E+14	1.117E+14	1.117E+14	1.115E+14	1.113E+14	1.111E+14	1.110E+14	1.108E+14	1.106E+14	1.104E+14	1.102E+14
i134	1.068E+14	1.134E+14	1.226E+14	1.259E+14	1.270E+14	1.267E+14	1.263E+14	1.259E+14	1.254E+14	1.250E+14	1.247E+14	1.242E+14	1.239E+14	1.235E+14
i135	8.785E+13	9.367E+13	1.017E+14	1.044E+14	1.054E+14	1.055E+14	1.054E+14	1.054E+14	1.053E+14	1.052E+14	1.051E+14	1.051E+14	1.050E+14	1.049E+14
kr85	1.505E+10	3.074E+10	6.372E+10	9.780E+10	1.319E+11	1.650E+11	1.970E+11	2.279E+11	2.577E+11	2.864E+11	3.142E+11	3.410E+11	3.669E+11	3.918E+11
kr87	3.187E+13	3.264E+13	3.382E+13	3.429E+13	3.410E+13	3.331E+13	3.246E+13	3.157E+13	3.077E+13	2.994E+13	2.928E+13	2.847E+13	2.778E+13	2.709E+13
kr88	4.307E+13	4.408E+13	4.568E+13	4.638E+13	4.612E+13	4.499E+13	4.381E+13	4.255E+13	4.141E+13	4.025E+13	3.932E+13	3.818E+13	3.720E+13	3.624E+13

Table 19 Isotopic composition of separately selected fuel rod with burnable absorber FA-A type 398GO depending on the depth of burnup (28 to 54 MWd/kg)

Burnup	28.00	30.00	32.00	34.00	36.00	38.00	40.00	42.00	44.00	46.00	48.00	50.00	52.00	54.00
cs134	5.168E+12	5.846E+12	6.568E+12	7.311E+12	8.063E+12	8.793E+12	9.597E+12	1.043E+13	1.123E+13	1.209E+13	1.301E+13	1.393E+13	1.476E+13	1.565E+13
cs135	1.928E+07	2.048E+07	2.168E+07	2.288E+07	2.407E+07	2.525E+07	2.643E+07	2.762E+07	2.881E+07	3.000E+07	3.119E+07	3.239E+07	3.360E+07	3.482E+07
cs137	4.403E+12	4.716E+12	5.029E+12	5.342E+12	5.651E+12	5.959E+12	6.268E+12	6.572E+12	6.876E+12	7.181E+12	7.481E+12	7.785E+12	8.085E+12	8.380E+12
cs138	1.017E+14	1.013E+14	1.009E+14	1.005E+14	1.002E+14	9.989E+13	9.954E+13	9.915E+13	9.889E+13	9.858E+13	9.828E+13	9.802E+13	9.776E+13	9.754E+13
cs139	9.471E+13	9.437E+13	9.393E+13	9.354E+13	9.319E+13	9.289E+13	9.250E+13	9.215E+13	9.184E+13	9.154E+13	9.124E+13	9.093E+13	9.067E+13	9.045E+13
xe133	1.044E+14	1.043E+14	1.041E+14	1.041E+14	1.039E+14	1.038E+14	1.036E+14	1.035E+14	1.034E+14	1.032E+14	1.031E+14	1.029E+14	1.029E+14	1.083E+14
xe135	2.853E+13	2.784E+13	2.760E+13	2.720E+13	2.660E+13	2.618E+13	2.595E+13	2.568E+13	2.521E+13	2.481E+13	2.453E+13	2.422E+13	2.411E+13	2.385E+13
xe137	9.876E+13	9.863E+13	9.845E+13	9.828E+13	9.815E+13	9.802E+13	9.784E+13	9.767E+13	9.758E+13	9.741E+13	9.728E+13	9.715E+13	9.706E+13	9.697E+13
xe138	9.284E+13	9.250E+13	9.206E+13	9.163E+13	9.128E+13	9.093E+13	9.058E+13	9.019E+13	8.989E+13	8.958E+13	8.924E+13	8.893E+13	8.867E+13	8.841E+13
i129	1.109E+06	1.199E+06	1.290E+06	1.381E+06	1.473E+06	1.565E+06	1.657E+06	1.750E+06	1.843E+06	1.936E+06	2.029E+06	2.123E+06	2.217E+06	2.310E+06
i131	5.416E+13	5.429E+13	5.438E+13	5.451E+13	5.459E+13	5.464E+13	5.472E+13	5.477E+13	5.490E+13	5.490E+13	5.494E+13	5.499E+13	5.512E+13	5.516E+13
i132	7.872E+13	7.880E+13	7.889E+13	7.898E+13	7.907E+13	7.907E+13	7.911E+13	7.915E+13	7.924E+13	7.924E+13	7.928E+13	7.928E+13	7.941E+13	7.989E+13
i133	1.101E+14	1.099E+14	1.097E+14	1.096E+14	1.094E+14	1.092E+14	1.091E+14	1.089E+14	1.088E+14	1.086E+14	1.084E+14	1.083E+14	1.082E+14	1.075E+14
i134	1.231E+14	1.228E+14	1.225E+14	1.221E+14	1.218E+14	1.216E+14	1.213E+14	1.210E+14	1.207E+14	1.204E+14	1.201E+14	1.199E+14	1.197E+14	1.195E+14
i135	1.049E+14	1.048E+14	1.048E+14	1.047E+14	1.046E+14	1.046E+14	1.045E+14	1.044E+14	1.044E+14	1.043E+14	1.042E+14	1.041E+14	1.041E+14	1.041E+14
kr85	4.158E+11	4.390E+11	4.616E+11	4.829E+11	5.038E+11	5.242E+11	5.438E+11	5.625E+11	5.807E+11	5.981E+11	6.151E+11	6.311E+11	6.472E+11	6.624E+11
kr87	2.638E+13	2.579E+13	2.515E+13	2.455E+13	2.401E+13	2.351E+13	2.296E+13	2.242E+13	2.196E+13	2.150E+13	2.104E+13	2.062E+13	2.019E+13	1.983E+13
kr88	3.523E+13	3.440E+13	3.350E+13	3.266E+13	3.190E+13	3.120E+13	3.042E+13	2.967E+13	2.902E+13	2.837E+13	2.773E+13	2.714E+13	2.652E+13	2.601E+13

Table 20 Isotopic composition of separately selected fuel rod FA-A type 398GO depending on the depth of burnup (1 to 26 MWd/kg)

Burnup	1.00	2.00	4.00	6.00	8.00	10.00	12.00	14.00	16.00	18.00	20.00	22.00	24.00	26.00
cs134	4.373E+09	2.451E+10	1.154E+11	2.712E+11	4.877E+11	7.563E+11	1.078E+12	1.453E+12	1.896E+12	2.360E+12	2.883E+12	3.439E+12	4.032E+12	4.668E+12
cs135	6.685E+05	1.357E+06	2.752E+06	4.153E+06	5.559E+06	6.959E+06	8.354E+06	9.750E+06	1.114E+07	1.251E+07	1.387E+07	1.523E+07	1.659E+07	1.792E+07
cs137	1.681E+11	3.360E+11	6.711E+11	1.005E+12	1.338E+12	1.670E+12	2.001E+12	2.330E+12	2.658E+12	2.986E+12	3.312E+12	3.637E+12	3.960E+12	4.283E+12
cs138	1.141E+14	1.135E+14	1.124E+14	1.114E+14	1.105E+14	1.098E+14	1.091E+14	1.085E+14	1.079E+14	1.074E+14	1.069E+14	1.064E+14	1.059E+14	1.054E+14
cs139	1.079E+14	1.072E+14	1.060E+14	1.049E+14	1.039E+14	1.032E+14	1.024E+14	1.017E+14	1.011E+14	1.005E+14	1.000E+14	9.945E+13	9.893E+13	9.850E+13
xe133	1.095E+14	1.144E+14	1.085E+14	1.084E+14	1.083E+14	1.082E+14	1.081E+14	1.079E+14	1.078E+14	1.077E+14	1.076E+14	1.074E+14	1.073E+14	1.072E+14
xe135	3.326E+13	3.354E+13	3.401E+13	3.415E+13	3.428E+13	3.398E+13	3.387E+13	3.382E+13	3.352E+13	3.306E+13	3.264E+13	3.239E+13	3.230E+13	3.140E+13
xe137	1.052E+14	1.050E+14	1.045E+14	1.041E+14	1.037E+14	1.034E+14	1.031E+14	1.028E+14	1.025E+14	1.023E+14	1.021E+14	1.019E+14	1.017E+14	1.016E+14
xe138	1.070E+14	1.062E+14	1.048E+14	1.036E+14	1.025E+14	1.017E+14	1.009E+14	1.001E+14	9.941E+13	9.880E+13	9.828E+13	9.767E+13	9.715E+13	9.667E+13
i129	2.558E+04	5.425E+04	1.173E+05	1.855E+05	2.575E+05	3.322E+05	4.093E+05	4.886E+05	5.694E+05	6.520E+05	7.355E+05	8.206E+05	9.071E+05	9.945E+05
i131	4.425E+13	4.990E+13	5.129E+13	5.190E+13	5.242E+13	5.281E+13	5.316E+13	5.346E+13	5.377E+13	5.399E+13	5.420E+13	5.442E+13	5.459E+13	5.477E+13
i132	7.550E+13	7.628E+13	7.659E+13	7.715E+13	7.767E+13	7.802E+13	7.837E+13	7.867E+13	7.894E+13	7.915E+13	7.937E+13	7.954E+13	7.972E+13	7.989E+13
i133	1.146E+14	1.145E+14	1.150E+14	1.148E+14	1.146E+14	1.144E+14	1.142E+14	1.141E+14	1.138E+14	1.137E+14	1.135E+14	1.134E+14	1.132E+14	1.130E+14
i134	1.341E+14	1.336E+14	1.327E+14	1.320E+14	1.313E+14	1.307E+14	1.301E+14	1.296E+14	1.291E+14	1.287E+14	1.283E+14	1.279E+14	1.275E+14	1.271E+14
i135	1.085E+14	1.084E+14	1.083E+14	1.081E+14	1.080E+14	1.079E+14	1.078E+14	1.078E+14	1.077E+14	1.076E+14	1.075E+14	1.075E+14	1.074E+14	1.074E+14
kr85	2.129E+10	4.228E+10	8.280E+10	1.216E+11	1.588E+11	1.946E+11	2.292E+11	2.625E+11	2.945E+11	3.255E+11	3.555E+11	3.843E+11	4.122E+11	4.390E+11
kr87	4.254E+13	4.165E+13	4.004E+13	3.865E+13	3.739E+13	3.634E+13	3.529E+13	3.433E+13	3.340E+13	3.257E+13	3.181E+13	3.098E+13	3.022E+13	2.954E+13
kr88	5.803E+13	5.677E+13	5.446E+13	5.251E+13	5.073E+13	4.925E+13	4.773E+13	4.638E+13	4.507E+13	4.390E+13	4.283E+13	4.166E+13	4.059E+13	3.962E+13

Table 21 Isotopic composition of separately selected fuel rod FA-A type 398GO depending on the depth of burnup (28 to 54 MWd/kg)

Burnup	28.00	30.00	32.00	34.00	36.00	38.00	40.00	42.00	44.00	46.00	48.00	50.00	52.00	54.00
cs134	5.312E+12	6.011E+12	6.737E+12	7.511E+12	8.306E+12	9.132E+12	9.915E+12	1.076E+13	1.158E+13	1.241E+13	1.331E+13	1.418E+13	1.510E+13	1.600E+13
cs135	1.925E+07	2.057E+07	2.188E+07	2.318E+07	2.448E+07	2.578E+07	2.707E+07	2.836E+07	2.963E+07	3.091E+07	3.220E+07	3.347E+07	3.476E+07	3.606E+07
cs137	4.603E+12	4.925E+12	5.242E+12	5.559E+12	5.877E+12	6.194E+12	6.507E+12	6.820E+12	7.133E+12	7.441E+12	7.750E+12	8.059E+12	8.367E+12	8.672E+12
cs138	1.050E+14	1.046E+14	1.042E+14	1.038E+14	1.035E+14	1.031E+14	1.028E+14	1.024E+14	1.021E+14	1.018E+14	1.014E+14	1.011E+14	1.008E+14	1.006E+14
cs139	9.802E+13	9.758E+13	9.715E+13	9.676E+13	9.637E+13	9.597E+13	9.563E+13	9.524E+13	9.497E+13	9.458E+13	9.419E+13	9.393E+13	9.358E+13	9.332E+13
xe133	1.071E+14	1.069E+14	1.068E+14	1.067E+14	1.065E+14	1.064E+14	1.064E+14	1.062E+14	1.061E+14	1.060E+14	1.058E+14	1.057E+14	1.056E+14	1.111E+14
xe135	3.121E+13	3.092E+13	3.017E+13	2.981E+13	2.944E+13	2.894E+13	2.857E+13	2.824E+13	2.735E+13	2.728E+13	2.707E+13	2.632E+13	2.624E+13	2.595E+13
xe137	1.014E+14	1.012E+14	1.011E+14	1.009E+14	1.008E+14	1.006E+14	1.005E+14	1.003E+14	1.002E+14	1.000E+14	9.989E+13	9.976E+13	9.963E+13	9.954E+13
xe138	9.619E+13	9.571E+13	9.528E+13	9.489E+13	9.445E+13	9.406E+13	9.367E+13	9.328E+13	9.297E+13	9.258E+13	9.219E+13	9.193E+13	9.154E+13	9.132E+13
i129	1.083E+06	1.172E+06	1.262E+06	1.352E+06	1.444E+06	1.536E+06	1.628E+06	1.721E+06	1.814E+06	1.908E+06	2.002E+06	2.096E+06	2.190E+06	2.285E+06
i131	5.494E+13	5.507E+13	5.520E+13	5.529E+13	5.546E+13	5.555E+13	5.568E+13	5.577E+13	5.581E+13	5.594E+13	5.598E+13	5.607E+13	5.616E+13	5.620E+13
i132	8.002E+13	8.015E+13	8.024E+13	8.037E+13	8.050E+13	8.054E+13	8.067E+13	8.076E+13	8.076E+13	8.089E+13	8.093E+13	8.098E+13	8.107E+13	8.159E+13
i133	1.129E+14	1.127E+14	1.125E+14	1.124E+14	1.122E+14	1.121E+14	1.119E+14	1.118E+14	1.116E+14	1.115E+14	1.113E+14	1.112E+14	1.110E+14	1.104E+14
i134	1.267E+14	1.264E+14	1.261E+14	1.257E+14	1.254E+14	1.251E+14	1.248E+14	1.245E+14	1.243E+14	1.240E+14	1.237E+14	1.234E+14	1.231E+14	1.230E+14
i135	1.073E+14	1.072E+14	1.072E+14	1.071E+14	1.071E+14	1.070E+14	1.070E+14	1.069E+14	1.069E+14	1.068E+14	1.068E+14	1.067E+14	1.066E+14	1.066E+14
kr85	4.651E+11	4.903E+11	5.146E+11	5.381E+11	5.607E+11	5.825E+11	6.038E+11	6.237E+11	6.437E+11	6.629E+11	6.811E+11	6.985E+11	7.159E+11	7.320E+11
kr87	2.881E+13	2.813E+13	2.749E+13	2.685E+13	2.624E+13	2.565E+13	2.508E+13	2.454E+13	2.407E+13	2.350E+13	2.297E+13	2.254E+13	2.202E+13	2.161E+13
kr88	3.861E+13	3.766E+13	3.676E+13	3.585E+13	3.499E+13	3.415E+13	3.336E+13	3.260E+13	3.194E+13	3.113E+13	3.038E+13	2.977E+13	2.904E+13	2.846E+13

Table 22 Isotopic composition of separately selected fuel rod with burnable absorber FA-A type 439GT depending on the depth of burnup (1 to 26 MWd/kg)

Burnup	1.00	2.00	4.00	6.00	8.00	10.00	12.00	14.00	16.00	18.00	20.00	22.00	24.00	26.00
cs134	6.142E+09	3.203E+10	1.363E+11	2.902E+11	4.799E+11	7.272E+11	1.029E+12	1.380E+12	1.760E+12	2.192E+12	2.668E+12	3.183E+12	3.729E+12	4.324E+12
cs135	1.151E+06	2.282E+06	4.215E+06	5.798E+06	7.228E+06	8.606E+06	9.967E+06	1.133E+07	1.266E+07	1.399E+07	1.532E+07	1.663E+07	1.793E+07	1.923E+07
cs137	1.258E+11	2.598E+11	5.481E+11	8.528E+11	1.165E+12	1.480E+12	1.793E+12	2.105E+12	2.416E+12	2.726E+12	3.034E+12	3.342E+12	3.649E+12	3.954E+12
cs138	8.798E+13	9.228E+13	9.889E+13	1.015E+14	1.028E+14	1.027E+14	1.022E+14	1.017E+14	1.013E+14	1.008E+14	1.003E+14	9.993E+13	9.954E+13	9.910E+13
cs139	8.337E+13	8.719E+13	9.311E+13	9.537E+13	9.645E+13	9.628E+13	9.580E+13	9.519E+13	9.476E+13	9.424E+13	9.371E+13	9.332E+13	9.293E+13	9.245E+13
xe133	8.385E+13	9.284E+13	9.676E+13	1.001E+14	1.018E+14	1.022E+14	1.021E+14	1.020E+14	1.019E+14	1.018E+14	1.016E+14	1.015E+14	1.014E+14	1.012E+14
xe135	6.042E+13	5.707E+13	4.899E+13	3.918E+13	3.490E+13	3.362E+13	3.313E+13	3.318E+13	3.229E+13	3.217E+13	3.206E+13	3.162E+13	3.108E+13	3.093E+13
xe137	8.246E+13	8.680E+13	9.341E+13	9.593E+13	9.719E+13	9.732E+13	9.715E+13	9.689E+13	9.676E+13	9.654E+13	9.632E+13	9.619E+13	9.602E+13	9.584E+13
xe138	8.267E+13	8.624E+13	9.184E+13	9.393E+13	9.497E+13	9.476E+13	9.419E+13	9.354E+13	9.315E+13	9.254E+13	9.202E+13	9.158E+13	9.119E+13	9.071E+13
i129	2.107E+04	4.681E+04	1.081E+05	1.771E+05	2.501E+05	3.254E+05	4.024E+05	4.812E+05	5.607E+05	6.420E+05	7.242E+05	8.072E+05	8.911E+05	9.758E+05
i131	3.439E+13	4.123E+13	4.681E+13	4.903E+13	5.016E+13	5.068E+13	5.090E+13	5.116E+13	5.129E+13	5.151E+13	5.168E+13	5.186E+13	5.199E+13	5.207E+13
i132	5.994E+13	6.437E+13	7.046E+13	7.285E+13	7.411E+13	7.455E+13	7.476E+13	7.502E+13	7.515E+13	7.533E+13	7.546E+13	7.563E+13	7.576E+13	7.585E+13
i133	8.989E+13	9.502E+13	1.035E+14	1.064E+14	1.078E+14	1.080E+14	1.079E+14	1.077E+14	1.076E+14	1.074E+14	1.072E+14	1.071E+14	1.069E+14	1.068E+14
i134	1.048E+14	1.101E+14	1.182E+14	1.212E+14	1.227E+14	1.227E+14	1.224E+14	1.219E+14	1.216E+14	1.211E+14	1.208E+14	1.204E+14	1.201E+14	1.198E+14
i135	8.606E+13	9.076E+13	9.789E+13	1.005E+14	1.018E+14	1.020E+14	1.020E+14	1.019E+14	1.018E+14	1.018E+14	1.017E+14	1.017E+14	1.016E+14	1.015E+14
kr85	1.496E+10	3.040E+10	6.233E+10	9.515E+10	1.281E+11	1.603E+11	1.916E+11	2.218E+11	2.511E+11	2.794E+11	3.067E+11	3.331E+11	3.586E+11	3.833E+11
kr87	3.143E+13	3.193E+13	3.283E+13	3.309E+13	3.312E+13	3.253E+13	3.180E+13	3.092E+13	3.030E+13	2.951E+13	2.877E+13	2.813E+13	2.751E+13	2.684E+13
kr88	4.248E+13	4.314E+13	4.434E+13	4.473E+13	4.477E+13	4.394E+13	4.291E+13	4.168E+13	4.080E+13	3.969E+13	3.865E+13	3.775E+13	3.687E+13	3.593E+13

Table 23 Isotopic composition of separately selected fuel rod with burnable absorber FA-A type 439GT depending on the depth of burnup (28 to 54 MWd/kg)

Burnup	28.00	30.00	32.00	34.00	36.00	38.00	40.00	42.00	44.00	46.00	48.00	50.00	52.00	54.00
cs134	4.933E+12	5.577E+12	6.224E+12	6.937E+12	7.641E+12	8.350E+12	9.106E+12	9.854E+12	1.061E+13	1.143E+13	1.227E+13	1.311E+13	1.397E+13	1.481E+13
cs135	2.052E+07	2.179E+07	2.305E+07	2.431E+07	2.556E+07	2.680E+07	2.805E+07	2.928E+07	3.052E+07	3.175E+07	3.298E+07	3.421E+07	3.544E+07	3.668E+07
cs137	4.258E+12	4.560E+12	4.864E+12	5.164E+12	5.464E+12	5.764E+12	6.059E+12	6.355E+12	6.650E+12	6.942E+12	7.237E+12	7.528E+12	7.820E+12	8.107E+12
cs138	9.871E+13	9.841E+13	9.806E+13	9.767E+13	9.737E+13	9.706E+13	9.671E+13	9.645E+13	9.615E+13	9.584E+13	9.558E+13	9.532E+13	9.502E+13	9.489E+13
cs139	9.206E+13	9.171E+13	9.137E+13	9.098E+13	9.067E+13	9.032E+13	8.998E+13	8.967E+13	8.937E+13	8.911E+13	8.880E+13	8.850E+13	8.819E+13	8.806E+13
xe133	1.011E+14	1.010E+14	1.009E+14	1.008E+14	1.006E+14	1.005E+14	1.004E+14	1.002E+14	1.001E+14	9.997E+13	9.989E+13	9.976E+13	9.967E+13	1.050E+14
xe135	3.047E+13	2.982E+13	2.956E+13	2.907E+13	2.875E+13	2.829E+13	2.823E+13	2.746E+13	2.724E+13	2.674E+13	2.639E+13	2.594E+13	2.578E+13	2.547E+13
xe137	9.567E+13	9.554E+13	9.537E+13	9.524E+13	9.510E+13	9.497E+13	9.480E+13	9.471E+13	9.458E+13	9.445E+13	9.432E+13	9.419E+13	9.406E+13	9.402E+13
xe138	9.028E+13	8.993E+13	8.954E+13	8.919E+13	8.885E+13	8.850E+13	8.811E+13	8.785E+13	8.750E+13	8.724E+13	8.689E+13	8.663E+13	8.628E+13	8.611E+13
i129	1.061E+06	1.148E+06	1.234E+06	1.322E+06	1.410E+06	1.498E+06	1.586E+06	1.675E+06	1.764E+06	1.853E+06	1.943E+06	2.033E+06	2.123E+06	2.213E+06
i131	5.225E+13	5.233E+13	5.242E+13	5.251E+13	5.259E+13	5.264E+13	5.277E+13	5.281E+13	5.290E+13	5.290E+13	5.299E+13	5.303E+13	5.312E+13	5.316E+13
i132	7.598E+13	7.607E+13	7.611E+13	7.620E+13	7.624E+13	7.628E+13	7.637E+13	7.641E+13	7.650E+13	7.646E+13	7.654E+13	7.659E+13	7.663E+13	7.715E+13
i133	1.066E+14	1.064E+14	1.063E+14	1.061E+14	1.060E+14	1.058E+14	1.057E+14	1.055E+14	1.054E+14	1.052E+14	1.051E+14	1.049E+14	1.048E+14	1.042E+14
i134	1.194E+14	1.191E+14	1.188E+14	1.185E+14	1.183E+14	1.180E+14	1.177E+14	1.174E+14	1.172E+14	1.169E+14	1.167E+14	1.164E+14	1.162E+14	1.161E+14
i135	1.015E+14	1.014E+14	1.014E+14	1.013E+14	1.012E+14	1.012E+14	1.011E+14	1.011E+14	1.010E+14	1.009E+14	1.009E+14	1.008E+14	1.008E+14	1.008E+14
kr85	4.072E+11	4.303E+11	4.525E+11	4.742E+11	4.951E+11	5.155E+11	5.351E+11	5.538E+11	5.720E+11	5.898E+11	6.068E+11	6.233E+11	6.394E+11	6.546E+11
kr87	2.621E+13	2.568E+13	2.509E+13	2.455E+13	2.406E+13	2.353E+13	2.299E+13	2.254E+13	2.208E+13	2.167E+13	2.118E+13	2.080E+13	2.037E+13	2.003E+13
kr88	3.503E+13	3.430E+13	3.347E+13	3.271E+13	3.201E+13	3.128E+13	3.051E+13	2.988E+13	2.923E+13	2.865E+13	2.797E+13	2.743E+13	2.683E+13	2.635E+13

Table 24 Isotopic composition of separately selected fuel rod FA-A type 439GT depending on the depth of burnup (1 to 26 MWd/kg)

Burnup	1.00	2.00	4.00	6.00	8.00	10.00	12.00	14.00	16.00	18.00	20.00	22.00	24.00	26.00
cs134	4.306E+09	2.390E+10	1.121E+11	2.630E+11	4.768E+11	7.420E+11	1.041E+12	1.402E+12	1.819E+12	2.291E+12	2.776E+12	3.288E+12	3.851E+12	4.477E+12
cs135	7.307E+05	1.481E+06	3.006E+06	4.529E+06	6.051E+06	7.568E+06	9.067E+06	1.057E+07	1.205E+07	1.352E+07	1.500E+07	1.646E+07	1.790E+07	1.933E+07
cs137	1.681E+11	3.360E+11	6.711E+11	1.005E+12	1.338E+12	1.670E+12	2.001E+12	2.331E+12	2.659E+12	2.987E+12	3.313E+12	3.638E+12	3.962E+12	4.284E+12
cs138	1.141E+14	1.136E+14	1.126E+14	1.117E+14	1.109E+14	1.102E+14	1.096E+14	1.090E+14	1.084E+14	1.080E+14	1.074E+14	1.070E+14	1.066E+14	1.061E+14
cs139	1.080E+14	1.074E+14	1.062E+14	1.052E+14	1.044E+14	1.036E+14	1.030E+14	1.023E+14	1.017E+14	1.011E+14	1.006E+14	1.001E+14	9.967E+13	9.919E+13
xe133	1.095E+14	1.144E+14	1.086E+14	1.085E+14	1.084E+14	1.083E+14	1.082E+14	1.081E+14	1.079E+14	1.078E+14	1.077E+14	1.076E+14	1.075E+14	1.073E+14
xe135	3.636E+13	3.651E+13	3.720E+13	3.712E+13	3.707E+13	3.682E+13	3.649E+13	3.636E+13	3.605E+13	3.546E+13	3.557E+13	3.500E+13	3.445E+13	3.415E+13
xe137	1.053E+14	1.050E+14	1.046E+14	1.042E+14	1.038E+14	1.035E+14	1.033E+14	1.030E+14	1.028E+14	1.026E+14	1.024E+14	1.022E+14	1.020E+14	1.018E+14
xe138	1.071E+14	1.063E+14	1.051E+14	1.040E+14	1.030E+14	1.022E+14	1.015E+14	1.008E+14	1.001E+14	9.954E+13	9.889E+13	9.841E+13	9.793E+13	9.741E+13
i129	2.552E+04	5.403E+04	1.166E+05	1.840E+05	2.547E+05	3.281E+05	4.037E+05	4.812E+05	5.603E+05	6.411E+05	7.233E+05	8.067E+05	8.911E+05	9.767E+05
i131	4.421E+13	4.986E+13	5.120E+13	5.177E+13	5.220E+13	5.259E+13	5.294E+13	5.320E+13	5.351E+13	5.368E+13	5.394E+13	5.412E+13	5.429E+13	5.446E+13
i132	7.546E+13	7.624E+13	7.646E+13	7.702E+13	7.741E+13	7.781E+13	7.815E+13	7.841E+13	7.867E+13	7.885E+13	7.911E+13	7.928E+13	7.941E+13	7.959E+13
i133	1.145E+14	1.145E+14	1.150E+14	1.148E+14	1.146E+14	1.145E+14	1.143E+14	1.141E+14	1.140E+14	1.138E+14	1.137E+14	1.135E+14	1.134E+14	1.132E+14
i134	1.341E+14	1.337E+14	1.329E+14	1.322E+14	1.316E+14	1.310E+14	1.305E+14	1.300E+14	1.296E+14	1.292E+14	1.287E+14	1.284E+14	1.280E+14	1.276E+14
i135	1.085E+14	1.084E+14	1.083E+14	1.082E+14	1.081E+14	1.080E+14	1.079E+14	1.078E+14	1.077E+14	1.077E+14	1.076E+14	1.075E+14	1.075E+14	1.074E+14
kr85	2.132E+10	4.237E+10	8.311E+10	1.222E+11	1.599E+11	1.963E+11	2.315E+11	2.654E+11	2.983E+11	3.301E+11	3.608E+11	3.905E+11	4.194E+11	4.473E+11
kr87	4.263E+13	4.183E+13	4.034E+13	3.907E+13	3.797E+13	3.694E+13	3.601E+13	3.511E+13	3.425E+13	3.350E+13	3.265E+13	3.196E+13	3.128E+13	3.055E+13
kr88	5.811E+13	5.698E+13	5.485E+13	5.307E+13	5.151E+13	5.007E+13	4.877E+13	4.747E+13	4.629E+13	4.521E+13	4.399E+13	4.303E+13	4.208E+13	4.105E+13

Table 25 Isotopic composition of separately selected fuel rod FA-A type 439GT depending on the depth of burnup (28 to 54 MWd/kg)

Burnup	28.00	30.00	32.00	34.00	36.00	38.00	40.00	42.00	44.00	46.00	48.00	50.00	52.00	54.00
cs134	5.125E+12	5.807E+12	6.520E+12	7.237E+12	7.963E+12	8.715E+12	9.528E+12	1.032E+13	1.119E+13	1.208E+13	1.295E+13	1.386E+13	1.477E+13	1.566E+13
cs135	2.075E+07	2.215E+07	2.354E+07	2.492E+07	2.631E+07	2.768E+07	2.904E+07	3.039E+07	3.174E+07	3.309E+07	3.443E+07	3.576E+07	3.710E+07	3.844E+07
cs137	4.607E+12	4.925E+12	5.246E+12	5.564E+12	5.881E+12	6.194E+12	6.511E+12	6.824E+12	7.137E+12	7.446E+12	7.754E+12	8.063E+12	8.372E+12	8.676E+12
cs138	1.057E+14	1.053E+14	1.049E+14	1.045E+14	1.041E+14	1.038E+14	1.035E+14	1.031E+14	1.028E+14	1.024E+14	1.021E+14	1.018E+14	1.015E+14	1.013E+14
cs139	9.876E+13	9.832E+13	9.793E+13	9.750E+13	9.710E+13	9.671E+13	9.637E+13	9.606E+13	9.563E+13	9.528E+13	9.497E+13	9.463E+13	9.437E+13	9.415E+13
xe133	1.072E+14	1.071E+14	1.070E+14	1.069E+14	1.068E+14	1.066E+14	1.065E+14	1.064E+14	1.062E+14	1.061E+14	1.061E+14	1.059E+14	1.058E+14	1.114E+14
xe135	3.363E+13	3.305E+13	3.245E+13	3.229E+13	3.189E+13	3.147E+13	3.087E+13	3.015E+13	3.003E+13	2.953E+13	2.886E+13	2.854E+13	2.808E+13	2.758E+13
xe137	1.017E+14	1.015E+14	1.013E+14	1.012E+14	1.010E+14	1.008E+14	1.007E+14	1.006E+14	1.004E+14	1.003E+14	1.001E+14	1.000E+14	9.989E+13	9.989E+13
xe138	9.697E+13	9.650E+13	9.610E+13	9.567E+13	9.524E+13	9.484E+13	9.445E+13	9.415E+13	9.371E+13	9.337E+13	9.302E+13	9.267E+13	9.237E+13	9.215E+13
i129	1.063E+06	1.150E+06	1.238E+06	1.327E+06	1.417E+06	1.507E+06	1.597E+06	1.689E+06	1.780E+06	1.873E+06	1.965E+06	2.058E+06	2.151E+06	2.244E+06
i131	5.459E+13	5.477E+13	5.490E+13	5.503E+13	5.516E+13	5.525E+13	5.538E+13	5.542E+13	5.555E+13	5.564E+13	5.577E+13	5.581E+13	5.585E+13	5.594E+13
i132	7.972E+13	7.985E+13	7.998E+13	8.007E+13	8.020E+13	8.028E+13	8.037E+13	8.041E+13	8.054E+13	8.063E+13	8.072E+13	8.072E+13	8.080E+13	8.133E+13
i133	1.131E+14	1.129E+14	1.128E+14	1.126E+14	1.124E+14	1.123E+14	1.121E+14	1.120E+14	1.118E+14	1.117E+14	1.116E+14	1.114E+14	1.113E+14	1.107E+14
i134	1.273E+14	1.270E+14	1.267E+14	1.263E+14	1.260E+14	1.257E+14	1.254E+14	1.251E+14	1.248E+14	1.245E+14	1.242E+14	1.240E+14	1.237E+14	1.236E+14
i135	1.074E+14	1.073E+14	1.073E+14	1.072E+14	1.071E+14	1.071E+14	1.070E+14	1.070E+14	1.069E+14	1.069E+14	1.068E+14	1.068E+14	1.067E+14	1.068E+14
kr85	4.742E+11	5.003E+11	5.255E+11	5.503E+11	5.738E+11	5.964E+11	6.185E+11	6.398E+11	6.607E+11	6.807E+11	6.998E+11	7.185E+11	7.363E+11	7.537E+11
kr87	2.993E+13	2.926E+13	2.863E+13	2.801E+13	2.737E+13	2.680E+13	2.623E+13	2.571E+13	2.512E+13	2.461E+13	2.412E+13	2.362E+13	2.319E+13	2.272E+13
kr88	4.018E+13	3.923E+13	3.835E+13	3.747E+13	3.656E+13	3.576E+13	3.497E+13	3.423E+13	3.340E+13	3.269E+13	3.200E+13	3.130E+13	3.068E+13	3.003E+13

6.5 Summary

The best-estimate models for the SCALE software package were developed for the selected representative types of fuel assemblies used in WWER-1000 reactors of Ukrainian NPPs.

With use of the developed models the best-estimated source term for LOCA radiological consequences analysis is evaluated. As result the relevant knowledge on WWER-1000 fuel characteristics and its evolution characterization during in-core irradiation is enhanced. It gives possibility to decrease level of conservatism of assessment of LOCA radiological consequences.

6.6 References

[1] SCALE User's Manual. NUREG/CR-0200 Revision 6. RNL/NUREG/CSD-2/V2/R6

[2] U 0401.21.00.000 DKO. Complex components of the WWER-1000 fuel core (type V-320, 338), Catalog descriptions

7 VTT

VTT Technical Research Centre of Finland is developing new severe accident models for the Apros code. A general description of the Apros code is given in R2CA report D2.1.2 *Review of simulation codes and*

methodologies for LOCA and SGTR. The code is used extensively for analysis of design-basis accidents. The severe accident models of Apros have been limited to VVER-440 reactors, and they have not had many active users. Now the goal is to extend the capabilities of Apros from design-basis accidents towards more severe cases, applicable to all light-water reactors. The code is being developed with VTT's own funding. In the R2CA project, a validation calculation of the gravitational deposition of aerosols was performed.

7.1 Model description

The size distribution of aerosol particles is discretized into size bins. Because size distributions are generally modelled with logarithmic discretization, the ratio of particle diameters in successive size bins is kept constant. The default discretization in Apros is the same as in MELCOR: 10 size bins, minimum diameter of the smallest size bin 0.1 µm, and maximum diameter of the largest size bin 10 µm.

The deposition rate (kg/s) of aerosols on heat structures is calculated from

$$\frac{dm_k}{dt} = A_{dep} u_{dep,k} \frac{m_k}{V_{gas}}, \tag{10}$$

where m_k is the mass of aerosol particles in the node in size bin k, A_{dep} is the deposition area, and V_{gas} is the gas volume of the node. [1]

The deposition velocity (m/s) of gravitational deposition is calculated from

$$u_{dep,k} = \frac{\rho_p g C_c d_{p,k}^2}{18 \mu_{gas} \chi}, \tag{11}$$

where ρ_p is the density of the particles, g is the acceleration of gravity, $d_{p,k}$ is the geometric mean particle diameter in size bin k, and μ_{gas} is the dynamic viscosity of the gas in the node. [1] The particle dynamic shape factor χ is assumed to be unity (corresponding to spherical particles) but can be modified by the user.

The Cunningham slip correction factor [2] is

$$C_c = 1 + \frac{2\lambda}{d_p}\left(1.142 + 0.558 \exp\left(-0.999 \frac{d_p}{2\lambda}\right)\right). \tag{12}$$

For the mean free path of gas molecules, λ = 0.0673 µm is used, corresponding to air at atmospheric pressure and 23 °C.

7.2 AHMED experiment

The AHMED (Aerosol and Heat Transfer Measurement Device) experiment was chosen for the first validation case of the gravitational deposition model of Apros because it was performed in very simple thermal-hydraulic conditions: the test vessel was kept at a constant temperature, pressure and humidity. Due to the simple thermal hydraulics set-up of the experiment, the device was modelled as a single homogeneous, fully mixed volume without any spatial discretization. Because the vessel walls were kept at the same temperature as the air, gravitational deposition was the only significant deposition mechanism.

The AHMED tests were conducted at VTT Technical Research Centre of Finland in 1993 and 1994. [3] They were designed for studying the hygroscopic phenomenon, in which aerosol particles absorb moisture from air. However, the selected experiment was performed at a very low relative humidity, so that hygroscopic effects did not play any role in that test. A hygroscopic model has not yet been developed for Apros.

The test vessel was a cylindrical 1.81 m^3 vessel with diameter of 63.5 cm and height 142.5 cm. During the experiment, the aerosol particles deposited by gravitation on the 1.27 m^2 floor of the vessel. The selected NaOH test number 1 has been used in an OECD NEA code comparison exercise [4], [5]. The test was conducted at the atmospheric pressure. The vessel was filled with 50 °C air with relative humidity of 22 %. In the beginning of the test, NaOH particles were injected to the vessel so that their concentration was 0.112 g/m^3. The aerodynamic mass median diameter (*ammd*) of the injected aerosols was 2.4 µm and geometric standard deviation (*gsd*) 1.6. The density of NaOH is 2 130 kg/m^3. The NaOH mass concentration in the air was measured for 210 min, during which it decreased to about 17 % of the initial concentration. The mass median diameter of the particles decreased during the experiment because large particles deposited faster than small particles.

7.3 Results

The calculated aerosol concentration in the air is compared to the measurement in Figure 36. The same test was calculated with the MELCOR code, too. Both codes overestimate the aerosol concentrations, i.e. they underestimate the deposition rate. However, the MELCOR result is slightly better than the Apros result. The difference is partly explained by the agglomeration model, which MELCOR has, but it has not yet been developed for Apros. The agglomeration of small particles increases their deposition velocity. The Apros result can be considered satisfactory, and it is expected to improve when the agglomeration model is added in the future.

Both calculations were run with the default 10 aerosol size bins. The Apros model was tested also with 50 size bins, but the difference in the result was so small that it cannot be discerned in a plot.

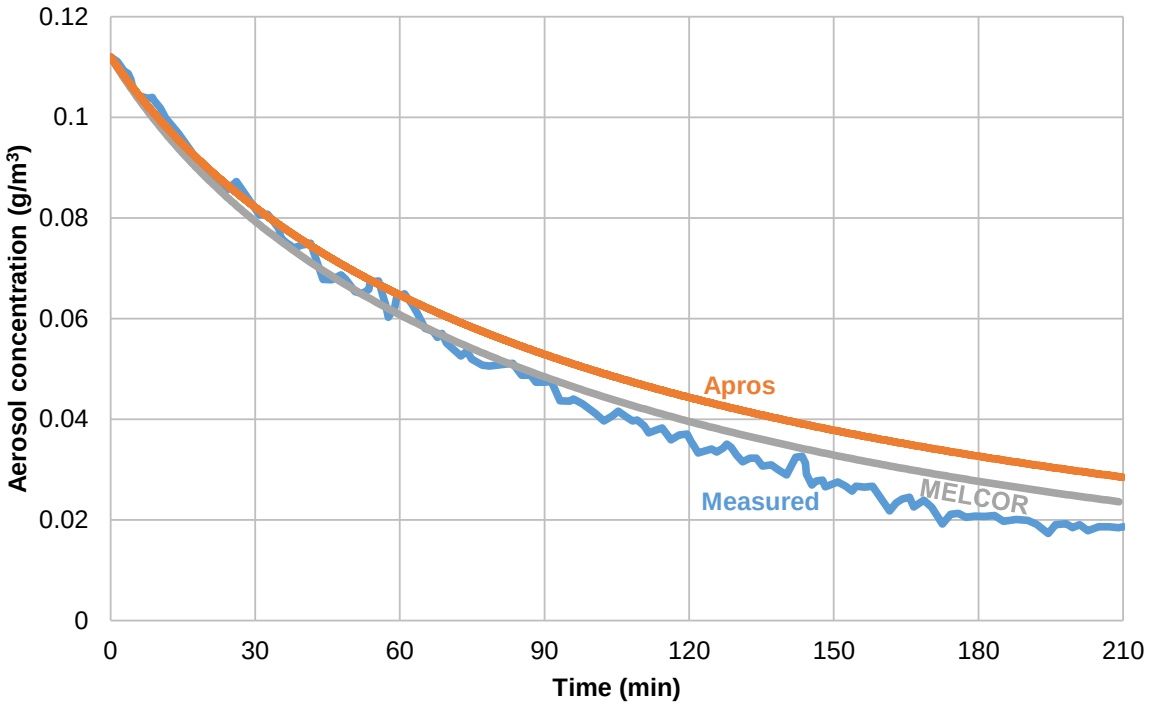

Figure 36. Aerosol concentration in the AHMED test, measurement compared with Apros and MELCOR calculations.

7.4 References

[1] NEA. 2009. State-of-the-Art Report on Nuclear Aerosols. OECD Nuclear Energy Agency. (NEA/CSNI/R(2009)5) https://www.oecd-nea.org/upload/docs/application/pdf/2021-03/csni-r2009-5.pdf
[2] Allen, M.D. & Raabe, O.G. 1985. Slip correction measurements of spherical solid aerosol particles in an improved Millikan apparatus. Aerosol Science and Technology, vol. 4, p. 269–286. https://doi.org/10.1080/02786828508959055
[3] Mäkynen, J.M. et al. 1997. AHMED experiments on hygroscopic and inert aerosol behaviour in LWR containment conditions: experimental results. Nuclear Engineering and Design, vol. 178, p. 45–59. https://doi.org/10.1016/S0029-5493(97)00174-X
[4] Mäkynen, J.M. & Jokiniemi, J.K. 1995. AHMED Code Comparison Exercise. Comparison Report. OECD Nuclear Energy Agency. (NEA/CSNI/R(95)23)
[5] https://www.oecd-nea.org/upload/docs/application/pdf/2020-01/csni-r1995-23.pdf

8 Summary

The work conducted by partners within this task can be separated into following areas, which cover the main issues related to fission product transport during LOCA transient:

- Fission product release from the fuel rod,
- Fission product transport in the primary circuit,
- Fission product behaviour in the containment.

Activities of ENEA, HZDR and VTT aimed at fission product release from fuel. ENEA conducted research on validation activities related to ASTEC/ELSA module. This revealed the lack of information from high burnup fuel tests as well as problem with other initial and boundary conditions, typical for DBA LOCA (high burnup, low temperatures). Furthermore, ENEA conducted recalculation of VERCORS RT1 and RT6 experiments aiming at grain size distribution. The recalculation revealed several discrepancies, which should be assessed in the future.

HZDR dedicated the workforce to detailed analysis of fission product release from fuel during DBA LOCA conditions with ATHLET-CD code. The simulations were done on a German PWR Konvoi NPP model. The simulations revealed that due to the physical nature of the LOCA transient majority of the fission product release originates from the fission products accumulated in the fuel-cladding gap. ATHLET-CD I equipped with three burst models, where two of them exhibit sever issues. The only fission release model applicable for DBA-LOCA is the one based on CORSOR. Future effort should be aimed on precise estimation of the fuel-cladding gap inventory.

VTT worked on validation of the aerosol gravitational deposition model implemented in Apros. Experimental data from the AHMED experiment were compared to the Apros and MELCOR calculation. For both codes a very good agreement was observed.

The fission product transport in the primary circuit and containment was in the scope of IRSN. The ASTEC-TR module SOPHAEROS was originally validated on several experiments (Phébus-PF, ISTP, OECD/STEM) aiming mainly at iodine behaviour. Unfortunately, initial and boundary conditions of these experiments are representative to DEC-B conditions (higher temperature, dose rate). The goal of the activity was to reassess the models implemented in ASTEC-TR module SOPHAEROS and to verify their applicability for DBA and DEC-A. The comparison revealed good agreement with experiment chosen from the R2CA database.

Transport in the containment and estimation of the source term was the subject of UJV activities. UJV conducted validation of several BIP experiments aiming at adsorption on dry painted surface. The models implemented in COCOSYS were fine tuned to the Ameron Amerlock paint. Further validation aimed at RTF experiment, where the impact of pH on iodine revolatilization was studied. The results were then transferred to the VVER-1000/V-320 containment model, where sensitivity studied aiming at sump pH proved the consonance with the RTF experiment. Finally, a BEPU analysis using the GRS methodology and Spermanns correlation ratio marked important initial and boundary conditions – sump pH, spray droplet diameter, spraying angle and environment pressure.

SSTC NRS activities aimed at precise estimation of the core inventory, which is an essential part of the radiological consequences estimation and preceding fission product transport within the primary circuit and containment. The

recalculation was done with SCALE code, using state of the art methods and best estimate approach to reduce the conservativism.

The main goal of the project, reduction of uncertainties, is the linking element of all the activities conducted by the partners within the Task 3.1. The expectations were fulfilled. Furthermore, several areas for future development have been targeted. The main issue is the validation, where many of the implemented models were validated against conditions, which are typical to DEC-A (high temperature, high pressure, high dose rate etc.) and a proper validation on DBA and DEC-A conditions should be conducted. Future effort should be aimed at precise definition of typical LOCA conditions (for fuel, primary circuit, and containment). Based on that, a complex reassessment of existing experiments should be done to select relevant experiments for validation and to reveal knowledge gaps, i.e. missing data and conditions. These gaps may become corner stones of future research projects both in national and international level. The need of research of the DBA and DEC-A conditions is even more important for SMRs (small modular reactors), where the DEC-B conditions are expected to be practically eliminated due to inherent safety.